2013-01-01

Experimental Study on the Fabrication of Advanced Materials for Energy Applications Using High Energy Mechanical Milling

Ashvin Kumar Narayana Swamy
University of Texas at El Paso, anarayanaswamy@miners.utep.edu

EXPERIMENTAL STUDY ON THE FABRICATION OF ADVANCED MATERIALS FOR ENERGY APPLICATIONS USING HIGH ENERGY MECHANICAL MILLING

ASHVIN KUMAR NARAYANA SWAMY

Environmental Science and Engineering Doctoral Program

APPROVED:

EVGENY SHAFIROVICH, Ph.D., Chair

CHINTALAPALLE RAMANA, Ph.D., Co-Chair

AHSAN R. CHOUDHURI, Ph.D.

YIRONG LIN, Ph.D.

CESAR J. CARRASCO, Ph.D.

Benjamin C. Flores, Ph.D.
Dean of the Graduate School

Dedication

Dedicated to my mom Rashmi and my dad Narayana Swamy for their unconditional support and love.

EXPERIMENTAL STUDY ON THE FABRICATION OF ADVANCED MATERIALS FOR ENERGY APPLICATIONS USING HIGH ENERGY MECHANICAL MILLING

by

ASHVIN KUMAR NARAYANA SWAMY, B.S., M.S.

DISSERTATION

Presented to the Faculty of the Graduate School of

The University of Texas at El Paso

in Partial Fulfillment

of the Requirements

for the Degree of

DOCTOR OF PHILOSOPHY

Environmental Science and Engineering Doctoral Program

THE UNIVERSITY OF TEXAS AT EL PASO

August 2013

Abstract

The reaction of aluminum (Al) powder with water has the potential for on demand hydrogen generation. Conventional Al powders, however, react with water slowly due to a highly protective oxide layer on the particle surface. Current methods for Al activation involve harmful and expensive materials. The nano-scale Al powders also remain very expensive and have problems such as a large amount of oxide on the surface. The use of aluminum in an energy generation cycle is also hindered by the fact that, although Al is the most abundant metal in the Earth's crust, its recovery from ore consumes a lot of energy. Recycling aluminum hydroxide, formed as a result of Al reaction with water, would also require large amounts of energy. The energy consumption for production of Al powder and hence its cost could be significantly reduced by using recycled aluminum scrap and waste where aluminum is contained in metallic, non-oxidized form.

The research work presented here investigates the preparation of an activated aluminum powder from aluminum foil that is widely available as scrap and waste. The obtained results demonstrate that a highly reactive, fine powder can be obtained from Al foil by high-energy ball milling with sodium chloride (NaCl). The obtained powder readily reacts with hot water, releasing hydrogen. Note that NaCl is an environment-friendly additive that can easily be removed after milling and recycled. After washing NaCl out, the powders retain a high reactivity with respect to hot water. As compared to previously studied activation of commercial Al powders, a major advantage of the investigated process is the feasibility of using secondary aluminum.

Another area of research presented here is the synthesis of gallium oxide (Ga_2O_3) nanostructures for their use as high-temperature sensors. Quasi one-dimensional nanomaterials are of great interest due to increased focus on their importance in physics research and also their applications in the nanodevices industry. Since the mid 1950's, considerable research has been reported on the synthesis of filamentary crystals from alloys and metals. Since the discovery of carbon nanotubes (CNTs), there has been a tremendous surge in research activities for development and characterization of one-dimensional nanostructures. Most of the research is targeted towards the development of semiconductors such ZnO, Si, SnO_2, and GaAs. Gallium oxide nanostructures have the ability to withstand high temperatures and

also act as high-temperature sensors. In particular, they can be used as oxygen sensors at temperatures over 900 °C. These properties make gallium oxide nanostructures attractive for use in exhaust systems of the combustion chambers in power plants.

β-Ga_2O_3 nano-rods and nano-sheets were successfully synthesized by a simple method based on heating GaN in inert gas environment with traces of oxygen. Characterization of the obtained products showed nano-belts in the size range from 10 nm to 15 nm. Several other unique nano-structures were also synthesized. The results show a vapor-solid mechanism to be the prevailing growth route for the synthesis of nano-structures.

Table of Contents

Abstract v

Table of Contents vii

List of Tables ix

List of Figures x

List of Illustrations xiii

Chapter 1: Introduction 1

1.1 Aluminum: Brief History and Properties 2

1.2 Gallium Oxide Based High Temperature Sensors 4

1.3 History of Mechanical Milling 5

1.1.1 Types of Mechanical Milling 6

1.1.2 Types of Mills 6

1.1.3 Mechanism of Milling 6

1.4 Research Objectives 8

1.5 Organization of Thesis 8

Chapter 2: Literature Review 9

2.1 Hydrogen Generation 9

2.2 Synthesis of Ga_2O_3 Nanostructures 20

Chapter 3: Experimental Setups and Procedures 25

3.1 Hydrogen Generation 25

3.1.1 Sample Preparation 25

3.1.2 Overview of Experimental Apparatus 28

3.1.3 Experimental Procedure – Reactions of the Activated Al powders with warm water 29

3.1.4 Experimental Procedure – Combustion of the Activated Al Powder with Water 30

3.2 Gallium Oxide Synthesis 31

3.2.1 Sample Preparation 31

3.2.2 Overview of Experimental Apparatus 33

3.2.3 Experimental Procedure 34

3.3 Characterization Techniques 35

3.3.1 Surface Area Analysis 35
3.3.2 Particle Size Analysis 37
3.3.3 Scanning Electron Microscopy 38
3.3.4 X-Ray Diffraction Analysis 39
3.3.5 Tumbler Mixer 41

Chapter 4: Results-Hydrogen Generation 43
4.1 Commercially Available Aluminum Powder 43
4.2 Investigation of Activated Powder Obtained from Aluminum Foil 44
4.2.1 Characterization of the Obtained Al/NaCl powders and Al powders 44
4.2.2 Reactions of the Obtained Powders with Warm Water 48
4.3 Investigation of Activated Powder Obtained from Aluminum Cans 55
4.3.1 Characterization of the Obtained Al/NaCl and Al powders 55
4.3.2 Reactions of the Obtained Powders with Hot Water 57
4.4 Discussion of the Effect of Leaching on the Induction Period and the Final Reaction Extent 60
4.5 The Activation Energy of Al-H_2O Reaction 62
4.6 Combustion of Activated Aluminum Powder with Water 63
4.7 Energy Considerations 70
4.8 Summary 71

Chapter 5: Results-Gallium Oxide Synthesis 72
5.1 Characterization of Ball Milled GaN Powders 72
5.2 Oxidation Reactions of Ball Milled GaN Powders 74
5.2.1 Case 1 74
5.2.2 Case 2 77
5.2.3 Case 3 78
5.2.4 Case 4 78
5.2.5 Case 5 80
5.2.6 Case 6 81
5.3 Summary 85

Chapter 6: Conclusions 86

Bibliography 88

Appendix A 93

Vita 95

List of Tables

Table 3.1 Different milling parameters for ball milling GaN.....32
Table 4.1 Elemental composition of the obtained powder and the oxygen-to-aluminum atomic ratio for powders obtained by milling Al foil with NaCl in air atmosphere.....46
Table 4.2. Elemental composition and the oxygen-to-aluminum atomic ratio for the powders obtained by milling Al foil with NaCl in argon atmosphere. 47
Table 5.1 Elemental composition of nano structures seen in fig. 5.7b obtained from spot analysis using EDS.....79

List of Figures

Figure 1.1 Schematic showing the different forms of impact during high-energy ball milling [13]. 7
Figure 2.1: Hydrogen evolution rates from Al-NaCl and Al- salt-free systems [25]. 11
Figure 2.2: Portable H_2 generators a) reactor-water supply-air compressor b) reactor and water pump, Al powder cartridge (black cylinder-far right) [27]. 12
Figure 2.3: Combustion rate (1) in a stoichiometric mixture of aluminum with water versus pressure [45]. 15
Figure 2.4 Adiabatic flame temperatures of various mixtures of nano-aluminum and water [50]. 17
Figure 2.3: Growth of a silicon crystal by VLS: a) Liquid droplet on a substrate and b) Growing crystal with liquid droplet [63]. 21
Figure 2.4: SEM image of ball-milled GaN powder annealed at 930 °C [67]. 23
Figure 3.1: Aluminum foil (15 µm) cut into square pieces (10 mm x 10 mm). 26
Figure 3.2: (a) Fritsch Pulverisette 7 Premium Line planetary ball mill and (b) zirconium oxide grinding media. 27
Figure 3.3: (a) Pepsi can pieces (b) Can pieces after removal of paint and film. 28
Figure 3.4: Experimental apparatus for H_2 generation. 29
Figure 3.5: Schematic of the combustion chamber. 31
Figure 3.6: Experimental setup for GaN combustion 33
Figure 3.7: Microtrac BET Specific Surface Area Analyzer 37
Figure 3.8: Microtrac Bluewave S3500 Particle Size Analyzer 38
Figure 3.9: Hitachi S-4800 Scanning Electron Microscope 39
Figure 3.10: Bruker D8 Discover X-ray Diffractometer 41
Figure 3.11: Bioengineering INVERSINA 2L 42
Figure 4.1: Kinetic curves obtained from the reaction of commercially available Al powders with water at two different water temperatures (50 °C and 65 °C) 43
Figure 4.2: Powder obtained by milling Al foil with NaCl. 44
Figure 4.3: Microphotographs of powders obtained from 23 µm Al foil by milling with NaCl (a) magnification: 6000 and (b) magnification: 30000. 45
Figure 4.4. Particle size distribution for Al Powder obtained by milling of 23 µm Al foil with NaCl in Ar, after leaching by methanol. 47
Figure 4.5: XRD pattern of the solid products obtained after reaction of the Al powder with water at temperatures of 35 °C, 50 °C, 65 °C, and 80 °C. 48
Figure 4.6: Kinetic curves for the powders obtained from Al foils of different thicknesses (15 µm, 23 µm, and 36 µm) by ball milling with NaCl: (a) Al/NaCl powders and (b) Al powders after leaching-out NaCl. 50
Figure 4.7: Time variation of the reaction rate for the powders obtained from Al foils of different thicknesses (15 µm, 23 µm, and 36 µm) by ball milling with NaCl: (a) Al/NaCl powders and (b) Al powders after leaching-out NaCl. 51
Figure 4.8: Kinetic curves for the powders obtained by ball milling of Al foil with NaCl in Ar: (a) Al/NaCl and (b) salt-free (leached by water) Al. 53
Figure 4.9: Time variation of the reaction rate for the powders obtained from Al foil by ball milling with NaCl in Ar: (a) Al/NaCl and (b) salt-free (leached by water) Al. 54
Figure 4.10: SEM microphotographs of the ball milled Al can powders (a) 30 min milled unleached and (b) 60 min milled unleached 55
Figure 4.11: EDS spectrum for Al can unleached powder after 30 min milling with NaCl 56

Figure 4.12: Kinetic curves for the powders obtained from Al cans by milling with NaCl in air (the milling time: 30 min): (a) Al/NaCl and (b) salt-free (leached by water) Al. 58
Figure. 4.13: Kinetic curves for the powders obtained from Al cans by milling with NaCl in air (the milling time: 60 min): (a) Al/NaCl and (b) salt-free (leached by water) Al. 59
Figure 4.14: Kinetic curves for the powder obtained by ball milling of Al foil with NaCl in Ar and leached by methanol. 61
Figure 4.15: Arrhenius plot for the maximum rates of the reactions between the obtained powders and water. 63
Figure 4.16: Propagation of the combustion front over Al/H_2O mixture at 40 wt% Al. Time zero was selected arbitrarily. 64
Figure 4.17: Propagation of the combustion front over Al/H_20 mixture at 60 wt% Al. Time zero was selected arbitrarily. 65
Figure 4.18: Propagation of the combustion front over Al/H_2O mixture at 80 wt% Al. Time zero was selected arbitrarily. 65
Figure 4.19: Maximum temperatures measured in the front (points) and calculated adiabatic flame temperatures (curve) for Al/H_2O mixtures. 66
Figure 4.20: The front propagation velocities measured for Al/H_2O mixtures. 67
Figure 4.21: EDS spectrum of the combustion products for Al/H_2O mixture with 50 wt% Al. 68
Figure 4.22: XRD patterns of the combustion products for Al/H_2O mixtures with 40 wt% Al and 70 wt% Al. 69
Figure 5.1: SEM microphotographs of GaN powders: (a) Original GaN powder, (b) Ball milled GaN powder, and (c) Ball milled GaN powder at higher magnification. 72
Figure 5.2: XRD pattern of the GaN powders showing comparison of the peaks obtained for different milling parameters: (a) Green peaks: Original powder and (b) Black peaks: 04/13/12 powder (see section 3.2.1) 73
Figure 5.3: SEM microphotographs of the reaction products obtained by heating ball milled GaN powder in a tube furnace: (a) nanobelts seen, (b) sheet like structures (see arrow), (c) magnified view of the belts, and (d) saw-like nano structures 75
Figure 5.4: EDS spectra of the reaction products (a) EDS spectrum of the nanobelts by spot analysis (b) EDS spectrum of the obtained powder by area analysis 76
Figure 5.5 XRD pattern of the reaction products obtained by heating GaN powder: peaks consistent with Ga0.97N0.9O0.09. 77
Figure 5.6: SEM microphotograph of the reaction products obtained by heating ball milled GaN powder in a helium atmosphere 78
Figure 5.7: SEM microphotographs of the reaction products obtained by heating GaN pellet: (a) closely pack structure, (b) small, wire-like structures embedded in a dense powder matrix, and (c) thin sheet-like structures on the surface of the pellet 79
Figure 5.8: Digital photographs of the alumina crucible retrieved after heating ball milled GaN powder: (a) white wool like structures on the outer rim of the crucible, and (b) top view of the crucible with unreacted GaN powder inside 80
Figure 5.9: SEM microphotographs of the reaction products obtained by heating ball milled GaN powder: (a) Extensive belts/wire like structures, and (b) rod-like structures 80
Figure 5.10: SEM microphotographs of the products obtained by haeting GaN powder: (a) three-dimensional nanorods of different sizes, (b) nanorods, nanosheets, nanowires seen in between agglomerated particles, (c) close up view of a nanorod grown from the GaN nanoparticles, and (d) clusters of sheets 82
Figure 5.11: EDS spectra using area analysis of the nanosheets shown in fig. 5.10d: (inset: elemental composition) 83

Figure 5.12: XRD pattern of the products obtained by heating GaN powder: red lines show presence of β-Ga_2O_3 mixed with unreacted GaN powder (green lines) 84

List of Illustrations

Illustration 3.1: Bragg's law of diffraction. 40

Chapter 1: Introduction

In this thesis, the effect of high energy mechanical milling on the fabrication of advanced materials for energy applications is studied. Specifically, the investigated materials include activated aluminum powder and gallium oxide nanostructures. The activated aluminum could be used for generation of hydrogen from water and in energetic materials such as rocket propellants, explosives, and pyrotechnics, while gallium oxide nanostructures are promising materials for use as high-temperature sensors in advanced fossil fuel power plants.

The United States uses about 10 million tons of hydrogen each year for industrial purposes like making fertilizers and refining petroleum [1]. It has approximately three times more energy content per unit mass than gasoline [2]. At present, 95% of all hydrogen in the U.S. is produced from fossil fuels (natural gas, liquid hydrocarbons, and coal) through the processes such as steam methane reformation and coal gasification. Hydrogen is a clean fuel as the only product of is combustion is H_2O. The production of hydrogen, however, releases large amounts of carbon dioxide, a greenhouse gas. To reduce greenhouse gas emissions and the nation's dependence on fossil fuels, other ways of hydrogen generation are required.

However, hydrogen has a number of drawbacks in terms of use and storage. It has a low energy density, which makes it difficult to store under standard atmospheric conditions. Liquid hydrogen occupies four times more volume than gasoline to produce the same amount of energy [2]. As a result, heavy and bulky tanks are used to store hydrogen gas at high pressures. Liquid hydrogen requires the temperature as low as 20 K and also has a relatively low density. Extensive studies of metal hydrides, the so-called chemical hydrides, metal-organic networks, and other systems for hydrogen storage have been conducted, but storage still remains a major hurdle for hydrogen economy.

Significant research has been conducted over the last four decades on hydrogen production from water. One approach is based on Al – H_2O reactions. These reactions could be used for the production of hydrogen and for on-demand hydrogen generation in applications such as portable fuel cell power systems, underwater propulsion, space propulsion, mobile, and stationary power generation systems. Unfortunately, a major problem of using Al as reactant is the protective oxide layer on its surface.

Hence, Al has to be used in an activated form for the reaction with H_2O. Prior research has shown that the protective oxide layer can be removed by corrosion in strong alkaline solutions, high-energy ball milling, and alloying with bismuth, gallium and other dopants.

Operating conditions of advanced fossil fuel power plants require sensor and controls that can withstand high temperature, pressure, and corrosive environment [3], [4]. The desired characteristics of those sensors are long shelf life and stability, high sensitivity, and low threat of poisoning or contamination. One promising material is gallium oxide (β-Ga_2O_3). The second part of the thesis investigates the synthesis of gallium oxide nanostructures using ball-milling technique and subsequent annealing. Since the advent of carbon nanotubes, one dimensional nanostructures have garnered much interest in the nano/micro devices industry owing to their unique properties. β-Ga_2O_3 is the most stable form of gallium oxide with a melting point of 1900°C [5], making it desirable for high-temperature sensors. Also, it has good chemical and thermal stability. Previous studies have reported use of laser ablation, thermal evaporation, and carbon thermal reduction for the synthesis of β-Ga_2O_3. More recently, ball-milled gallium nitride powders were used to produce gallium oxide nanostructures.

The following sections describe the motivations for studying Al-H_2O reactions and the synthesis of β- Ga_2O_3 nanostructures, and their importance to the above mentioned fields of interest.

1.1 Aluminum: Brief History and Properties

Aluminum is the third most abundant element in the universe making up approximately 8% of the earth's crust [6]. Humphrey Davy proved the existence of Al in 1808 and a few years later Hans Oersted was able to produce small amounts of the metal. It was in 1880 when Charles Martin Hall learned how to make aluminum oxide from alumina (Al_2O_3). He placed cryolite and alumina in a container and passed electric current through it. A congealed mass was formed which had various Al particles in it.

In the present day, the production of Al begins with mining bauxite. The bauxite ore is crushed to a correct particle size and alumina is then extracted by dissolving in hot sodium hydroxide. The resulting aluminum trihydrate crystals are precipitated in fluidized beds to produce alumina. Finally, Al is produced by the electrolytic reduction of the alumina through the so-called Hall-Heroult process. This

involves carbon electrodes which are oxidized to carbon dioxide during the process. As a result, the production of 1 mol (27 g) of aluminum also produces 0.75 mol (33 g) of CO_2:

$$2\,Al_2O_3 + 3\,C \rightarrow 4\,Al + 3\,CO_2 \quad (1)$$

This does not include CO_2 emissions during the production of required (large) electrical energy, aluminum refining, and other involved processes.

The so-called secondary aluminum is produced from the byproducts of aluminum smelting, scrap and waste. Aluminum is recovered by melting the scrap in a gas- or oil-fired furnace and the impurities are removed using chlorine or other fluxes until the Al reaches the desired purity. As compared to the production of primary Al (i.e., from bauxites), production of secondary Al requires less energy and emits less CO2.

Aluminum is a shiny, silvery white colored metal that is light in weight and strong. It is crystallized in a face-centered lattice with an atomic radius of 1.43 Å. The density of Al is 2.7 g/cm^3. It is a good conductor (electrical conductivity ranges from 156 * 10^4 Ω^{-1}.cm^{-1} (-189 °C) to 12.5 * 10^4 Ω^{-1}.cm^{-1} (400 °C)). The standard enthalpy of formation of Al_2O_3 is -1669 kJ/mol (only behind B and Be). The high exothermicity of Al oxidation makes it desirable for energetic applications such as solid rocket propellants, thermites, pyrotechnics, and explosives.

However, the surface of Al metal is covered with an oxide layer that prevents any reaction with air. The Pilling and Bedworth coefficient β determines the ratio of the oxide volume to the metal. Metals with β not excessively greater than 1 have good oxide layer properties. For Al, β is equal to 1.28 making the oxide layer highly protective [7]. This means that for Al - H_2O reactions, the oxide layer becomes a deterrent. Thus, it is necessary to break the oxide layer so that Al can be used as a reactive material.

The goal of the present research is to develop scientific basis for environment-friendly preparation of an activated Al powder from foil that is widely available as scrap and waste. Such a powder could be used for various applications such as on demand hydrogen generation from water, green Al-H_2O propulsion systems, rocket propellants, and other energetic materials. Specifically, the project investigates the feasibility of converting aluminum foil to activated Al powder using high-energy mechanical milling.

1.2 GALLIUM OXIDE BASED HIGH TEMPERATURE SENSORS

Gallium oxide is mostly used in integrated circuits (ICs), laser diodes, light-emitting diodes (LEDs), photodetectors, and solar cells and temperature sensors. Gallium oxide has a polymorphic crystal structure with α, β, and γ phases. Of the three phases β-Ga_2O_3 is the most stable form of gallium oxide. It is a wide-band-gap (>5 eV) semiconductor material with good chemical and thermal stabilities [8]. Gallium oxide is usually prepared by heating gallium in air or by decomposing gallium nitrate at 200- 250 °C.

Pollutant emissions have been a cause of great concern for industrial plants and automobiles. Typically, nitrogen oxides (NO_X), carbon monoxide, and hydrocarbons are released into the atmosphere. To detect these emissions, oxygen sensors are installed in the exhaust pipes of the combustion systems. These sensors are usually at an operating temperature of 700 °C or above. To better understand the combustion characteristics for precise measurement and control, the oxygen sensors need to be installed as close as possible to the combustion chamber. Hence, these sensors need to be thermally stable to withstand the stresses that occur at high temperatures.

The desired characteristics of a temperature sensor are long shelf life and stability, high sensitivity, and no threat of poisoning or contamination. Ga_2O_3 is one such material which exhibits n-type semiconductor properties above 600 °C and is sensitive to reducing gases like CO and H_2 below 700 °C and to oxygen above 900 °C [9]. This makes gallium oxide ideally suited for high temperature applications as mentioned above. One-dimensional nanostructures of Ga_2O_3 are especially of great interest since they can be easily integrated to nano-electronics due to their high melting point and stable structure.

The overarching goal of this part of the research is to develop high-temperature oxygen sensors by employing Ga_2O_3-based nanostructures (nano belts, sheets, and wires). The underlying concept of this research is to use mechanically milled GaN powders for fabrication of Ga_2O_3 through heating in inert gas environment with traces of oxygen. The hypothesis is that use of high-energy mechanical milling in a planetary ball mill for preliminary treatment of GaN powders may increase the yield and quality of the obtained gallium oxide nanostructures.

1.3 HISTORY OF MECHANICAL MILLING

Mechanical milling is a powder processing technique for production of homogeneous materials from elemental powders, one elemental phase and another intermetallic compound, or two or more intermetallic compounds. It usually involves repeated welding, fracturing, and rewelding of powder particles in a high-energy ball mill. This process was developed in around 1966 by John Benjamin and his colleagues at the Paul D. Merica Research Laboratory of the International Nickel Company [10] (INCO). They found that milling a nickel or Al alloy powder in an oxidizing atmosphere, new powder with each of the powder particles containing a dispersion of oxide particles was produced. This proved that during the milling process oxide layers formed on the surface of the particles are fractured and embedded into the powder particles through cold welding. It was found that fracturing and cold welding of particles occurs during milling, which results in the formation of a new material which is totally different from the starting powders.

In the 1980's Koch *et al.* [11] demonstrated that mechanical milling can also be used for alloying metals. They milled Ni and Nb powders, and after milling, the powder became an amorphous Ni-Nb alloy powder. During the late 1980's, McCormick *et al.* [12] reported chemical reactions between Ca and CuO induced by high-energy mechanical milling. Since then, mechanical milling has diversified into other areas of interest like mechanochemical synthesis, mechanically activated self-propagated high-temperature synthesis (MASHS), etc.

Currently, there are many processes in commercial use for the production of advanced composites such as, rapid solidification from liquid state, plasma processing, and vapor deposition. There are several attributes of mechanical milling which make it desirable e.g., production of fine dispersion of second phase particles, refinement of grain sizes into nanometer range, development of amorphous phases, possibility of alloying difficult to alloy elements and inducement of chemical reactions at lower temperatures. An important factor that comes in to the picture is that mechanical milling is relatively inexpensive when compared to other processes as mentioned above.

1.1.1 Types of Mechanical Milling

a) Reaction Milling: A mechanical alloying process wherein a solid-state reaction occurs as a result of high temperature and pressure during the milling process.

b) Cryomilling: Milling is carried out at very low temperatures or milling is carried out in cryogenic liquids such as liquid nitrogen.

c) Rod Milling: In a conventional ball mill, the grinding balls are replaced by long rods to exert shear forces on the material.

d) Mechanical Activated Annealing (M2A): It involves a short period of mechanical milling followed by low-temperature annealing.

e) Double Mechanical Alloying: A two stage milling process wherein, in the first stage the elemental powders are refined and this mixture is then subjected to heat treatment at high temperatures. During the second stage, the heat treated powder is milled again to further refine the particle size.

1.1.2 Types of Mills

a) SPEX Shaker Mill: This mill works on back and forth shaking motion and can mill about 10-20 g in a cycle. The ball velocities can reach up to 5 m/s.

b) Attritor Mill: This mill consists of a vertical drum with series of impellers inside and can mill about 0.5- 40 kg in a cycle. The ball velocities can reach up to 0.5 m/s.

c) Planetary Ball Mill: It works on the planetary motion of the grinding bowls and can mill about 10 -250 g in a cycle. The ball velocities are higher than the SPEX mill.

In the present research, a planetary ball mill (Fritsch Pulverisette 7 Premium Line) was used to produce fine powders required for the Al – H_2O reactions and for the synthesis of gallium oxide nanostructures.

1.1.3 Mechanism of Milling

During the milling process the particles are repeatedly fractured and cold welded. The colliding grinding balls trap some amount of powder in between them during each impact (see fig.1.1). The force of the impact causes the powder particles to plastically deform and fracture. This allows the particles to

weld together again at the fracture plane. Soft particles have a tendency to weld together and form bigger particles (agglomeration). This leads to a varied particle size distribution where a broad range of particle sizes develops. The bigger particles continue to undergo further deformation by fragmentation of fragile flakes. In the absence of strong cohesive forces between the particles, further reduction in particle size occurs. As the grinding balls continue to collide, the structure of the particle is refined although the particle size continues to remain the same. As the milling continues for a certain amount of time, a state of equilibrium is achieved where further impact of the grinding media does not affect the particle size. Smaller particles are able to withstand the impact forces and agglomerate to form bigger particles with continued milling.

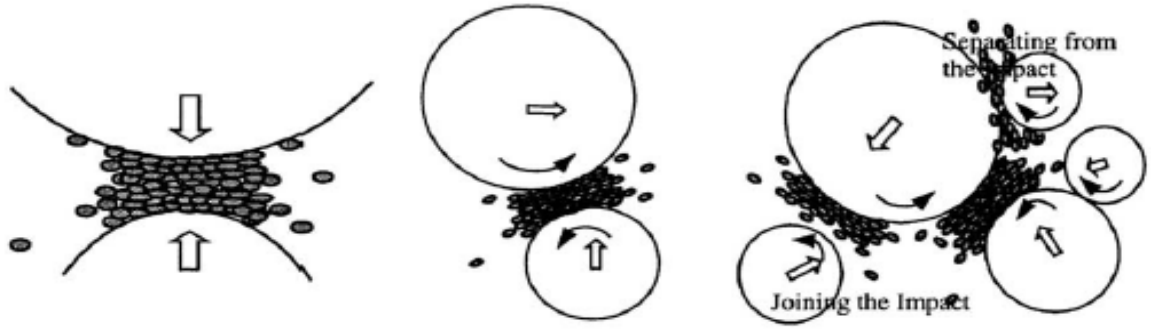

Figure 1.1 Schematic showing the different forms of impact during high-energy ball milling [13].

As seen in fig 1.1, three possible types of impact during high-energy ball milling can occur: a) Head-on impact, b) Oblique impact, and c) Multi-ball impact. It can be seen that, impact forces depend upon how the grinding balls collide with each other during the milling process. Head-on impact exerts more force than the oblique impact. Multi-ball impact traps more particles and thus greatly reduces the time required to achieve the desired particle size.

1.4 RESEARCH OBJECTIVES

a) To investigate and optimize the fabrication of activated Al powder from Al foil using high-energy ball milling with environment-friendly additives.
b) To determine the reaction kinetics and mechanisms of the obtained Al powder with hot water.
c) To determine the combustion characteristics of mixtures of the obtained Al powder with liquid water.
d) To fabricate high-quality Ga_2O_3-based materials using high-energy ball milling and optimize conditions to produce unique architectures and morphology at the nano scale.

1.5 ORGANIZATION OF THESIS

A literature review is presented in Chapter 2, where prior studies on Al-H_2O reactions (both low temperature and combustion reactions) and also Ga_2O_3 synthesis procedures are examined. The experimental setups and characterization techniques used in this research are presented in Chapter 3. Chapter 4 details the results obtained from the Al-H_2O reactions for different Al powders. GaN oxidation experiments and the subsequent results obtained are presented in Chapter 5. A summary of all the research work presented in this thesis and suggestions for future work are presented in Chapter 6.

Chapter 2: Literature Review

As mentioned in Chapter 1, the research presented in this thesis is focused on hydrogen generation and Ga_2O_3 synthesis. Thus, the literature review is divided into two sections.

2.1 Hydrogen Generation

Fossil fuel resources are depleting at an alarming rate with increased industrial activity among all nations of the world and a surge in the vehicular traffic. Clean, renewable energy technologies need to be devised for reducing our dependence on conventional energy resources. Fuel cells for transport applications can utilize hydrogen as an energy carrier. The main current method of producing hydrogen is via steam-reforming of natural gas. However, capital costs, storage requirements, transportation costs, and operation and maintenance costs associated with producing hydrogen from natural gas [14] make it expensive. Not to forget the cost associated with CO_2 sequestration, which is a byproduct of steam-reforming process. The need for cheaper and efficient hydrogen production systems has sparked tremendous research over the last few decades.

Reaction of Al with H_2O to produce H_2 is a well-known process. A typical Al-H_2O reaction is given by the equations below [15], [16]

$$2\,Al + 3\,H_2O \rightarrow Al_2O_3 + 3\,H_2 \quad (2)$$

$$Al + 3\,H_2O \rightarrow Al(OH)_3 + 1.5\,H_2 \quad (3)$$

It can be seen that 1 mole of Al produces 1.5 moles of H_2. One of the earliest methods for hydrogen generation through the reactions of water with metals was proposed by Brewer and Allgeier [17]. They reported hydrogen gas production in an Al foil envelope by the reaction of magnesium metal, zinc chloride, sodium chloride and water.

Kozin *et al* [18] reported that activated Al is highly reactive with water, producing hydrogen. Aluminum activation is usually the process of decreasing the protective properties of the oxide layer on the surface of Al with different kinds of additives. The additives penetrate the oxide layer forming a

stratified system with the primary Al. A theoretical discussion is presented by Zasukha *et.al* [19], wherein they report that additives not only eliminated the passivation on the Al surface but also change the position of the Fermi level. This decreases the activation energy for electron transfer from Al to the H_2O molecule and increases the rate constant of the reaction.

Mechanical milling of Al with other metals to produce metal matrix composites and fine grain structure has been reported by Hanada *et al* [20]. They found that mechanical milling increases the mechanical properties of the powder like Vickers hardness number and Young's modulus. Also, grain sizes were less than 1μm with a homogeneous matrix. Gas bubbles were observed by Uehara *et.al* [21] during drilling of an Al alloy in water (85 °C). Upon testing with a gas detector, it was confirmed that the bubbles were filled with hydrogen, presumably formed by the reaction of Al with H_2O. Examination of the by-product using SEM revealed that it fitted well with the aluminum hydroxide structure. It also confirms the reaction given by equation (2).

Kravchenko *et al* [16] reported the mechanical activation of aluminum by amalgamation with dopants such as gallium, tin, indium, lead, bismuth, magnesium, and calcium. They achieved a hydrogen evolution of about 1000 cc/g of alloy in one hour of reaction with water at 82 °C. It was also noted that hydrogen yield decreased when the doping metal content was over 20 %. Another technique of activation of aluminum by milling with graphite powders in a vibratory ball mill was reported by Streletskii *et al* [22]. The reaction of the produced powders (Al/C = 4:1) with water at 75 °C yielded up to 800 cc/g powder of hydrogen. It was also seen that almost 20 % of the Al atoms were oxidized by air, while the remaining, non-oxidized part of metallic Al (80%) reacted completely with water.

A liquid eutectic mixture of Ga-In was used to produce an activated aluminum powder by Parmuzina *et al* [23]. Hydrogen yield of up to 1100 cc/g of Al was obtained when the powder was treated with water at room temperature. It is believed that Ga creates a thin layer on Al surface, penetrating it and causing the oxide layer to fracture. Thus, upon contact with water, the Al powder reacts vigorously evolving hydrogen.

Recently, Alinejad *et al* [24] reported the ball milling of commercially available (CA) Al powder with sodium chloride (NaCl) in an argon atmosphere for 20 hours. The produced powder was treated

with water at 70 °C and a conversion yield of up to 70 % was achieved for salt to Al mole ratio of 0.5 (NaCl/Al = 50/50 wt%). Closer to 100 % conversion yield was seen for powders with salt to Al mole ratio of 1.5. A similar method was also reported by Czech *et.al* [25], where CA Al powder and NaCl (50/50 wt %) were treated in a SPEX mill under air atmosphere. Sodium chloride was leached out of the produced mixture by dissolution in cold water (< 15 °C) and the mixture was then dried in air. The resulting powder was treated with water at 55 °C. Hydrogen yield of up to 1000 cc/g Al or a 73 % conversion rate was achieved. Kinetic curves of the hydrogen evolution over a period of 60 min are shown in figure 2.1.

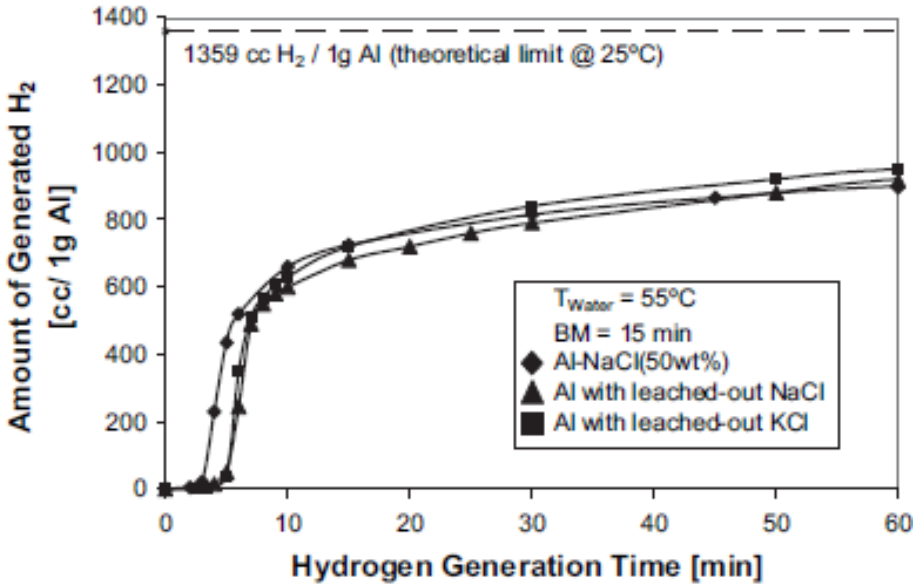

Figure 2.1: Hydrogen evolution rates from Al-NaCl and Al- salt-free systems [25].

Soler *et al* [26] used CA Al powder to perform corrosion experiments in seawater at 75 °C. To prevent passivation of the Al surface, an aqueous solution of $NaAlO_2$ with seawater was prepared. A 100 % conversion yield was achieved in 5 min. A 88 % conversion yield was achieved when aluminum hydroxide ($Al(OH)_3$) was used with 35 g/dm^3 of NaCl in distilled water at 75 °C. It was also noted that no passivation of Al was observed when NaOH was used in seawater. The reaction rate was significantly higher when using NaOH than that of $NaAlO_2$ although the final yield was much higher in $NaAlO_2$.

Watanabe [27] has developed portable H_2 generators (see fig. 2.2) using Al scrap generated from the auto industry. Stone mortars were used to crush the crystals, which created micro-cracks in the Al particles. Activation in sufficiently cold (<5 °C) water prevented hydrogen generation. The resulting powder was freeze dried and kept at low temperatures in an N_2 atmosphere. Hydrogen yield of up to 1500 cc/min was achieved using the activated Al powder with water at room temperature.

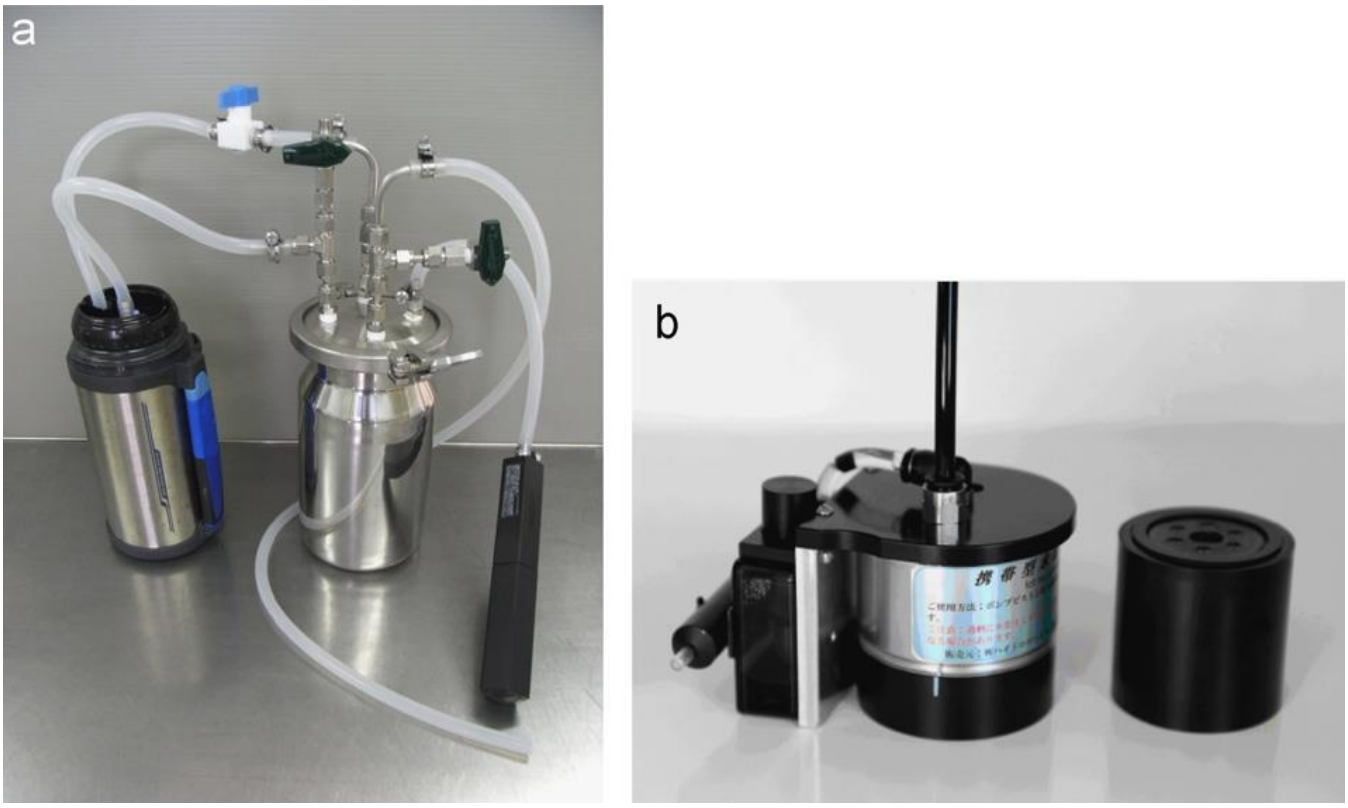

Figure 2.2: Portable H_2 generators a) reactor-water supply-air compressor b) reactor and water pump, Al powder cartridge (black cylinder-far right) [27].

Corrosion of Al in a sodium stannate (Na_2SnO_3) solution to produce H_2 from H_2O was reported by Soler *et al* [28]. Very high reaction rates were observed. Formation of Sn particles on the Al surface, which acted as a corroding agent, yielded high H_2 evolution when treated with water at 75 °C. Macanas *et al* [29] reported the use of aqueous alkaline solutions (NaOH, Na_2SnO_3, $NaAlO_2$, $NaBO_2$, and Na_2SiO_3) to promote Al corrosion in water (a similar process was reported in Refs. 24 and 26). A 100 % yield was achieved when Al powder was used in the $NaBO_2$ solution at 75 °C.

Rosenband *et al* [30] devised a lithium based thermo-chemical process for activation of Al. The activated powder was treated with tap water at temperatures ranging from 50 to 80 °C. Hydrogen yield was highest at 80 °C, revealing that temperature does play an important role in H_2 evolution. The Al powder was also treated with sea water and pure water. It was determined that the extent of hydrogen yield was independent of the type of water used.

Ilyukhina *et al* [31] used gallams for activation of Al. A similar method has been reported in [16]. The gallams alloy (Ga-In-Zn-Sn) was ground with Al pellets in a planetary mill at 2,220 rpm for 3 min. The resulting activated powder was treated with water at room temperature. 90 % H_2 yield was achieved in 5 hours of reaction, while 100 % conversion was achieved in 20-30 hours. It was also seen that increasing the water temperature resulted in faster reaction rates and higher H_2 yields. Zhao *et al* [32] used calcium (Ca) to activate Al in a ball mill. Initially Al-Ca-H_2O reactions resulted in low hydrogen yields (< 40 %). However, addition of NaCl to the Al-Ca alloy during ball milling and it subsequent treatment with water (10 – 80 °C) increased the yield to 100 % in 30 min. It was believed that chloride ions from NaCl cause pitting corrosion of Al, thereby creating numerous reaction sites for H_2O to penetrate the Al surface.

Mechanically milled Al-metal oxide powders were reacted with H_2O by Dupiano *et al* [33]. The metal oxides (Al_2O_3, MgO, CuO, MoO_3, and Bi_2O_3) were each milled with Al powders in a planetary ball mill. Stearic acid or hexane were added as process control agents (to achieve finer particle sizes and prevent agglomeration) during the milling process. The resulting activated Al powders were treated in hot water (80 °C). Only Al-Bi_2O_3 powder had a 100 % hydrogen yield. All other composite powders had hydrogen yields of about 75 – 85 %.

From the literature review above, it is clearly visible that considerable amount of research has been reported on Al-H_2O reactions. Several points need to be noted. Aluminum activation has been the primary focus of research for a better hydrogen yield. Aluminum reactions in alkaline solutions have been reported [26], [28], and [29]. Ball milling of commercially available Al powders with metals [18]-[20], salts [24], [25], [32], and metal oxides [33] has been reported as well. Most of the reviewed papers reported using water at an elevated temperature (70-80 °C), as it is believed to enhance reaction rates. It

is also noticeable that changing the additive content has a remarkable effect on hydrogen yield and reaction rate [16], [24], [25], [31], [33].

The goal of the research, as mentioned earlier, is to utilize Al foil which is widely available as scrap and waste, and produce a fine activated Al powder which can be treated with water to yield hydrogen. Hong *et al* [34], [35] have reported the manufacturing of Al powder from Al foil using both dry and wet ball milling process. The Al foils were milled in an inert atmosphere in case of dry milling and with mineral spirits (isobutyl alcohol, etc.) in case of wet milling. Stearic acid or oleic acid was added in both processes to control the milling behavior and non-leafing of Al particles. The produced powders were used as additives for automotive paints. Aleksandrov *et al* [36] reported the hydrogen yields obtained from the reaction between Al powder (obtained from foil) and dilute NaOH. A similar reaction was reported by Martinez *et al* [37], where Al cans were used as the source material for Al-NaOH reactions. It was noted that the reactions were highly spontaneous producing significant amounts of hydrogen. Chromatographic analysis revealed a high purity of the H_2 gas. The gas was used in a fuel cell to produce electricity.

In the present research, Al foil and NaCl were treated in a planetary ball mill in either air or argon atmosphere for a brief period of time. The resulting activated powder was introduced to warm deionized water (50-80 °C) and the hydrogen yield was recorded via the gas displacement method using an inverted graduated cylinder. In addition, NaCl can be leached out of the Al/NaCl mixture by dissolution in cold water. This is important for onboard power generation systems where the mass of the hydrogen storage unit is a critical characteristic. Also, powders were obtained from Al cans using the same milling procedure. The kinetic curves for both Al foil and Al can powders are presented. The powders are characterized using specific surface area analysis, particle size analysis, SEM, XRD, and EDS.

Another area of research which has received significant focus recently is the combustion of aluminum and water mixtures for the production of hydrogen. The obtained hydrogen could be used in fuel cells for mobile and stationary power generation systems, due to its low environmental impact [38],

[39], [40]. Also, combustion of aluminum with water has been studied for underwater propulsion ([41], [42]) and for hydrogen production for high-speed air breathing propulsion [43].

Ivanov *et al* [44], [45] studied the combustion of stoichiometric mixture of nano-aluminum (120 nm) and gelled-water (3 wt% polyacrylamide) at constant pressure in an argon atmosphere. They observed that at a pressure of 0.1 MPa the combustion front velocity was 2 mm/s. It was also noted that the front velocity increased with increasing pressure (fig. 2.3). Interestingly, for a mixture of 40% Al-60% H_2O, the combustion rates were higher than the ones observed for stoichiometric mixtures.

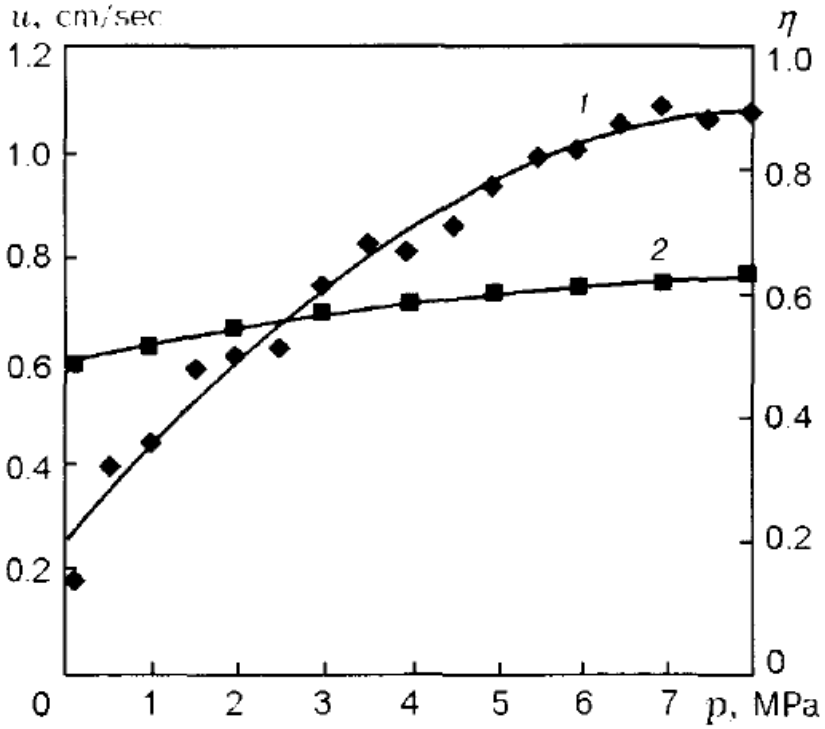

Figure 2.3: Combustion rate (1) in a stoichiometric mixture of aluminum with water versus pressure [45].

Shafirovich *et al* [46], [47] studied the combustion of nano-Al (80nm)/H_2O/$NaBH_4$ mixtures as a method for hydrogen generation. Polyacrylamide was used as a gelling agent for water. The free metallic aluminum in the nano-aluminum powder was found to be 83%. The mixtures were placed in a quartz tube and ignited using nichrome wire. All experiments were conducted at 1 atm pressure in an argon environment. They observed that combustion front velocity depended on the Al content in the

$Al/NaBH_4$ mixture. The front velocity increased by a factor of 2 with Al concentration increasing from 50 to 70 wt%. At the same time a sharp rise in combustion temperature was seen.

Ignition was not achieved when micron-scale Al powders were used in the $Al/H_2O/NaBH_4$ system. This can be explained due to the fact that the ignition temperature of micron-scale Al is 2327 K which is close to the melting point of alumina (Al_2O_3). Also at lower metal content, the combustion efficiency decreased due to the low reaction heat effect. When magnesium (Mg) was substituted with aluminum in the $Al/H_2O/NaBH_4$ mixture, the reaction was favorable due to the lower ignition temperature of Mg. The maximum observed hydrogen yield was 7 wt%. It was concluded from the results that nano-scale Al could be used but they have problems with lower active Al content.

Another exciting compound for hydrogen generation: Ammonia Borane (AB, Molecular formula: NH_3BH_3), was studied by Diwan *et al* [48]. They reported the combustion of mixtures of nano-Al/H_2O with AB as a source of hydrogen for portable fuel cell applications. This system has a theoretical yield of 9.5 wt% H_2 from both AB and water. The experiments yielded 7.7 wt% hydrogen and a combustion front velocity of 3 mm/s. More recently, Risha *et al* [49], [50] reported the dependence of equivalence ratio and particle size on the combustion of nano-Al and water in an argon atmosphere. They studied four nano-Al powders: 38 nm, 50nm, 80 nm, and 130nm with an active Al content of 54.3%, 68%, 74%, and 84% respectively. The burning rates increased with increasing pressure. At a pressure of 0.1MPa the burning rate was 12 mm/s for 38 nm Al powder. Burning rate depended strongly on the equivalence ratio between 0.5 and 1.25. They achieved a maximum burning rate of 8.6 ± 0.4 cm/s at a pressure of 4.3MPa. Also the burning rate increased 2.6 times when Al particle size was reduced from 130 – 50 nm.

When micron-scale (5 μm) Al powders were used, ignition was difficult. They also tested the effect of the addition of polyacrylamide (Poly A) to the nano-Al/H_2O mixture. Specifically, 3 wt% of Poly A was added to water. This turned the water into a gel and later 38 nm Al was mixed into it. The burning rate observed for that mixture was about 7 mm/s. However, it was noted that addition of Poly A did not affect the burning rates. Over a pressure range of 0.1 – 10 MPa, the adiabatic flame temperatures were lower for 38 nm Al than for 80 nm and 130 nm Al powders (see fig. 2.4). This was attributed to the

fact that at higher pressures, the argon gas fills the void in the Al particles and acts as a heat sink. Combustion of 38 nm Al powder achieved 85% maximum theoretical efficiency. Efficiency was lower for larger Al nano particles.

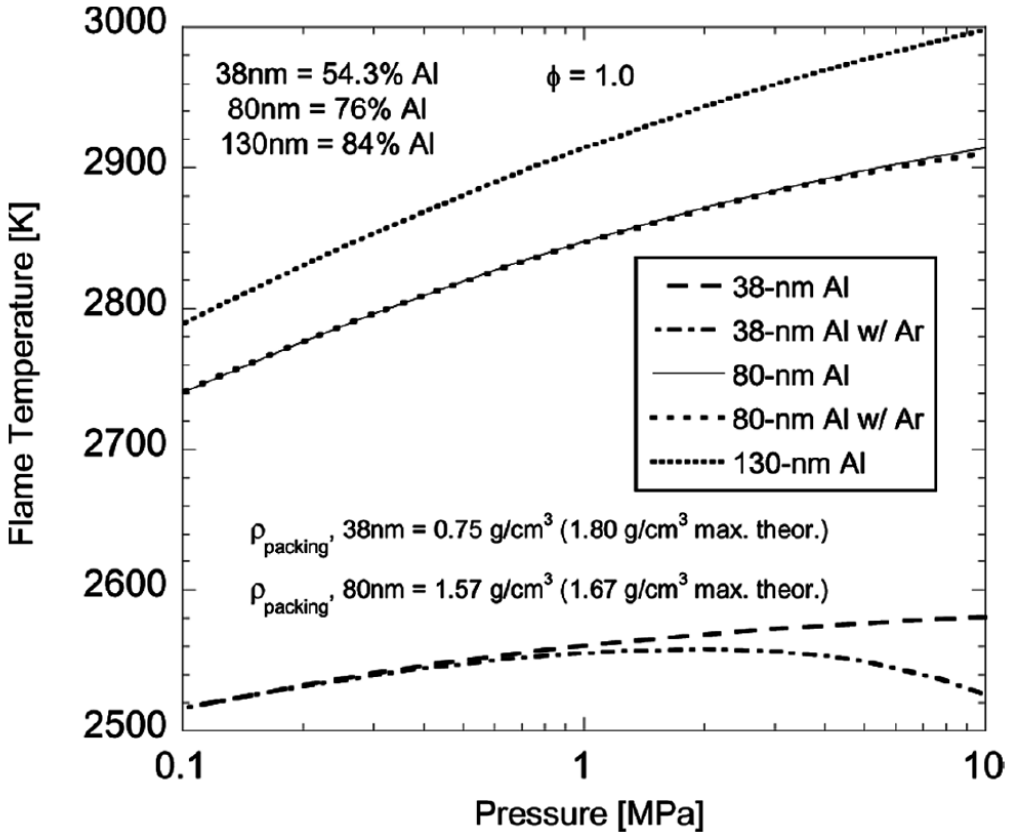

Figure 2.4 Adiabatic flame temperatures of various mixtures of nano-aluminum and water [50].

Ingenito *et al* [43] showed that the addition of hydrogen peroxide (H_2O_2) to nano-Al/H_2O mixtures theoretically increased the chemical heat release and specific impulse (Isp) performance. Sabourin *et al* [51] experimentally studied the nano-Al/H_2O/H_2O_2 mixtures using 38 nm Al particles. It was observed that addition of H_2O_2 significantly increased the flame temperature, mass burning rates, and combustion heat release. The burning rates and flame temperature strongly depended on equivalence ratio (Φ). They observed largest burning rates for Φ slightly greater than 1 with 10% H_2O_2 oxidizer. However, at above 32% H_2O_2, the burning of the reactant mixture was anomalous. This was due to the

Al oxidation by H_2O_2 and formation of product species like O_2, OH, and HO_2, which caused numerous cracks within the reactant system.

To improve the gravimetric yield of hydrogen and to minimize the mass of alumina, Connell *et al* [52] studied the effect of the addition of aluminum hydride (Alane) or micron-scale Al on the combustion of nano-Al and water in an argon atmosphere. Alane is an important compound as it has theoretically 10.1 wt% hydrogen storage capacity. For combustion experiments, 80 nm Al, 20 μm Al, and 20 μm Alane were used with deionized water. An important observation of these experiments was that increasing the additive wt% of Alane increased the specific impulse by 10% and reduced adiabatic flame temperatures by 5%. Also more hydrogen was found in products. The addition of micron-scale Al did not alter the burning rates or the chemical efficiency in the pressure range of 3 – 11 MPa. However, at pressure ranges below 3 MPa, addition of micron-scale Al dramatically reduced the burning rate. This observation is important for low pressure combustion reactions.

A similar system was studied by Sun *et al* [53] where they used polyoxyethylene (PEO) as a gelling agent/additive for the nano-Al/H_2O mixture. At an argon pressure of 0.1MPa, they observed that addition of PEO improved the burning rates and higher concentration of PEO increased the burning rate significantly. They mentioned that without the gelling agent, the nano-Al/H_2O mixture did not ignite. This may be erroneous as the literature review presented above clearly states otherwise. However, they also concurred that replacing a portion of the nano-Al with micron-scale Al reduced the combustion performance. This has been seen by other researchers as well.

An in-situ investigation of nano-Al/H_2O reaction was performed by Wan *et al* [54]. The results concluded that the optimal mole ratio interval of nano-Al and H_2O was between 1:2 and 1:2.2. They also determined that several reactions were performed during the whole process of the nano-Al/H_2O reaction as shown by the equations 4, 5, and 6 below. This research provides important information on the design of nano-Al/H_2O propellant system.

$$Al + H_2O \rightarrow AlO + H_2 \quad (4)$$

$$2\,Al + 4\,H_2O \rightarrow 2\,HAlO_2 + 3\,H_2 \quad (5)$$

$$2\,Al + 3\,H_2O \rightarrow Al_2O_3 + 3\,H_2 \quad (6)$$

Sundaram *et al* [55] studied the addition of micron-scale Al to stoichiometric aluminum-frozen water mixtures (ALICE) in the pressure range of 1 – 10 MPa. It was seen that the burning rate decreased significantly for micron-Al loading above 25 wt% and did not change when the loading was below 25 wt%. Also the flame thickness of the bimodal particle mix (nano-Al + micron-Al) was greater than the mono dispersed Al particles mixture. This indicated that the combustion of ALICE mixtures was dictated by the mass diffusion across the oxide layers of the Al particles.

Sippel *et al* [56] studied the effects of equivalence ratio and aging on the combustion of nano-Al/H_2O mixtures. It was reported that fuel-lean mixtures of nano-Al/H_2O have minimal effect on the burning rate and specific impulse performance. This observation has critical implications as it reduces cost (low nano-Al consumption). The aging experiment on ALICE mixtures showed no degradation after being stored at -30 °C for 200 days. This could be important for storage applications where the mixture could be used on demand without a loss of combustion performance.

Spontaneous ignition of nano-Al (300 nm) and water was studied by Phuoc *et al* [57]. Al concentrations of 17 and 27 wt % were used in the Al-water mixture. 0.1 wt% polyacrylamide was added to gellify the water. The resulting Al-H2O mixture was placed in a vial and heated using a hot plate with magnetic stirrer. It was observed that ignition occurred at temperatures as low as 303 K. This result was important for safety purposes as even a low concentration of nano-aluminum could spontaneously ignite under close to room temperature conditions.

It is obvious from the literature review presented above that the combustion nano-Al and water could be useful for hydrogen generation for propulsion and energy storage applications. It can be understood that nano-aluminum particles combust with water easily and provide faster burning rates and

improve specific impulse performance. Addition of additives like aluminum hydride, hydrogen peroxide does improve the hydrogen generation efficiency. Also, addition of gelling agents like polyacrylamide or polyoxyethylene may increase the combustion front velocities. However, it is also important to note that nano-aluminum particles are plagued with the presence of a thick oxide layer which decreases the gravimetric yield of hydrogen. Substitution of nano-Al with micron-scale powders has a negative effect on the combustion performance and in some cases reduces the ignitability of the Al-water mixtures. At high pressures (> 3 MPa), the combustion characteristics showed significant improvement.

Thus, it would be concluded that aluminum powder with low oxide content and high reactivity are desirable. In this thesis, combustion of activated micron-scale powders with water is investigated at a pressure of 1 atm (0.1 MPa). It was determined that combustion at lower pressures could be of significance where pressurization of the combustion chamber is not available.

2.2 SYNTHESIS OF Ga_2O_3 NANOSTRUCTURES

Quasi one-dimensional nanomaterials are of great interest due to increased focus on their importance in physics research and also their applications in the nanodevices industry. Since the mid 1950's, considerable research has been reported on the synthesis of filamentary crystals from alloys and metals. Since the discovery of carbon nanotubes (CNTs) [58], there has been a tremendous surge in research activities for development and characterization of one-dimensional nanostructures. Most of the research is targeted towards the development of semiconductors such as ZnO [59], Si [60], SnO_2 [61], and GaAs [62].

Several papers reported a vapor-liquid-solid (VLS) mechanism of crystal growth. The VLS mechanism was first reported by Wagner *et al* [63] in 1964. Silicon strands were grown using a small amount of gold as an impurity. Wagner reported that presence of gold is critical to crystal growth and it forms a liquid droplet with the base material when heated to a high temperature. This droplet is a nucleation site for the silicon vapor and strands grow by precipitation of the silicon from the droplet. This mechanism is shown in figure 2.3.

Zhang and Jiang [64] incorporated the VLS mechanism for catalytically growing Ga_2O_3 nanowires by physical evaporation. Indium was used as a catalyst in the form of a thin layer on an

alumina (Al_2O_3) substrate. Gallium (Ga) powder was placed on the substrate, inserted into a horizontal tube furnace (HTF), and heated to 960 °C for one hour under the flow of argon and oxygen (Ar/O_2 = 4:1). The products examined revealed nanowires with a mean diameter of 50 nm and a nanoparticle tip at the end of the wires, indicating growth by VLS.

For industrial purposes, Ga_2O_3 thin films of precise thickness and uniformity are desirable. Plasma-enhanced atomic layer deposition (PEALD) process was used by Shan *et al* [8] to develop Ga_2O_3 thin films. Oxygen gas was used as the plasma and $[(CH_3)_2GaNH_2]_3$ as the source. The chamber was maintained under vacuum. The thin films were deposited on Si and sapphire substrates and annealed in a rapid thermal cycling system at different temperatures. An important result from the XRD analysis of the annealed thin films revealed that with increasing temperature, the Ga_2O_3 thin film reached the desired β phase crystal structure.

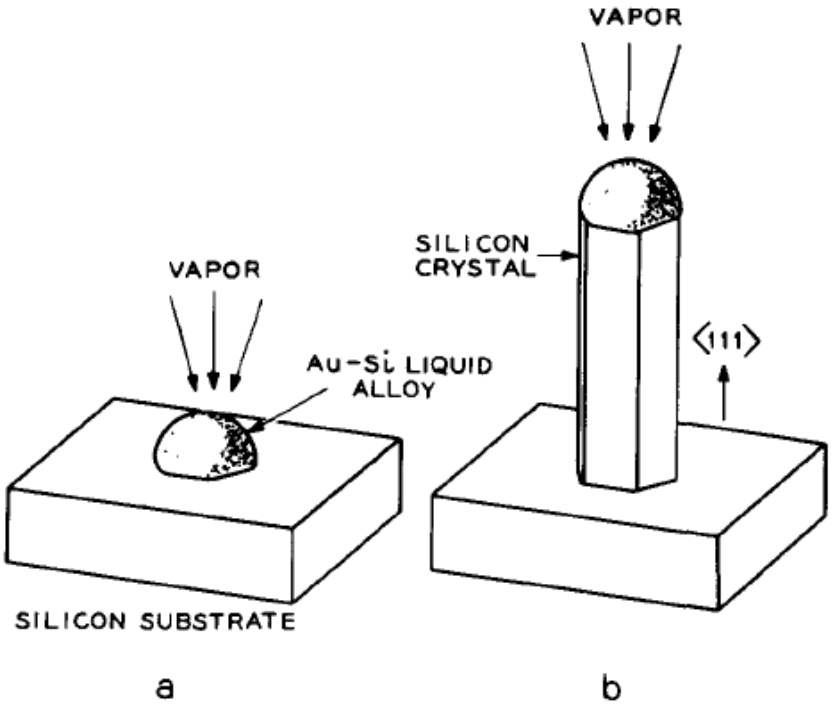

Figure 2.3: Growth of a silicon crystal by VLS: a) Liquid droplet on a substrate and b) Growing crystal with liquid droplet [63].

Zhang *et al* [65] reported the growth of Ga_2O_3 nanowires by evaporation of gallium powder with no catalyst. A Ga powder containing quartz combustion boat was placed in a high temperature furnace (HTF) and heated to 300 °C for about 24 hours. Before the combustion, the furnace was evacuated and pressure was kept at 0.3 atm. A mixture of argon (90%) and hydrogen gas (10%) was introduced into the furnace. After cooling, wool-like products, white in color, were found on the inner wall of quartz boat. Microphotographs from the scanning electron microscope (SEM) show Ga_2O_3 nanowires with an average of 60 nm diameter and up to 2 μm in length. X-ray diffraction (XRD) studies revealed that the nanowires were β-Ga_2O_3. However, Zhang *et al.* noted that the nanowires were not formed by the VLS mechanism. Instead, they found twin boundaries in the microstructures of the nanowires which implied that vapor-solid (VS) phase caused the growth.

Ogita *et al* [66] used an RF magnetron sputtering technique to develop Ga_2O_3 thin films for use as high-temperature gas sensors. They were able to obtain a 1 μm thick film in 2 hours using argon gas. Ar/O_2 gas ratio and sputtering pressure were varied to determine how it affected the formation of the thin films. It was found that 1:1 argon to oxygen gas ratio was too much for sputtering. The reason for this is that, for an ideal temperature sensor, the more the oxygen vacancies in the thin film, the better the gas sensing properties. At Ar/O_2 ratio of 10:1, the best crystallization was achieved.

In 2002, Lee *et* al [67] used ball-milled GaN powders to synthesize β-Ga_2O_3 nanowires. They used a SPEX mill to obtain finer and amorphous GaN powders. The powders were placed in a HTF at 930 °C for 15 hours under a nitrogen (ultra-high purity) flow. After cooling, wool-like products were formed on the inner wall of the alumina combustion boat. XRD analysis of the products confirmed Ga_2O_3 nanobelts. SEM microphotograph of the nanobelts can be seen in figure 2.4. This was also seen in the case of Zhang *et al* [65]. It was also seen that in an oxygen atmosphere, nanoparticles were formed instead of nanobelts. This further supports the hypothesis made by Ogita *et al* [66] that excessive oxygen inhibits the formation of nanobelts and other one-dimensional structures.

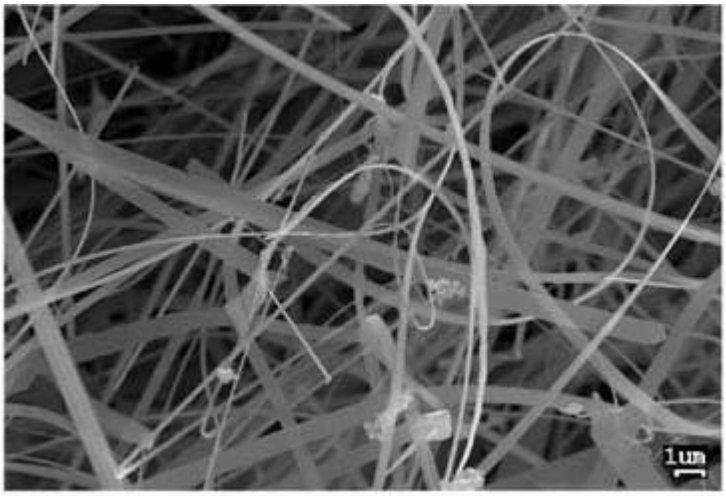

Figure 2.4: SEM image of ball-milled GaN powder annealed at 930 °C [67].

A similar method of ball milling and annealing was used by Glushenkov and Chen [68] for the synthesis of zinc oxide (ZnO) nanowires. Zinc powder was milled with 6 atomic percent (at%) germanium (Ge) in a ball mill for 100 h in an oxygen atmosphere. The milled powder was placed in a tube furnace and annealed at different temperatures in an argon atmosphere. Nanowires were found when the sample was heated to 1300 °C. No nanowires were seen when the annealing temperature was below 1000 °C suggesting that a higher temperature is indeed needed for successful crystallization of one-dimensional nanostructures.

Xiao *et al* [69] reported the ball milling of GaN powders with H_2O for 4 hours. After drying, the sample was placed in a HTF and annealed at 550 °C and 900 °C under a nitrogen atmosphere for 35 min. XRD analysis showed that powders annealed at 550 °C had peaks of α-Ga_2O_3, but at 900 °C β-Ga_2O_3 was synthesized. Thus, temperature again plays an important role in phase transition from α to β. These results again confirm the findings reported in [8] and [63].

To observe the effect of compaction on GaN powders for β-Ga_2O_3 synthesis, Jung *et al* [70] made a GaN pellet and placed it in an alumina tube furnace. The sample was heated to 1100 °C under a nitrogen (ultra-high purity) flow. After cooling, the products were examined by SEM. Nanowires and hillocks were observed. XRD analysis revealed the presence of β-Ga_2O_3 and unreacted GaN. The author also suggested a vapor-solid (VS) mechanism [65] through which the structures might have been grown.

Wang *et al* [71] found zigzag-shaped nanostructures of β-Ga_2O_3 after using NaN_3 and $GaCl_3$ as the starting materials. The detailed sample preparation process can be viewed in the aforementioned paper. An interesting point noted in the paper is the chemical reaction mechanism as shown by equations 7 and 8

$$GaCl_3 + NaN_3 \rightarrow GaN + 3\,NaCl + N_2 \tag{7}$$

$$2\,GaN + \left(\frac{3}{2} + x\right) O_2(g) \rightarrow\ Ga_2O_3 + 2\,NO_x \tag{8}$$

It is suggested that GaN vapors formed during the annealing process react with the residual oxygen in the nitrogen flow to form Ga_2O_3. The same mechanism was reported in [67] and [70].

In 2008, Cao *et al* [72] used pure Ga_2O_3 powder to develop nano/microbelts. The sample was placed in the center of a HTF and heated to 1150 °C under an argon (purity >99.9%) flow for 90 min. A Si substrate was placed downstream in the tube where the temperature was 600 °C. Analysis of the substrate using SEM and XRD revealed nanobelts of β-Ga_2O_3. Solid spherical droplets were observed at the end of the nanobelts, revealing a VLS growth mechanism, also reported in [63] and [64].

From the literature review presented above, it can be inferred that there are several factors that contribute to the synthesis of β-Ga_2O_3 nanostructures. A tube furnace was primarily used as the reaction chamber in most of the papers reviewed. Ultra-high purity gases were used as the atmospheres in the tube furnaces. The oxygen content in the gases played an important role in the final product structure. Also, the annealing temperature changed the final phase (α or β) of the Ga_2O_3 nanostructures. Ga, GaN, or Ga_2O_3 powders were used as the starting materials. Presence of a catalyst made little to no difference in the synthesis of nanowires. Ball milling process did produce finer and amorphous powders, which affected the growth mechanism of the nanowires/belts/hillocks.

For the present research, all the factors mentioned above were taken into account for the synthesis of β-Ga_2O_3 nanostructures. High energy ball milling was used to produce fine powders of GaN, which was used as the starting material for the fabrication of nanowires/sheets/belts.

Chapter 3: Experimental Setups and Procedures

Section 3.1 and 3.2 describe, in detail, the apparatus used to conduct the experiments. The materials characterization techniques are described in section 3.3.

3.1 Hydrogen Generation

Several experimental systems described in the literature usually consist of a reaction flask for Al reactions with alkaline solvents or H_2O. In the case of strong corrosive solvents like NaOH, reaction of Al occurs vigorously without any supply of heat. However, it was seen from previous studies that activated Al reacts well with hot water when no other solvents or dopants are used. It was also noted that resulting H_2 generated from the Al corrosion reactions was measured using a flowmeter or the inverted cylinder gas displacement method.

The apparatus described here combines the techniques drawn from the literature review. A simple experimental setup was designed to perform the Al-H_2O reactions and monitor the H_2 generation.

3.1.1 Sample Preparation

Aluminum foils (ultra-pure, thicknesses 15 μm, 23 μm, and 36 μm, VWR) and sodium chloride powder (>99.0% purity, Sigma-Aldrich) were used as starting materials. The aluminum foils were cut into square (10 mm x 10 mm) pieces (See figure 3.1). The sodium chloride was milled in a planetary ball mill (Fritsch Pulverisette 7 Premium Line) as shown in figure 3.2 (a). The ball mill has a maximum speed of 1100 rpm and a revolutionary acceleration of 95 times the force of gravity. The comminution takes place primarily through the high-energy impact of grinding balls. The grinding bowl, containing the material to be ground and the grinding balls, rotates around its own axis on a main disk rotating in the opposite direction, hence the name “planetary.” The huge centrifugal force causes the sample material and grinding balls to bounce off the inner wall of the grinding bowl, cross the bowl diagonally at an extremely high speed, and impact on the material to be ground on the opposite wall of the bowl. This mechanism allows us to achieve material fineness down into the nano range.

Milling was conducted in either air or argon atmosphere using 80-ml zirconia grinding bowls with zirconia grinding balls (diameter of 10 mm, total mass of 44.7 g, see figure 3.2 (b)). The milling time was 10 min and the rotation speed was 850 rpm. The Al foil pieces and the milled NaCl powder

were treated simultaneously in the planetary ball mill in air atmosphere. Specifically, in each milling process, 2 g of Al foil pieces and 2 g of the milled NaCl were treated, so that the mass ratio of the obtained Al/NaCl mixture was 1:1. The milling process involved several cycles. The first cycle employed 10-mm grinding balls (ZrO_2, 44.7 g) at 850 rpm for 10 min followed by a cooling pause of 45 min. The sample mixture retrieved from the first cycle was used as the starting material for the second cycle where 5-mm grinding balls (ZrO_2, 44.5 g) at 1000 rpm for 10 min were used to achieve a finer particle size. After a 60-min cooling pause, 2-mm grinding balls (ZrO_2, 44.5 g) at 1100 rpm for 5 min were used to further reduce the particle size. The last cycle was repeated after a 60-min cooling pause. Thus, the total milling time was 30 min. After milling and cooling, to break particle conglomerates, the powder was briefly (< 1 min) treated using a mortar and a pestle (both made of agate).

Figure 3.1: Aluminum foil (15 μm) cut into square pieces (10 mm x 10 mm).

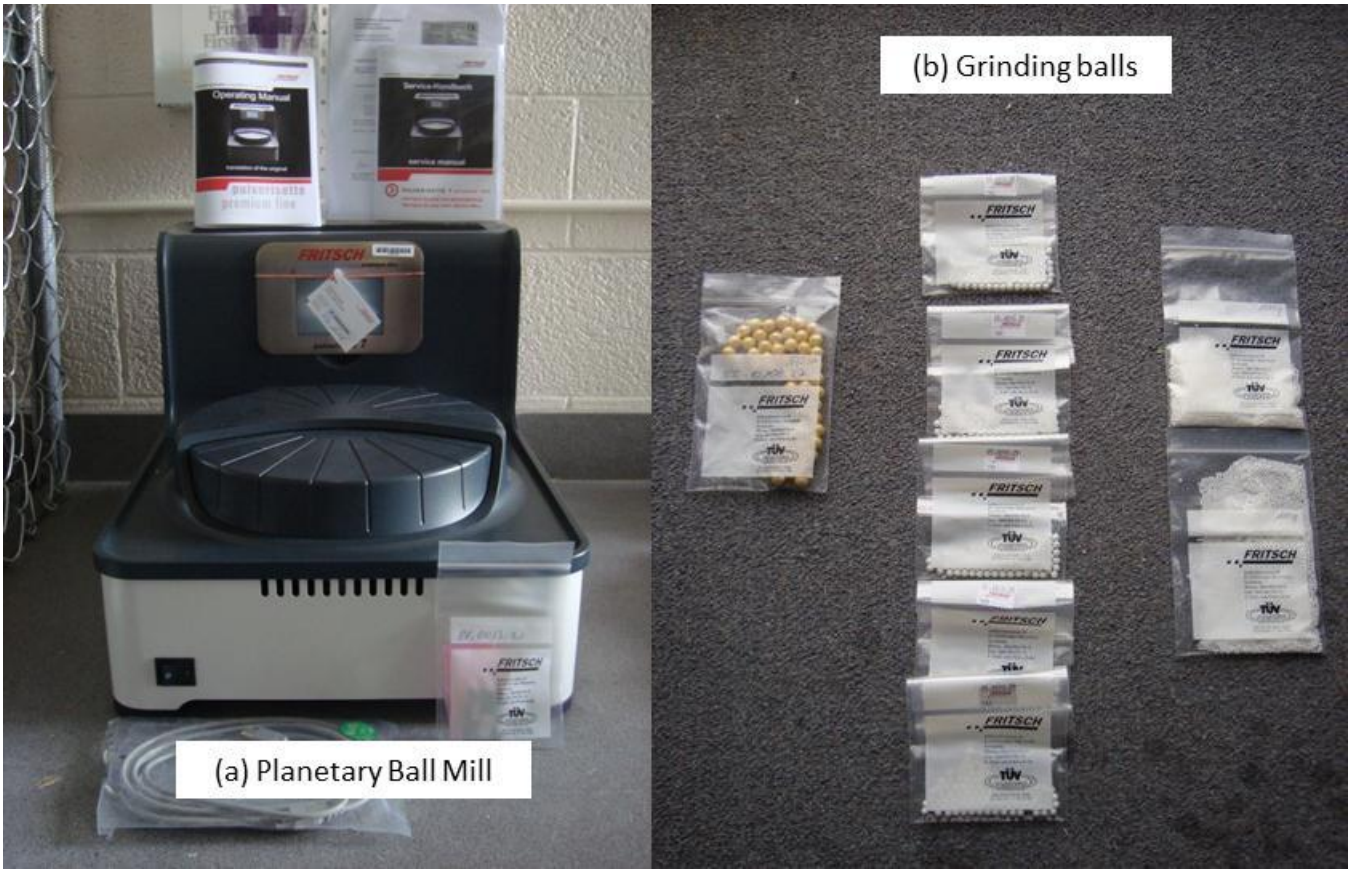

Figure 3.2: (a) Fritsch Pulverisette 7 Premium Line planetary ball mill and (b) zirconium oxide grinding media.

To determine the feasibility of using activated powders from Al soda cans, the top and bottom ends of a Pepsi can were cut off and the rest of the can was cut into four pieces as shown in figure 3.3 (a). To remove the paint and protective film on the cans, the pieces were immersed in concentrated sulfuric acid (H_2SO_4, ACS grade, 95 % w/w, Labchem Inc.) for 30 min. The pieces were removed from the acid and washed under cold tap water. The clean can pieces are shown in figure 3.3 (b). The can pieces were subjected to the same milling procedure in air atmosphere as described above for Al foil. Additionally, to see the effect of longer milling time on the reactivity of the Al powders, the can pieces were milled for 60 min instead of the previous 30 min used for Al foil. Specifically, the Al can pieces and NaCl were treated in the planetary ball mill in an air atmosphere. 2g of Al can and 2g of NaCl were milled for 15 min at 850 rpm using 10-mm zirconia grinding balls. After a 60 min cooling pause, the obtained powder was further milled for 15 min at 1000 rpm using 5-mm zirconia grinding balls. Finally,

after another 60 min cooling pause, a further milling of 30 min was carried out in 6 cycles (5 min/cycle) using 2-mm zirconia grinding balls.

For the experiments with leached out NaCl, the powders obtained by milling of Al foil with NaCl were washed in cold (< 10 °C) deionized water. The washing time was varied from 2 min to 60 min. After passing the solution through a filter paper, the resulting Al powder was left overnight to dry.

To investigate a potential effect of washing in water on the Al surface, the powders obtained by milling were washed in methanol (ACS grade, LabChem), which does not oxidize Al. The washing in methanol was followed by the same filtration and drying procedure as after washing in water.

Figure 3.3: (a) Pepsi can pieces (b) Can pieces after removal of paint and film.

3.1.2 Overview of Experimental Apparatus

Figure 3.4 shows the layout of primary components used for experimentation. A reaction flask (1000 ml, Pyrex) was placed on a digital hot plate stirrer (Scilogex, MS7- H550 Pro). The flask was sealed using a rubber stopper and vacuum grease. Two holes were made in the stopper; one for a thermocouple (Scilogex PT 1000 sensor), to measure the temperature of the water during the reaction, and the other for gas tubing (silicon, 5 mm I.D). The gas tubing was inserted into an inverted graduated cylinder (1000 ml, Pyrex, 10 ml graduations) full of tap water. The inverted graduated cylinder is immersed into a beaker (500 ml, polypropylene), which is about half full of water. As the hydrogen is generated in the reaction flask, it flows through the gas tubing and into the inverted graduated cylinder.

The gas bubbles displace the water in the graduated cylinder and H_2 yield is measured by reading the water level. The inverted cylinder is held by a support stand and support clamps as shown in the figure. All of the above mentioned apparatus is enclosed in a Plexiglass box (2 ft. x 3 ft.) with an exhaust opening in the top plate for safer venting of the evolved H_2 gas. Atmospheric pressure and temperature in the room was measured using a barometer (Cole-Parmer barometer with digital thermometer).

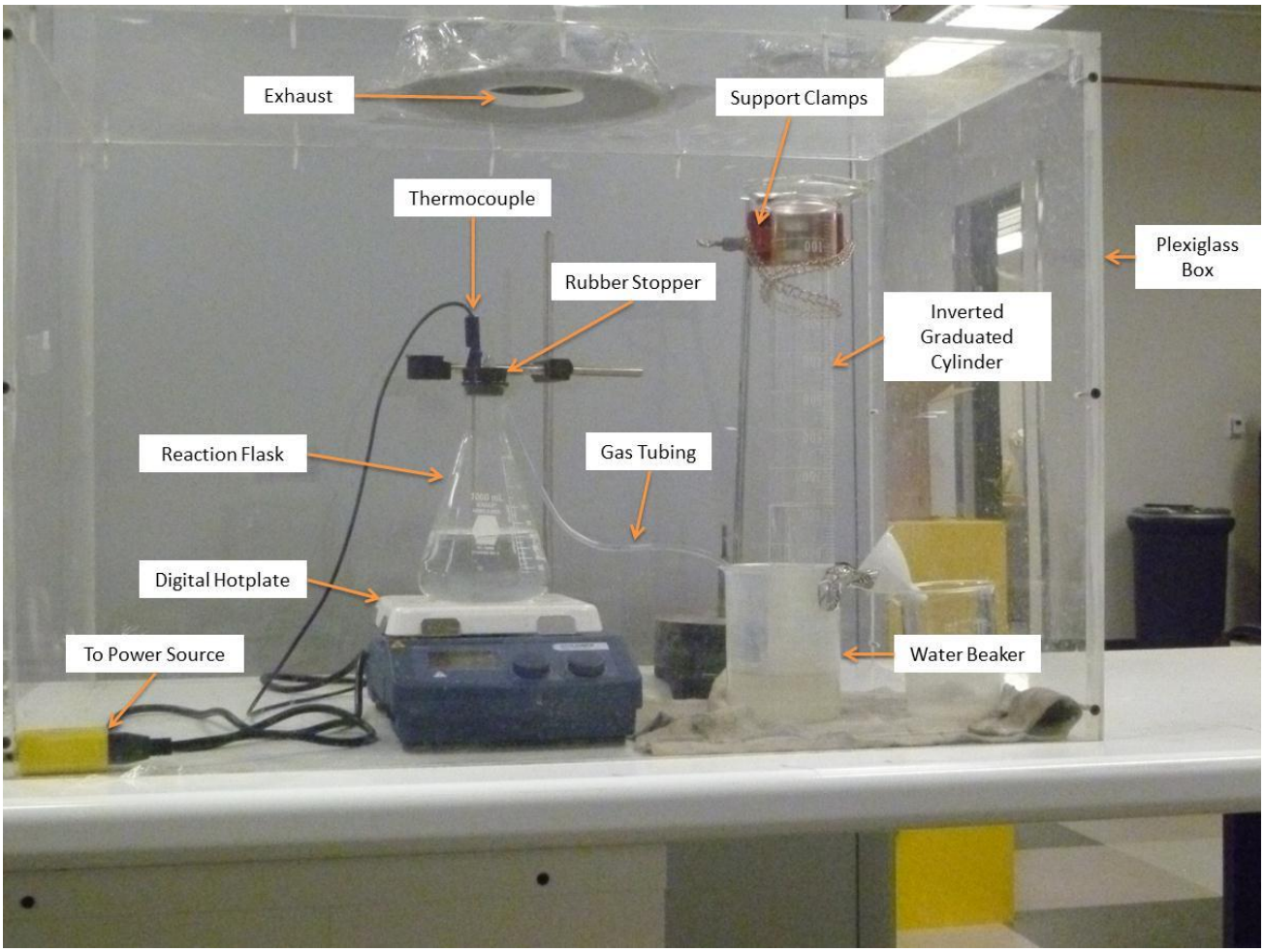

Figure 3.4: Experimental apparatus for H_2 generation.

3.1.3 Experimental Procedure – Reactions of the Activated Al powders with warm water

To observe the reaction with hot water, 0.7-g samples of the obtained powders (Al foil or Al cans) were submerged in 0.75 L of deionized water (i.e., the water/sample mass ratio was about 1070) and heated to 50°C, 65°C, or 80°C using the hot plate. During the process, the temperature of water increased by 2-2.5°C due to the exothermic reaction of Al with water and returned to the initial value

after the completion of the reaction. The amount of released gas was monitored for 90 min to 2 h using water displacement in an inverted graduated cylinder. Specifically, the water level in the inverted cylinder was recorded every minute until most hydrogen was released. Based on the measured volume of gas in the inverted cylinder, the number of moles of the released hydrogen was calculated using the ideal gas equation and assuming that the released gas is pure hydrogen and the gas temperature is equal to the water temperature in the inverted cylinder.

Solid products of the reaction were separated from the solution by filtering and, after drying, analyzed using X-ray diffraction analysis (Bruker D8 Discover XRD).

3.1.4 Experimental Procedure – Combustion of the Activated Al Powder with Water

The combustion experiments were conducted with Al powders obtained by milling Al foil (thickness: 23 μm) in argon and leached by cold water. Before mixing with aluminum powder, water was gelified by adding 3 wt% polyacrylamide (nonionic water-soluble polymer, MW 5×10^6, Sigma Aldrich), which is required for preventing sedimentation of micron-sized Al particles. The Al-H_2O mass ratio was varied from 3:7 to 9:1, which corresponds to the range of Al concentrations from 30 wt% to 90 wt% (this is the concentration of Al in the Al/H_2O mixture, not in the actual triple Al/H_2O/polyacrylamide mixture). Note that the combustion reaction is described by the equation:

$$2\,Al + 3\,H_2O \rightarrow Al_2O_3 + 3\,H_2 \tag{9}$$

which corresponds to Al-H_2O mass ratio of 1:1 (Al concentration of 50 wt%).

The mixture was placed in a thin-wall plastic tube (O.D. 7.62 mm, length 50 mm), which was then installed inside a steel chamber (diameter: 30 cm, height: 40 cm), equipped with glass windows, a pressure gage, and feedthroughs for the ignition system and thermocouple measurements (fig. 3.5). The chamber was repeatedly (3 to 5 times) evacuated and filled with ultra-high purity argon (99.999%) to establish an argon pressure of 1 atm. During the evacuation, pressure in the chamber remained higher than the saturation pressure of water at room temperature, so that the loss of water from the sample was negligible. The mixture was ignited using a Nichrome wire heated by a DC power supply (Mastech

HY3020E). Once the mixture ignited, the power supply was turned off. The combustion process was monitored using a high-resolution video camera (Sony XCD-SX90CR). Temperature inside the Al/water mixture during combustion was measured using a type C (W/Re5%–W/Re26%, wire diameter: 0.25 mm) thermocouple. Elemental composition of the reaction products was analyzed using XRD and EDS.

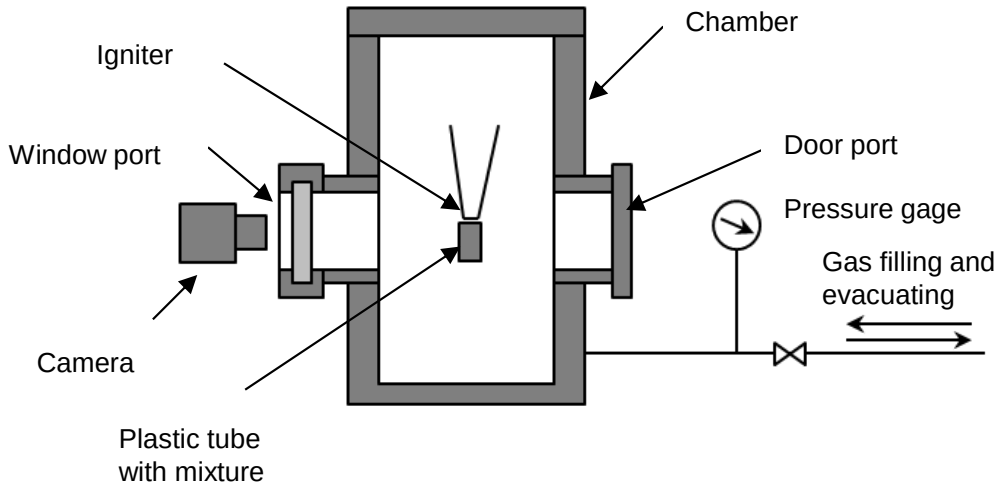

Figure 3.5: Schematic of the combustion chamber.

3.2 GALLIUM OXIDE SYNTHESIS

3.2.1 Sample Preparation

Lee *et al* [45] proposed ball milling of GaN powders to reduce particle size. The milling was performed in an air atmosphere for very long periods of time (as much as 40 h). The XRD peaks did show that after 10 h of milling all GaN peaks were lost and the powders became amorphous. For the present research, the GaN powders (> 99.9 % purity, Alfa Aesar) were milled in the planetary ball mill. Since the milling data for the ball milling of GaN powders are not very well established, it was decided to change several milling parameters till the XRD peaks showed a considerable reduction in particle size. Specifically, the milling time, the mass of sample, the diameter of grinding balls, and the total mass of grinding balls were varied as shown in table 3.1.

All milling procedures were conducted in an air atmosphere in 20-ml zirconia grinding bowls with zirconia grinding balls. It can be seen from the table that the mass ratio of sample/grinding balls is

maintained at approximately 1:15. After milling and cooling, it was noticed that the sample adhered to the walls of the grinding bowl. Hence, the sample was treated using a mortar and a pestle (both made from agate) briefly (5 min), to break down the agglomerates. The obtained powders were analyzed using XRD. The XRD peaks for all powders were superimposed to see the effect of milling.

Table 3.1 Different milling parameters for ball milling GaN

Date	Mass of GaN (g)	Mass of Grinding Balls (g)	Dia. Of Grinding Balls (mm)	Milling Time per Cycle (min)	Total Milling Time (min)	Speed (rpm)	Cooling Pause (min)
03/03/2012	1	12	1	3	12	1100	60
04/06/2012	1	20	1	5	70	1100	70
04/10/2012	1	15	0.5	5	35	1100	70
04/13/2012	2	30	0.5	5	70	1100	70

3.2.2 Overview of Experimental Apparatus

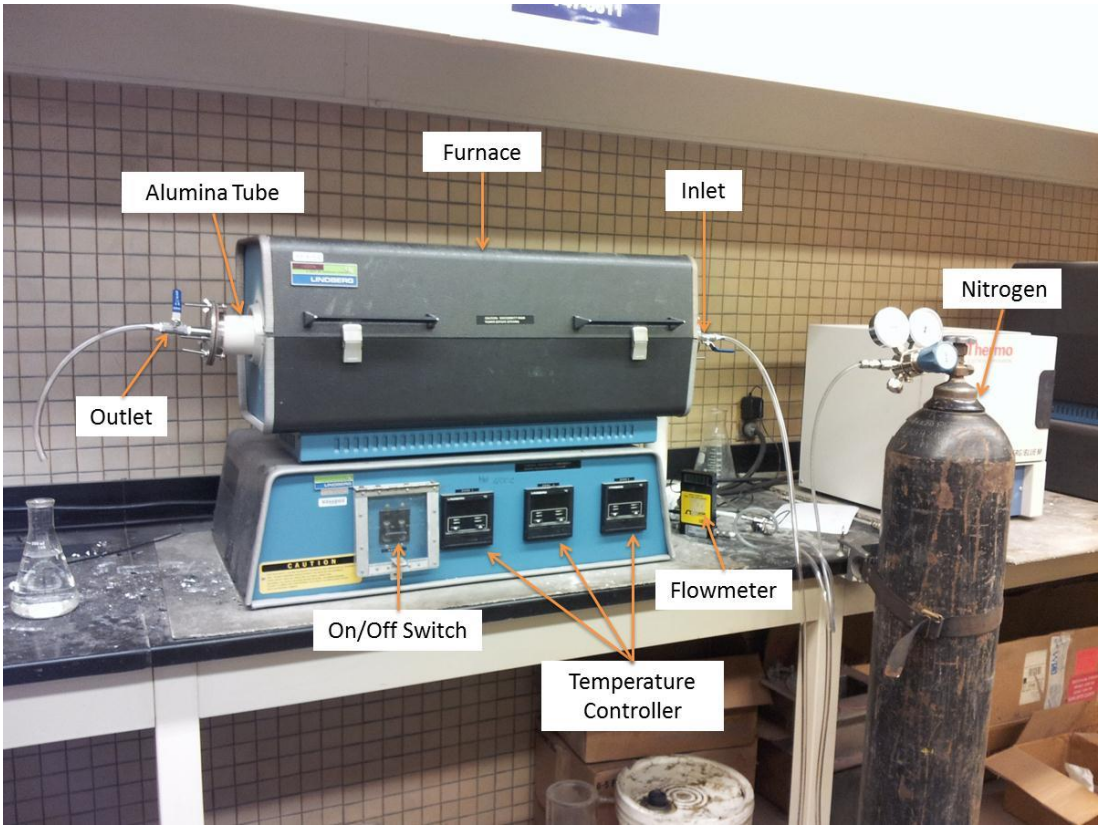

Figure 3.6: Experimental setup for GaN combustion

Figure 3.6 shows the experimental setup for combustion of ball milled GaN powders. An alumina tube (3 in. dia., 3 ft. long) was placed inside a horizontal tube furnace (Lindberg Blue M, three zones, max. temp. 1200 °C). To maintain a nitrogen atmosphere inside the tube, a nitrogen tank (ultra-high purity (UHP), Airgas, Size 200, CGA 580) was connected to the inlet. To monitor a constant flow rate, a digital flowmeter (2 L/min, Omega Engineering Inc.) was connected in between the nitrogen tank and inlet of the alumina tube. Both the inlet and outlet of the alumina tube were fitted with circular steel plates (5 in. dia.) which had a half inch hole in them for the flow of gases. The circular plates also have a ball valve attached to them to start/stop the flow. To prevent any gas leaks, vacuum grease was applied at the area of contact between the circular plates and the tube. To ensure gas flow through the alumina tube, a plastic tube (8 mm dia.) was connected to the outlet and immersed into a beaker full of water. Bubbling in water confirmed gas flow. The temperature of the furnace was set using the three temperature controllers available on the control module. This is useful in creating different temperature zones inside the tube.

3.2.3 Experimental Procedure

Case 1: 0.5 g of planetary ball milled (PBM) GaN powder is placed in an alumina crucible (1 in. dia., 1 in. height). The GaN-containing alumina crucible is loaded into the center of the horizontal tube furnace. The room temperature and pressure are recorded using a digital barometer (Cole-Parmer). To replace the air inside the tube, high-purity nitrogen is passed through the tube at the rate of 3 L/min for 15 min. After that the flow rate is reduced to 0.35 L/min (350 sccm). The regulator pressure is set to 60 psi. The furnace temperature is set to 930 °C and the annealing is carried out for 12 h. After 12 h, the furnace is turned off and cooled in a N_2 atmosphere until the sample reaches room temperature. After cooling the sample is retrieved and the obtained products are analyzed using SEM and XRD.

Case 2: The procedure is similar to case 1 except that helium gas (high purity (HP)) is used instead of UHP nitrogen and the furnace temperature is raised to 1000 °C.

Case 3: Similar to case 1 except: a pellet (4.5 mm height, 12.5 mm dia.) is made out 1.5 g of the PBM GaN powder and loaded into the tube furnace. The pellet is prepared by using a hydraulic press (Carver, Model 3851) by applying a load of 2 tons.

Case 4: Similar to case 1 except: pellet is made of 0.6 g of PBM GaN powder by applying a load of 3 tons. The pellet is loaded into the tube furnace. Furnace temperature is set to 1050 °C.

Case 5: Similar to case 1 except: the furnace temperature is raised to 1100 °C. The furnace is ran for 6.5 h and cooled in an N_2 atmosphere for 7 h. After 7 h, the N_2 flow is shut off and the furnace is cooled to room temperature.

Case 6: Similar to case 1 except: 0.2 g of the PBM GaN powder is placed into the tube furnace. Furnace temperature is set to 1100 °C and allowed to run for 15 h. After 15 h, the inlet end plate is removed and the tube is allowed to cool in air.

3.3 CHARACTERIZATION TECHNIQUES

To understand the reaction mechanisms and improve the reactivity/combustibility characteristics, it is important to characterize the ball milled Al and GaN powders and the reaction products,. The following section describes briefly the working principles of the instruments used to characterize the obtained powders.

3.3.1 Surface Area Analysis

Figure 3.7 shows the Brunauer-Emmett-Teller (BET) surface area analyzer (Microtrac SAA). The SAA consists of three main components: a measuring module, a sample pretreatment module, and a computer. The SAA makes use of two gases: helium and nitrogen (both UHP). It also had liquid nitrogen (LN2) Dewar cups for immersing the sample cells during the measurement process. To eliminate any moisture or contaminants that can result in erroneous surface area results, the sample is placed in a pretreatment module. This module can simultaneously perform three functions, i.e., vacuum, heat, and helium sweep. Heating the sample removes any moisture present in it. Vacuum removes contaminants and a flow of helium further removes any moisture that is left in the sample.

The technique is based on the adsorption of a flowing gas by the tested powder. At room temperature nitrogen will flow over the surface but when the sample is subjected to LN_2 temperature (-196 °C) molecules of nitrogen will adsorb or condense on the surface of the particles. Knowing the size of the nitrogen molecule and the number adsorbed to the surface allows calculation of surface area of the powder present. Measurement of the amount of nitrogen adsorbed is determined by allowing the

condensed nitrogen on the particles to evaporate from the surface by returning the sample to room temperature whereupon nitrogen is desorbed. The specific surface area (S_g) of a substance can be calculated using equation (10):

$$S_g = \frac{V_m \times N \times \sigma}{22410 \times W} \quad (10)$$

where:

V_m: is the monolayer capacity or the amount of nitrogen gas adsorbed, in mL;

N is Avogadro's number (6.024×10^{23});

σ is the cross-sectional area of a nitrogen molecule (0.162 nm^2);

W is the sample mass, in mg;

22410 is the volume, in mL, of 1 mole of an ideal gas at standard temperature and pressure

By knowing V_m and W, the specific surface area can be determined and presented as m^2/g. The SAA has a measurement range from 0.01 to 2000 m^2/g.

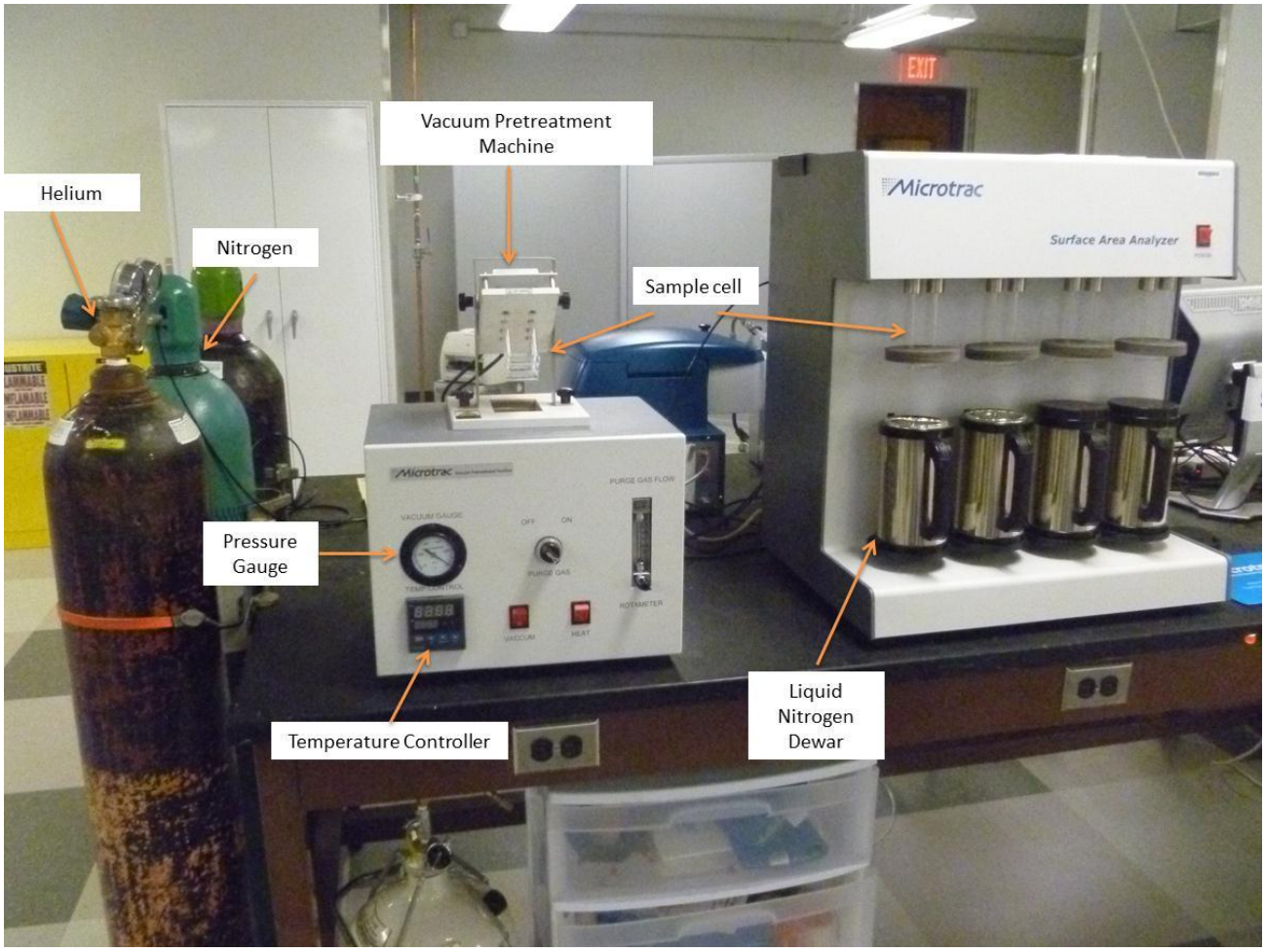

Figure 3.7: Microtrac BET Specific Surface Area Analyzer

3.3.2 Particle Size Analysis

Figure 3.8 shows the particle size analyzer (Microtrac Bluewave S3500) with two main components: a sample delivery controller (SDC) and a laser module. The SDC supports the Microtrac particle size analyzer by managing all sample delivery functions. Its capabilities depend on the options ordered. In wet operation it automates fill, circulate, rinse, de-aerate, dilute and ultrasonic dispersion. In dry operation the SDC acts as a communication interface and controller for optional Turbotrac dry delivery equipment.

The particle size analysis occurs through laser diffraction. The laser module houses three lasers (two red and one blue). The tri-laser system utilizes precise angular measurement of scattered light through a full 180 degree angular range. It utilizes full Mie compensation for spherical particles. It also

applies appropriately modified Mie calculations for non-spherical particles. The device measures the particle size over a range of 0.01 µm to 2000 µm.

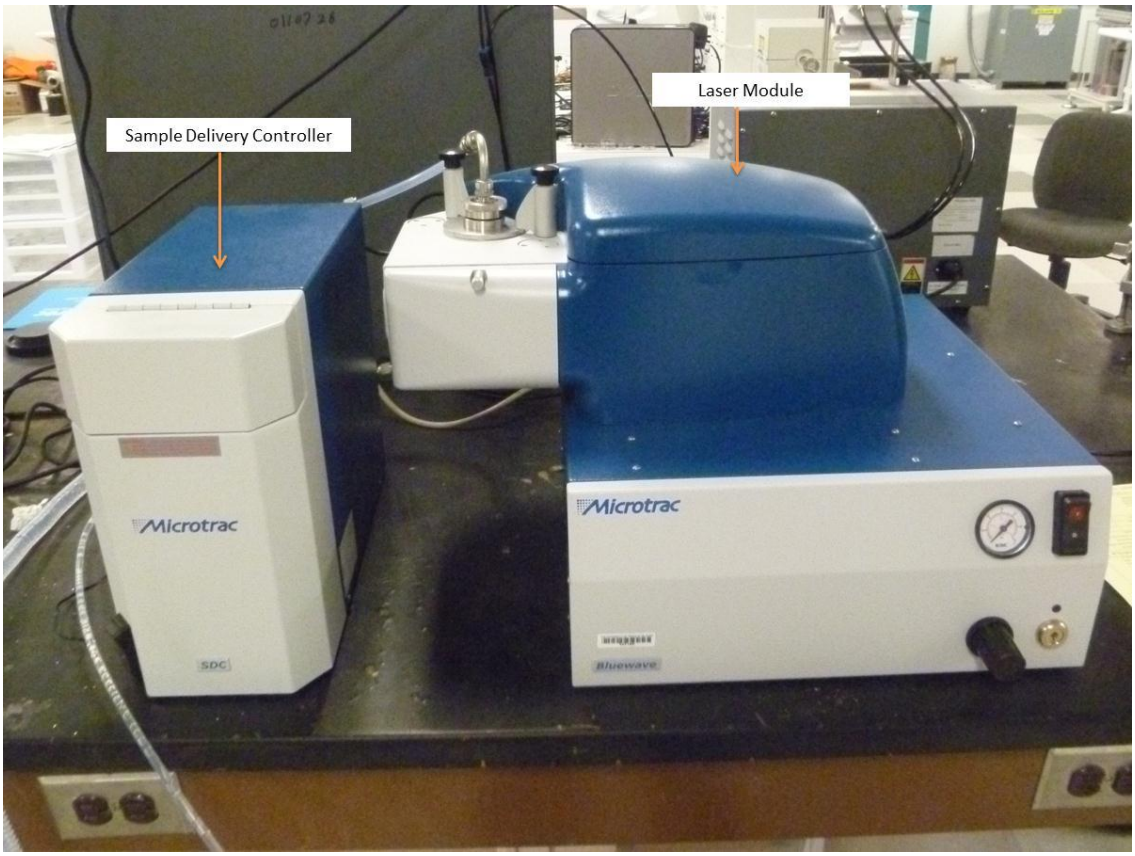

Figure 3.8: Microtrac Bluewave S3500 Particle Size Analyzer

3.3.3 Scanning Electron Microscopy

Figure 3.9 shows a scanning electron microscope (SEM, Hitachi S-4800). The device consists of four components: an electron gun, sample module, LN2 Dewar for EDAX operation, and a computer control. The sample is placed inside the chamber using a sample holder. The electron gun generates an intense beam of high-energy electrons which carry significant amounts of kinetic energy. When the beam hits the sample surface, a variety of signals are produced. These signals include secondary electrons, backscattered electrons, diffracted backscattered electrons, photons, visible light, and heat. Secondary and backscattered electrons are used for imaging.

The SEM also has an option for performing energy-dispersive X-ray spectroscopy (EDS) for elemental analysis or chemical characterization of a sample. It works on the principle of interaction

between an X-ray excitation and a sample. The EDS systems consists of three components: an X-ray detector which detects and converts X-ray into electronic signals, a pulse processor which measures the electronic signals to determine the energy of each X-ray detected, and a multiple channel analyzer which displays and interprets the X-ray data.

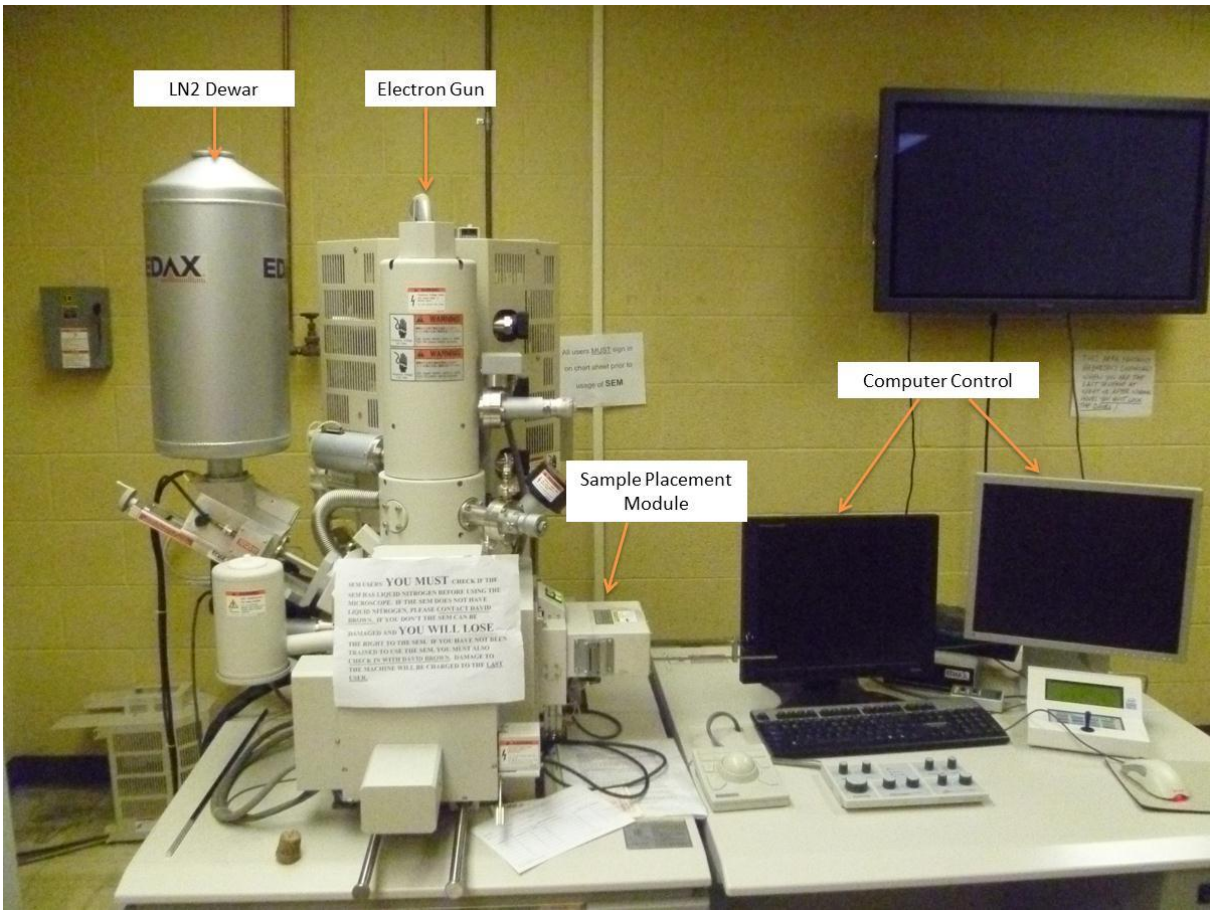

Figure 3.9: Hitachi S-4800 Scanning Electron Microscope

3.3.4 X-Ray Diffraction Analysis

Figure 3.10 shows an X-ray diffraction device (XRD, Bruker D8 Discover). It consists of a sample mount, an X-ray beam generator, a detector, and a camera. XRD is a nondestructive technique used to identify crystalline phases and orientation, determine structural properties like lattice parameters, strain, grain size, thickness of thin films and multi-layers, and determine atomic arrangement. The working principle of XRD is based on Bragg's law. The Bragg's law is given by equation (11) and is shown in illustration 3.1.

$$n\,\lambda = 2\,d\,Sin\,\theta \qquad (11)$$

where:

n is the order of diffraction

λ is the wavelength of incident radiation (nm)

d is the lattice spacing (nm)

θ is the diffraction angle (deg.)

Diffraction occurs when Bragg's law is satisfied for constructive interference (from two X-rays) from planes with spacing d. The present device uses a fixed Cu kα radiation with a wavelength of 1.54 Å.

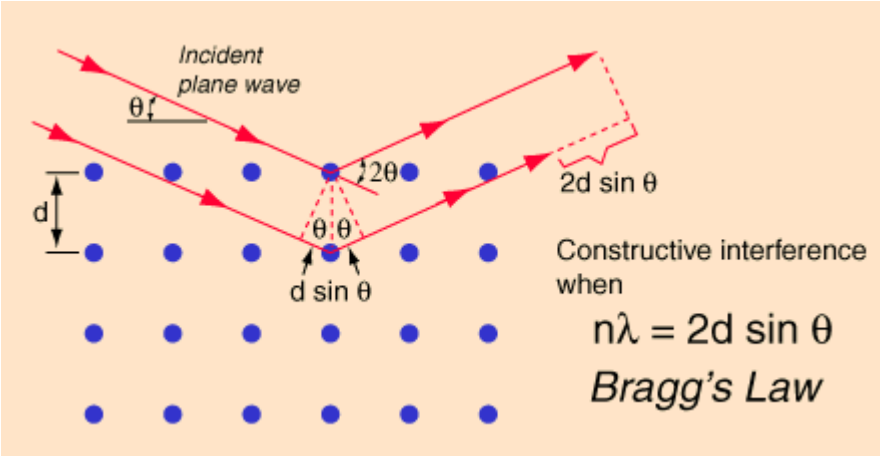

Illustration 3.1: Bragg's law of diffraction.

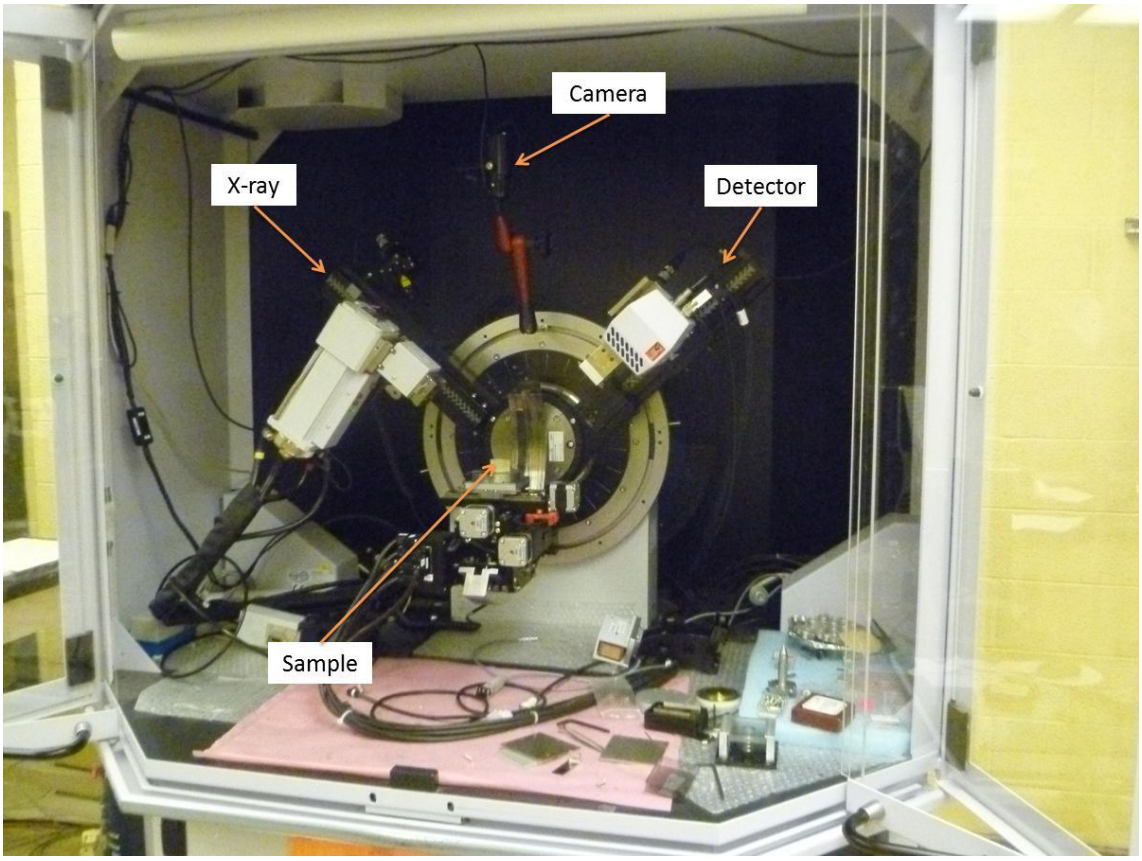

Figure 3.10: Bruker D8 Discover X-ray Diffractometer

3.3.5 Tumbler Mixer

For particle size analysis, it is important to have a homogeneous composition in the powder to obtain accurate particle size distribution. Figure 3.11 shows the tumbler mixer (Inversina 2L, Bioengineering) which was used to mix the Al powders. The device uses three-dimension inversion kinematics, also known as the Paul Schatz principle to homogeneously mix solids, liquids, and suspensions. It has a knob setting from 1 to 10 to maintain a continuous rpm setting. The mixer can hold containers of different sizes using a rubber-ring holder. It is also designed for automatic shut-off on opening of the hood. The Al powders were mixed for 30 min at a knob speed of 6.

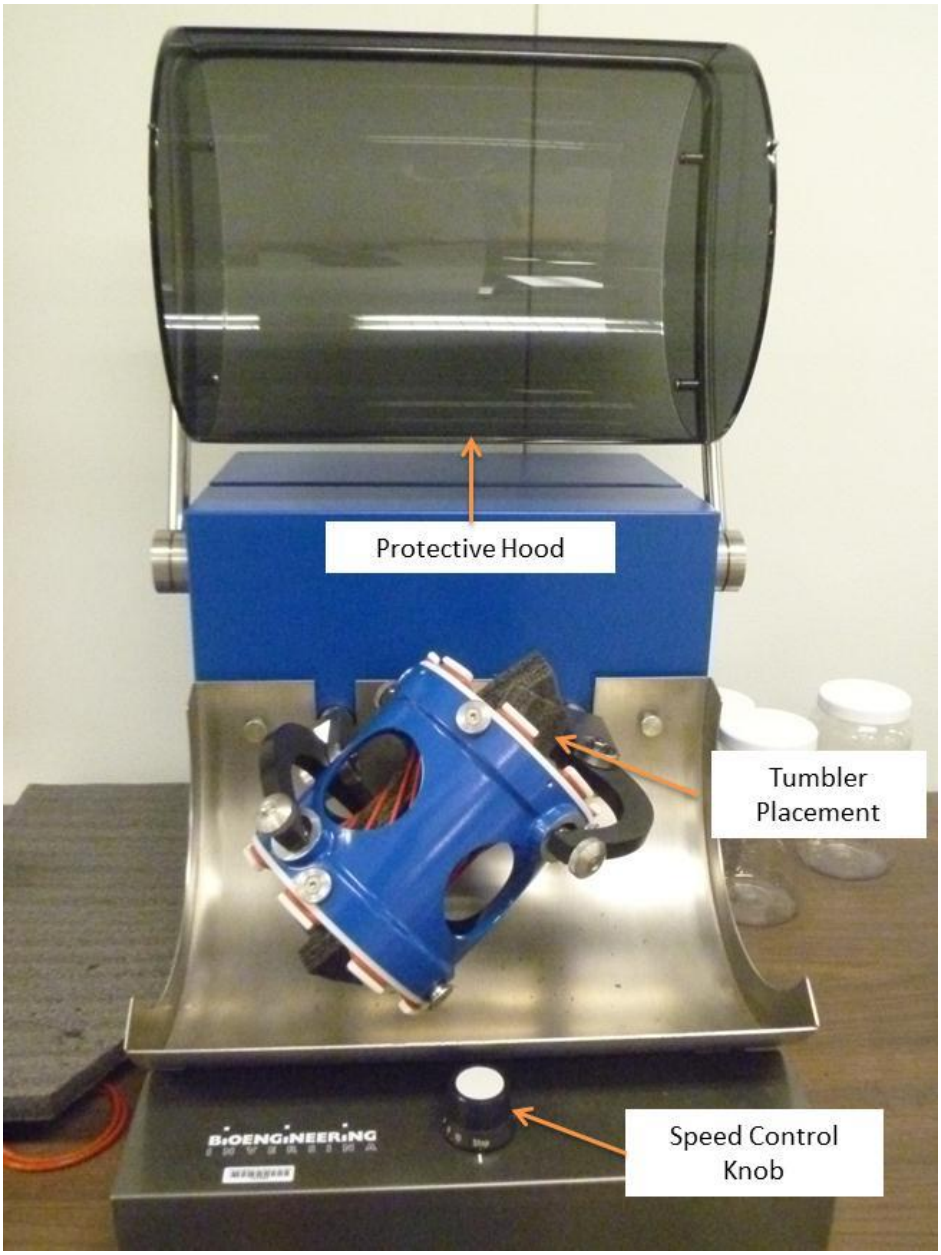

Figure 3.11: Bioengineering INVERSINA 2L

Chapter 4: Results-Hydrogen Generation

4.1 Commercially Available Aluminum Powder

To determine the feasibility of using commercially available Al powder, instead of Al powder obtained from foil, Al powder (97.5 % metals basis, 3 - 4.5 µm, Alfa Aesar) was used for reactions with hot water.

Figure 4.1 shows the obtained kinetic curves that present the extent of the reaction between aluminum and water as function of time. The experiments were carried out at two water temperatures (50 °C and 65 °C). The characteristic S-shaped curves are seen in the curves shown below.

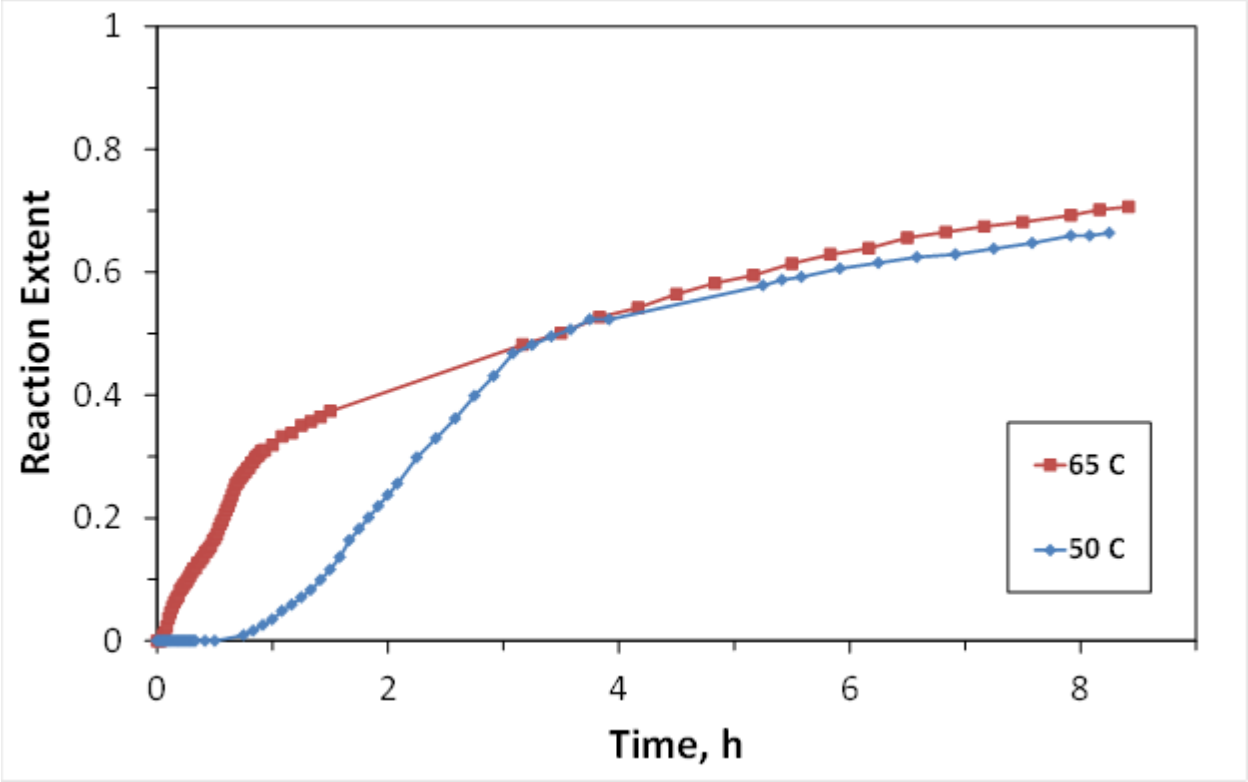

Figure 4.1: Kinetic curves obtained from the reaction of commercially available Al powders with water at two different water temperatures (50 °C and 65 °C)

The obtained kinetic curves show that the reaction was slow: it took 3 hours to reach 50% conversion and after 8 hours the reaction extent remains less than 70%. It is known that the commercially available Al powder has a large amount of oxide layer on the Al particles. Also, the

powder was not activated before it was subjected to hydrolysis reactions with water, due to its small particle size distribution.

4.2 Investigation of Activated Powder Obtained from Aluminum Foil

4.2.1 Characterization of the Obtained Al/NaCl powders and Al powders

Figure 4.2 shows that the employed high-energy ball milling of Al foil mixed with NaCl converted the Al foil pieces into a powder. Figure 4.3 shows SEM microphotographs of the obtained powders after breaking conglomerates. It is seen that the average particle size is 1 μm by the order of magnitude.

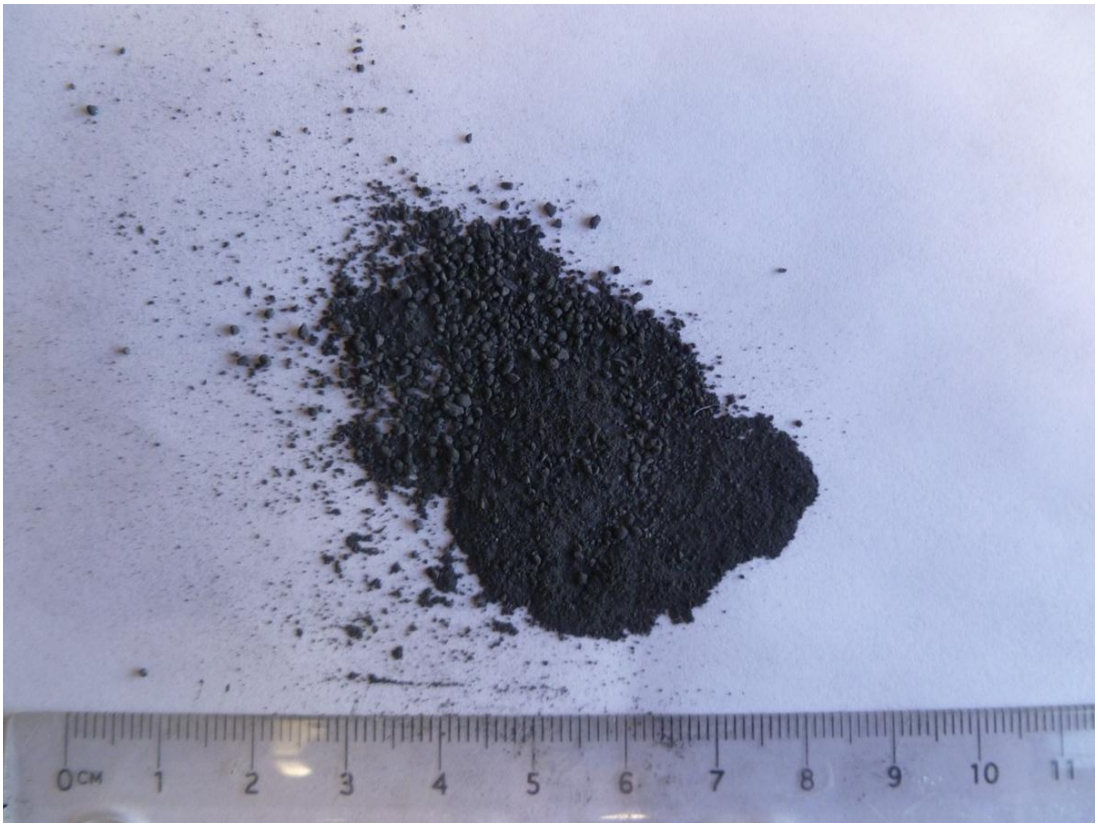

Figure 4.2: Powder obtained by milling Al foil with NaCl.

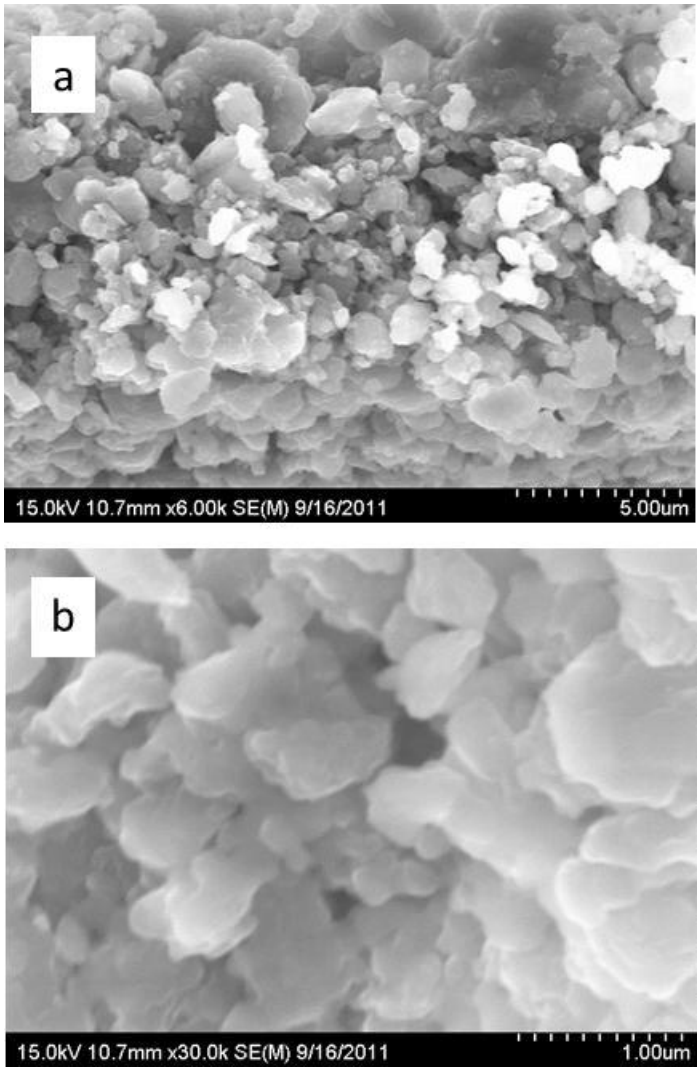

Figure 4.3: Microphotographs of powders obtained from 23 μm Al foil by milling with NaCl (a) magnification: 6000 and (b) magnification: 30000.

The BET specific surface area is 4.14 m^2/g, 4.54 m^2/g, and 4.74 m^2/g for the powders obtained from the foils of the thicknesses 15 μm, 23 μm, and 36 μm, respectively. According to the particle size analysis for the powder obtained from 15 μm foil, the mean volume particle size is 9.3 μm and the median diameter is 5.5 μm. Thus, the employed high-energy ball milling produces a fine powder from Al foil mixed with NaCl. The decrease in particle size is significant owing to repeated fracturing of the particles, while the presence of salt in the mixture prevents cold welding of the particles. Washing the obtained powder in cold distilled water for 2 min resulted in full dissolution of NaCl, which was confirmed by EDS (Table 4.1). For this reason, for the experiments with leached powders, 2-min washing time was used.

Table 4.1 Elemental composition of the obtained powder and the oxygen-to-aluminum atomic ratio for powders obtained by milling Al foil with NaCl in air atmosphere.

Foil thickness (μm)	Wash time, min	Elemental composition (at%)				O/Al (at%/at%)
		Al	O	Na	Cl	
15	0	49.52	5.85	25.32	19.32	0.118
15	0	48.92	9.36	21.32	20.39	0.191
23	0	53.56	8.92	19.07	18.45	0.166
23	0	49.79	10.80	21.00	18.41	0.217
36	0	41.83	4.31	25.28	28.58	0.103
36	0	48.75	12.67	19.43	19.15	0.260
15	2	82.88	17.12	0	0	0.207
15	5	72.73	27.27	0	0	0.375
15	10	76.22	23.78	0	0	0.312
15	60	76.78	23.22	0	0	0.302

The Al powder obtained after leaching out NaCl is finer than the original A/NaCl powder. The BET specific surface area is 13.5 m^2/g, 14.4 m^2/g, and 12.6 m^2/g for the powders obtained from the foils of the thicknesses 15 μm, 23 μm, and 36 μm, respectively. According to the particle size analysis for the powder obtained from 15 μm foil, the mean volume particle size is 3.1 μm and the median diameter is 2.9 μm. Note that elemental compositions of the obtained powders, determined by EDS for several samples (Table 4.1), contain significant amounts of oxygen. It is reasonable to suggest that for "unleached" powders, this oxygen is primarily a result of aluminum oxidation during milling, while the amounts of oxygen in the surface later of the original foil are likely much smaller. For "leached" powders, the content of oxygen is somewhat higher, which may be explained by additional oxidation of Al during the washing and filtering procedure.

Milling in argon did not lead to any significant changes in the particles size and specific surface area. For the unleached (Al/NaCl) powder, the mean volume diameter is 13.8 μm, median diameter is 6.6 μm, and specific surface area is 4.7 m^2/g. For the leached (Al) powder, the mean volume diameter is 8.5 μm, median diameter is 5.0 μm, and specific surface area is 10.6 m^2/g. EDS analysis has shown that the powders obtained in argon contained less oxygen (Table 4.2). It is also seen that leaching by cold

water increases the oxygen content, which may be explained by oxidation of Al during the washing and filtering procedure.

The powder obtained by milling in argon was also leached by methanol. The mean volume size and the median size of the obtained powder were 8.5 μm and 5.0 μm, respectively, i.e., the same as for the powder leached in water. Figure 4.4 shows the particle size distribution. EDS analysis (Table 4.2) confirmed that all salt was washed out and the oxygen content was less than in the case of leaching by water.

Table 4.2. Elemental composition and the oxygen-to-aluminum atomic ratio for the powders obtained by milling Al foil with NaCl in argon atmosphere.

Foil thickness (μm)	**Wash time (min)**	**Elemental Composition (at%)**				**O/Al (at%/at%)**
		Al	**O**	**Na**	**Cl**	
23	0	43.1	3.0	26.7	27.2	0.07
23	2 (water)	86.2	13.8	0	0	0.16
23	5 (methanol)	92.1	7.9	0	0	0.09

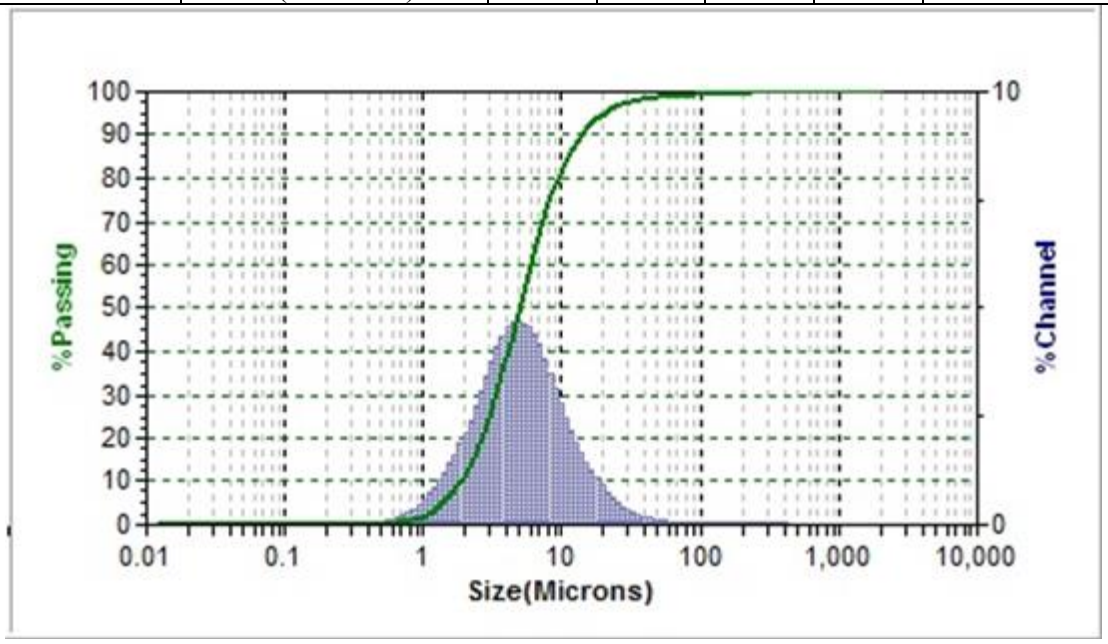

Figure 4.4. Particle size distribution for Al Powder obtained by milling of 23 μm Al foil with NaCl in Ar, after leaching by methanol.

4.2.2 Reactions of the Obtained Powders with Warm Water

Figure 4.5 shows XRD patterns of the solid products of the reaction between Al/NaCl powder and water. The powder was obtained by milling 23-μm Al foil in air At temperatures 50–80 °C the product is boehmite, while at the temperature of 35°C the product is a mixture of boehmite and bayerite. Thus, at temperatures 50–80 °C, the reaction follows Eq. (2). Note that these results accord with those obtained for the reaction of nanoscale (98 nm) Al powder with water: the product was a mixture of bayerite and boehmite at 40 °C and only boehmite at 60 °C [73].

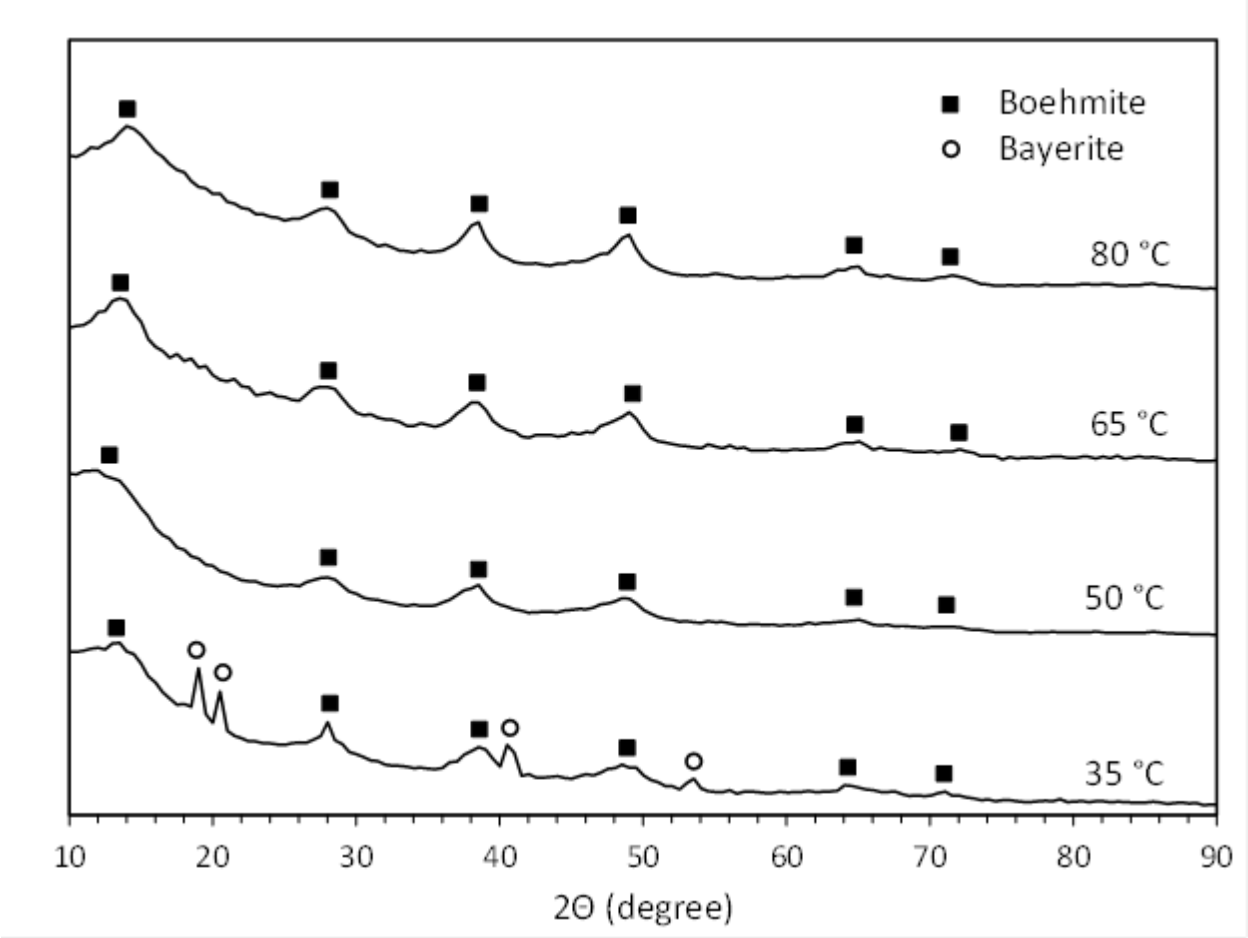

Figure 4.5: XRD pattern of the solid products obtained after reaction of the Al powder with water at temperatures of 35 °C, 50 °C, 65 °C, and 80 °C.

Figures 4.6 a and b show the kinetic curves for the Al/NaCl and salt-free Al powders obtained from foils of thicknesses 15, 23, and 36 μm by milling in air environment. It is seen that the reaction is much faster than in the case of the commercial powder despite the similar particle sizes. Apparently, the results are insensitive to the foil thickness in the range from 15 μm to 36 μm. At the temperature of 35 °C, the reaction was slow: the reaction extent after 2 hours was only 10 % and it took 8.5 hours to reach 87 % (unleached Al/NaCl powder obtained from 15 μm was tested). As in the experiments on milling of commercial Al powders with NaCl [[24], [25], [74]] or other additives [[22], [25], [33], [75]], the "S" shape of the kinetic curves indicates that the process involves three stages: the induction period, the middle stage where the reaction rate is the highest, and the final (saturation) stage. With increasing temperature, the induction period decreases, while the reaction rate (slope of the curve) at the middle stage and the final extent of reaction increase.

The high reactivity of the obtained powders is apparently caused by weakened protection properties of the oxide layer on the surface of formed particles. Multiple collisions with relatively hard NaCl particles during milling may create surface layer defects (e.g., grain boundaries, dislocations, and inclusions) that serve as reaction starting points after immersion in hot water. As shown experimentally for ball-milling of commercial Al powders with NaCl and other additives [25], it is the defected oxide film that enhances the reaction of Al with water, while the structural defects and microstrains induced in the aluminum lattice during milling do not affect the reactivity.

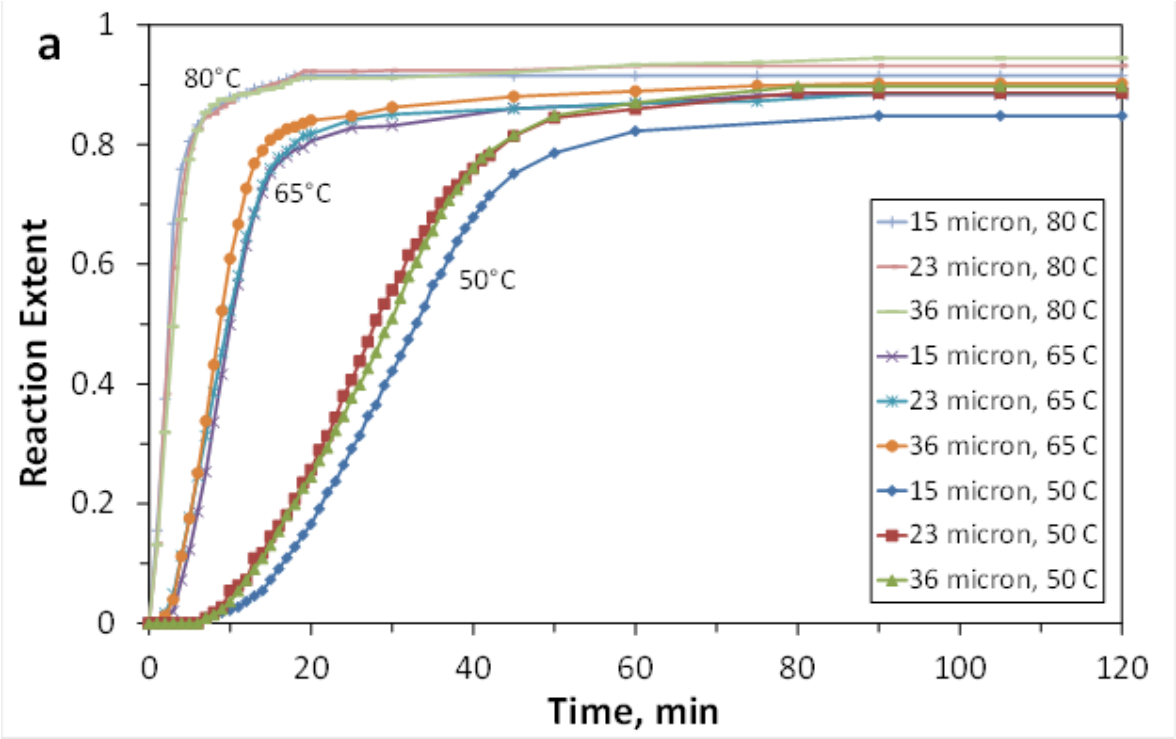

(a)

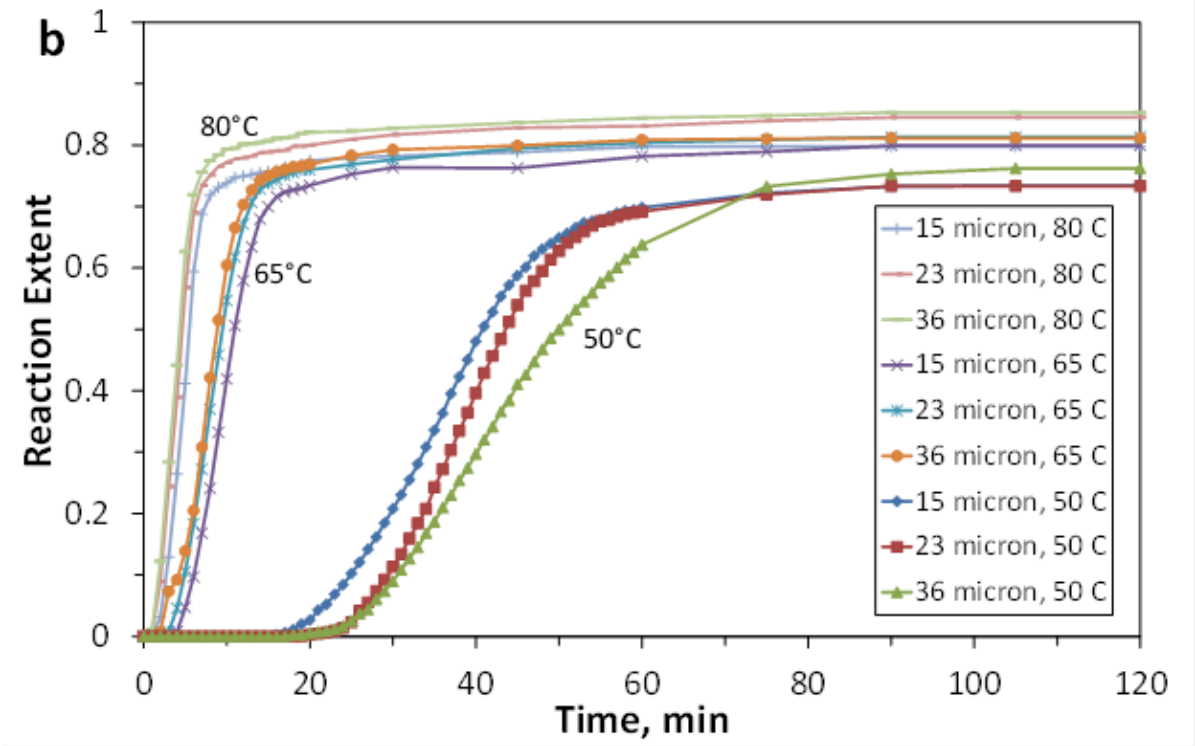

(b)

Figure 4.6: Kinetic curves for the powders obtained from Al foils of different thicknesses (15 µm, 23 µm, and 36 µm) by ball milling with NaCl: (a) Al/NaCl powders and (b) Al powders after leaching-out NaCl.

Figure 4.7 shows the curves for the reaction rate (the derivative of the reaction extent in respect to time) as function of time, obtained from the data presented in Figure 4.6.

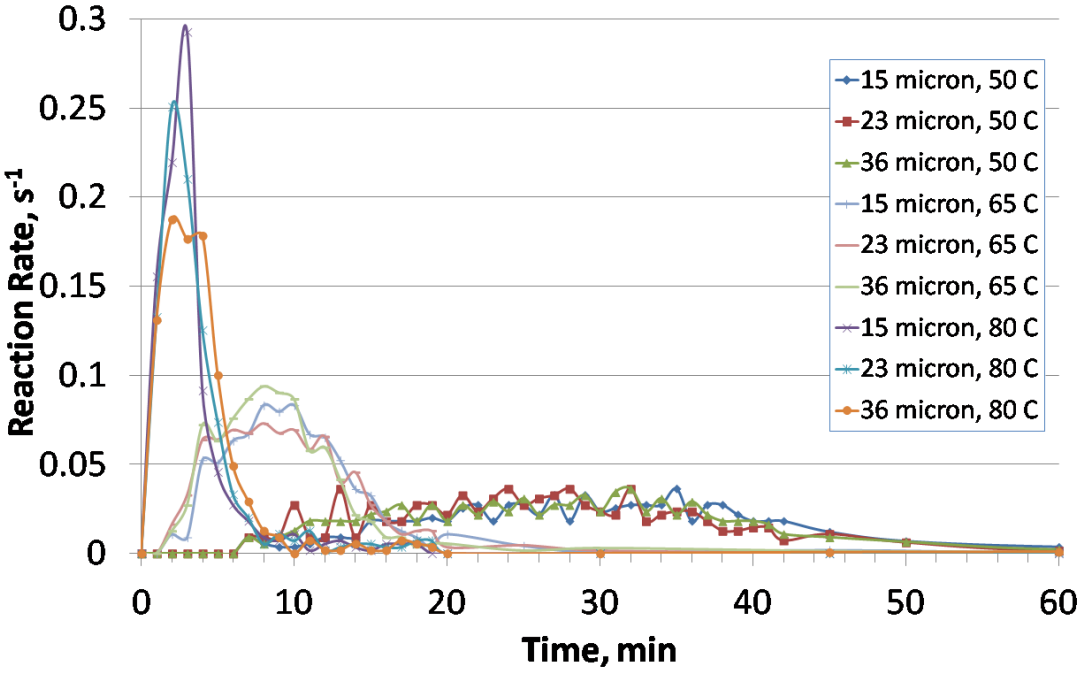

(a)

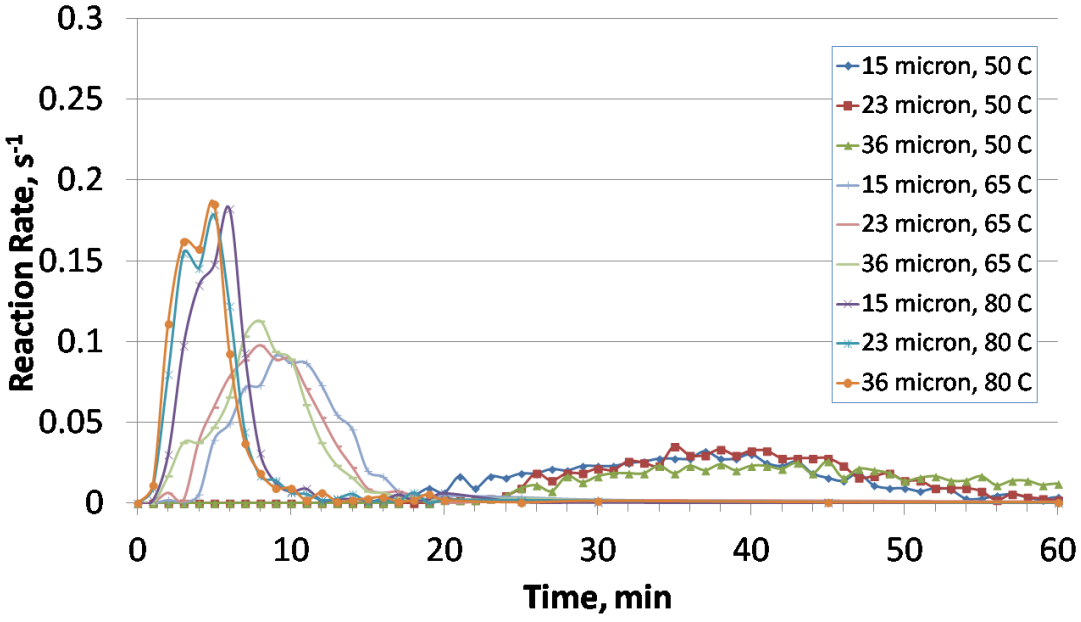

(b)

Figure 4.7: Time variation of the reaction rate for the powders obtained from Al foils of different thicknesses (15 µm, 23 µm, and 36 µm) by ball milling with NaCl: (a) Al/NaCl powders and (b) Al powders after leaching-out NaCl.

For each point, the reaction rate was determined as the change in the reaction extent between two consecutive measurements divided by the time between these measurements. The observed oscillations were apparently caused by experimental errors in recording the water level in the inverted cylinder.

Analysis of Figs. 4.6 and 4.7 show that the results are independent on the foil thickness over the range from 15 μm to 36 μm, which is explained by similar sizes of the particles obtained from these foils. Figures 4.4 and 4.5 also show that for leached powders, the induction period is longer and the maximum extent of the reaction is lower than in case of unleached Al/NaCl mixtures. At the same time, the reaction rate during the middle stage of the process is approximately the same for the unleached and leached powders.

The shorter induction period of Al/NaCl mixtures is apparently caused by the effect of pitting corrosion in the presence of chloride ions, which decreases protective properties of the oxide layer on the particle surface. During the middle stage of the process, pitting corrosion does not play a significant role because the surface of the reacting (shrinking) Al particle coated by a low-protective hydroxide phase. The decreased maximum extent of the reaction for the leached powders may be associated with the decreased content of free metallic Al, caused by oxidation during the leaching process.

Figure 4.8 shows the kinetic curves for the powder obtained by milling 23-μm Al foil in argon environment. Comparison with Fig. 4.6 shows that the final reaction extent for the powders milled in Ar is higher than that for the powders milled in air (for the unleached powders: 98% vs. 93%). This is apparently associated with lower oxidation during milling.

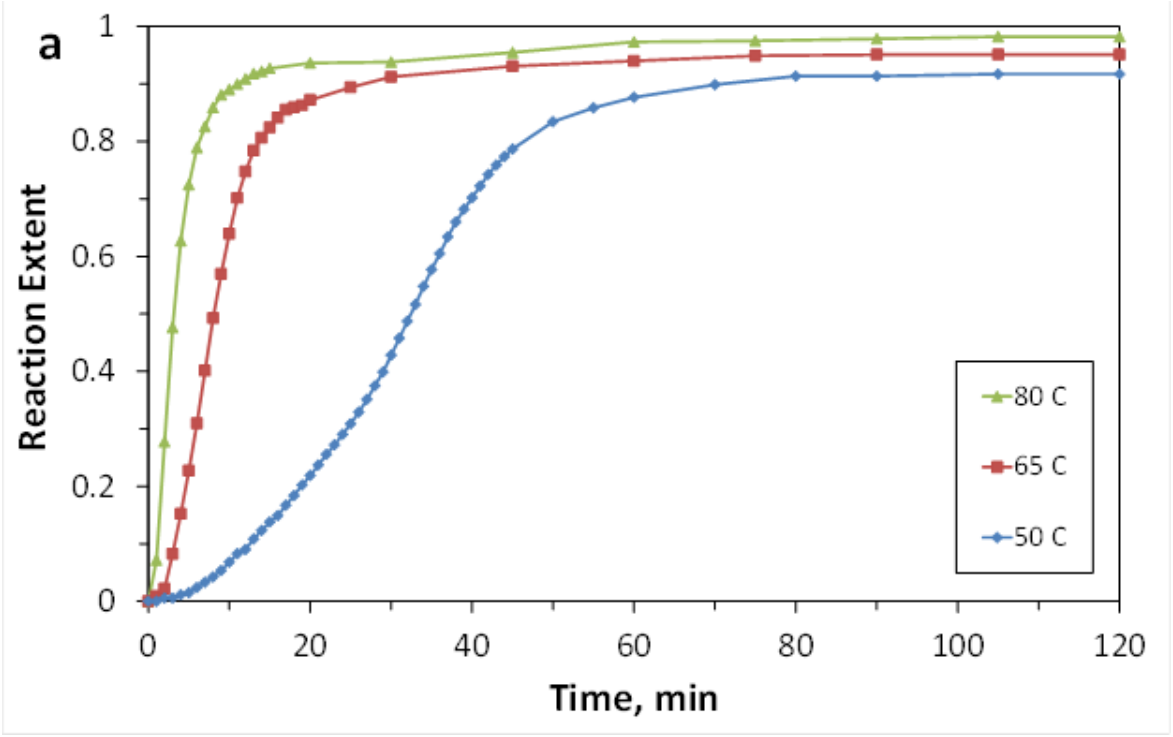

(a)

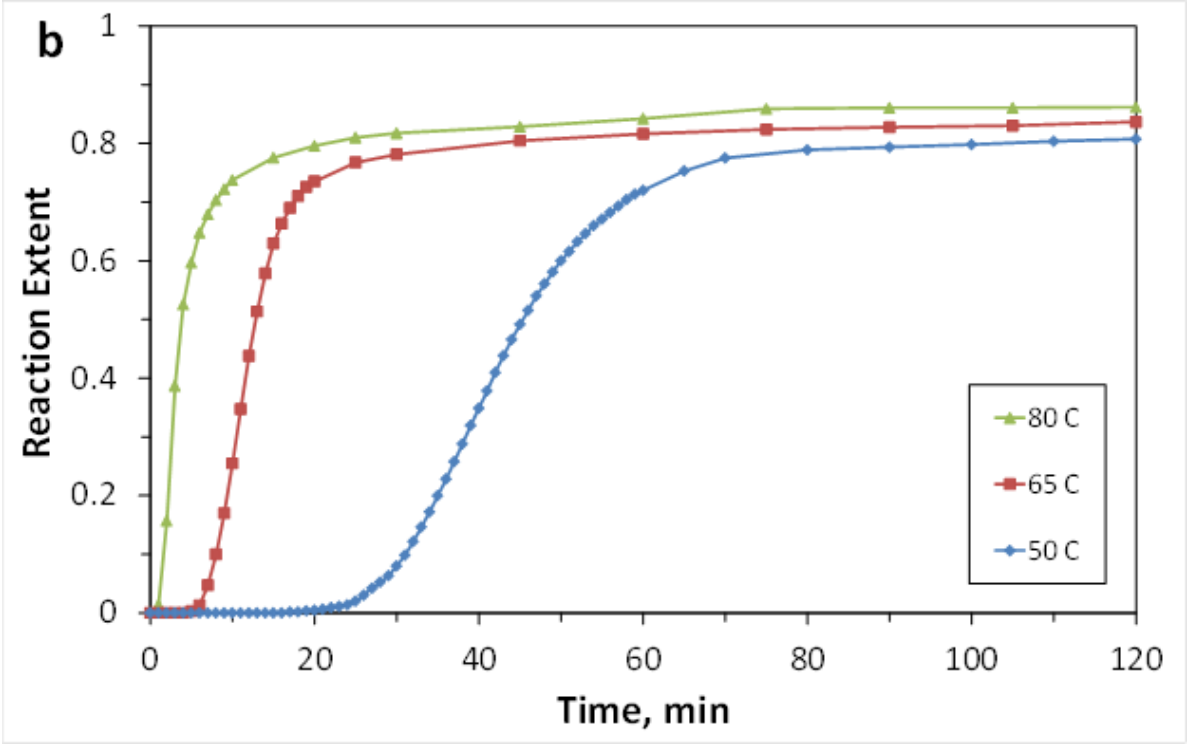

(b)

Figure 4.8: Kinetic curves for the powders obtained by ball milling of Al foil with NaCl in Ar: (a) Al/NaCl and (b) salt-free (leached by water) Al.

Figure 4.9 shows the reaction rate curves for the powders obtained by milling in argon environment, i.e., calculated using the data presented in Fig. 4.8. The observed oscillations were apparently caused by experimental errors in recording the water level in the inversed cylinder.

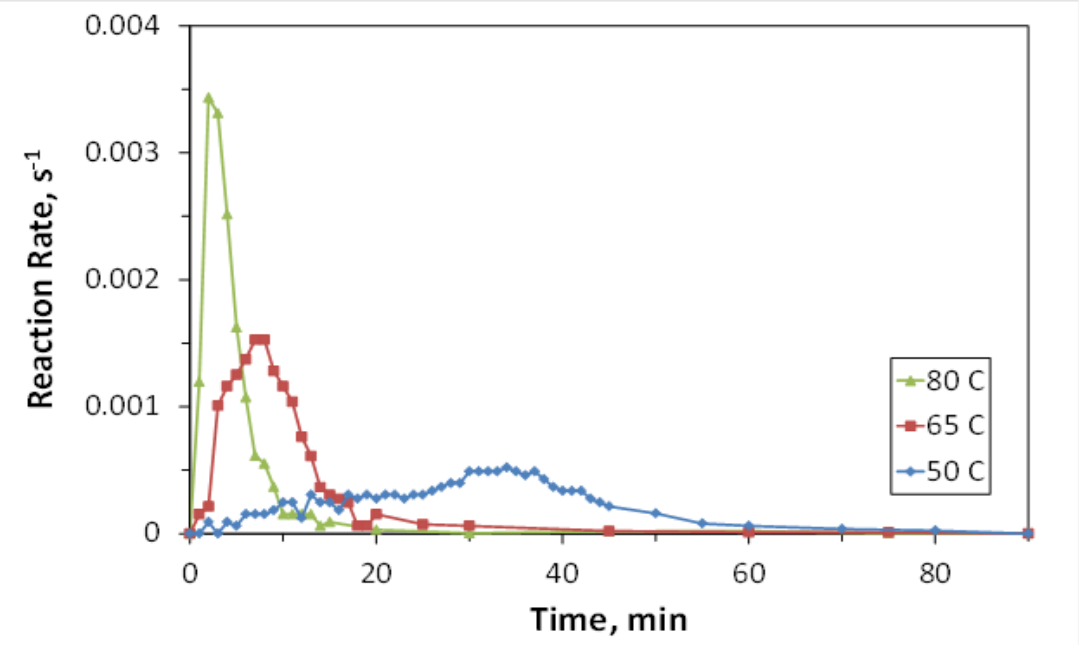

(a)

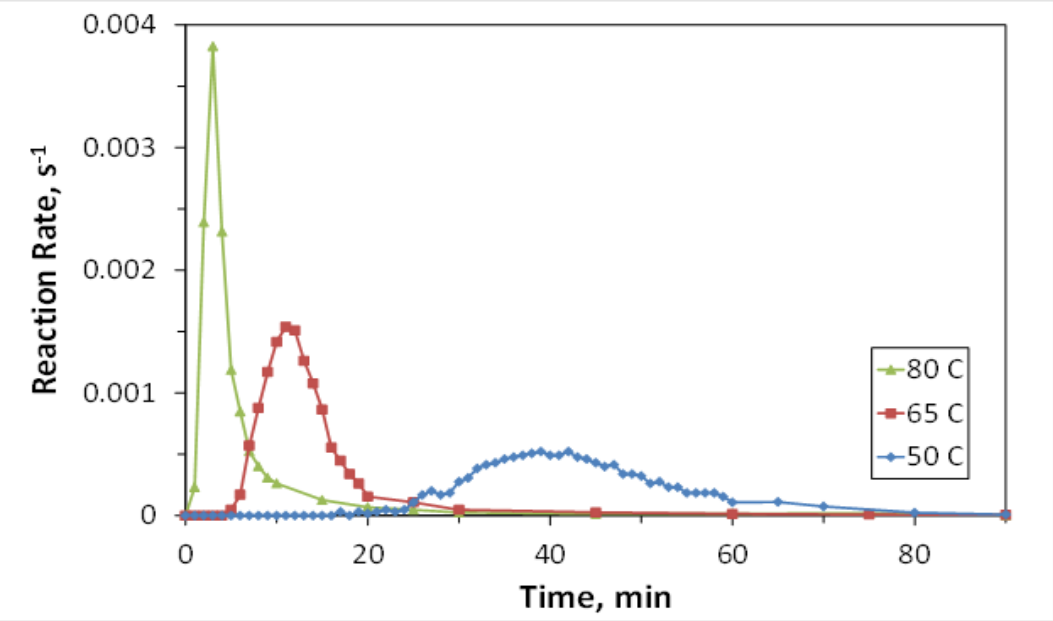

(b)

Figure 4.9: Time variation of the reaction rate for the powders obtained from Al foil by ball milling with NaCl in Ar: (a) Al/NaCl and (b) salt-free (leached by water) Al.

4.3 INVESTIGATION OF ACTIVATED POWDER OBTAINED FROM ALUMINUM CANS

4.3.1 Characterization of the Obtained Al/NaCl and Al powders

SEM of the powder obtained from 100-μm foil with a milling time of 30 min (Fig. 4.10a) revealed heavy agglomeration and a large difference in particle sizes. As compared to 15–36 μm foil, milling of 100-μm foil produced a coarser powder: the mean volume diameter was about 22 μm. At the same time, the specific surface area increased to 4.78 m^2/g, which may be explained by a less rounded shape of the particles. Increasing the milling time to 60 min reduced the particle size and made the powder more uniform (Fig. 4.10b). The mean volume diameter decreased to 17 μm and the specific surface area increased to 5.88 m^2/g.

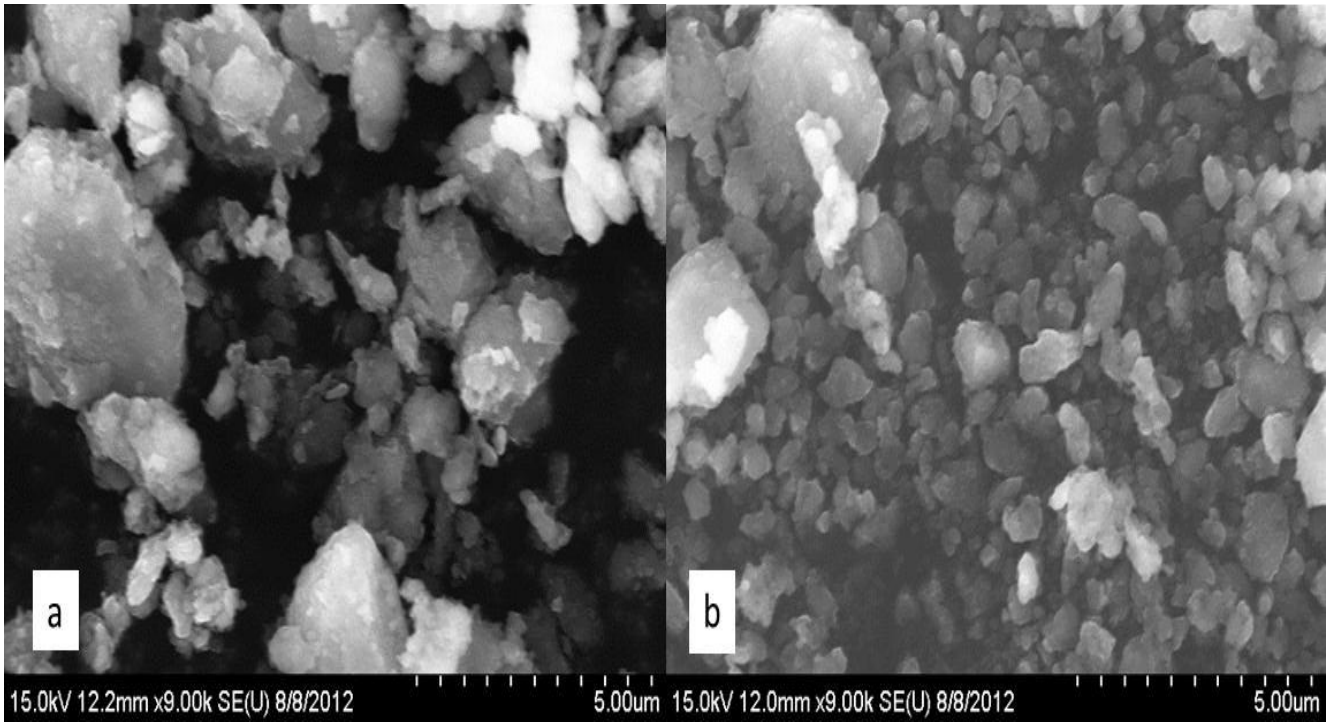

Figure 4.10: SEM microphotographs of the ball milled Al can powders (a) 30 min milled unleached and (b) 60 min milled unleached

EDS analysis of the powders obtained from 100-µm foil was performed to confirm the removal of paint and protective coating from the Al cans after immersion in sulfuric acid. Indeed, the EDS spectrum for the obtained powder (Fig. 4.11) shows only peaks for Al, O, Na, Cl, and C. The latter peak, located to the left of O peak, is explained by the fact that a carbon tape was used to place the powder sample onto the holder. Carbon was not included in the elemental analysis.

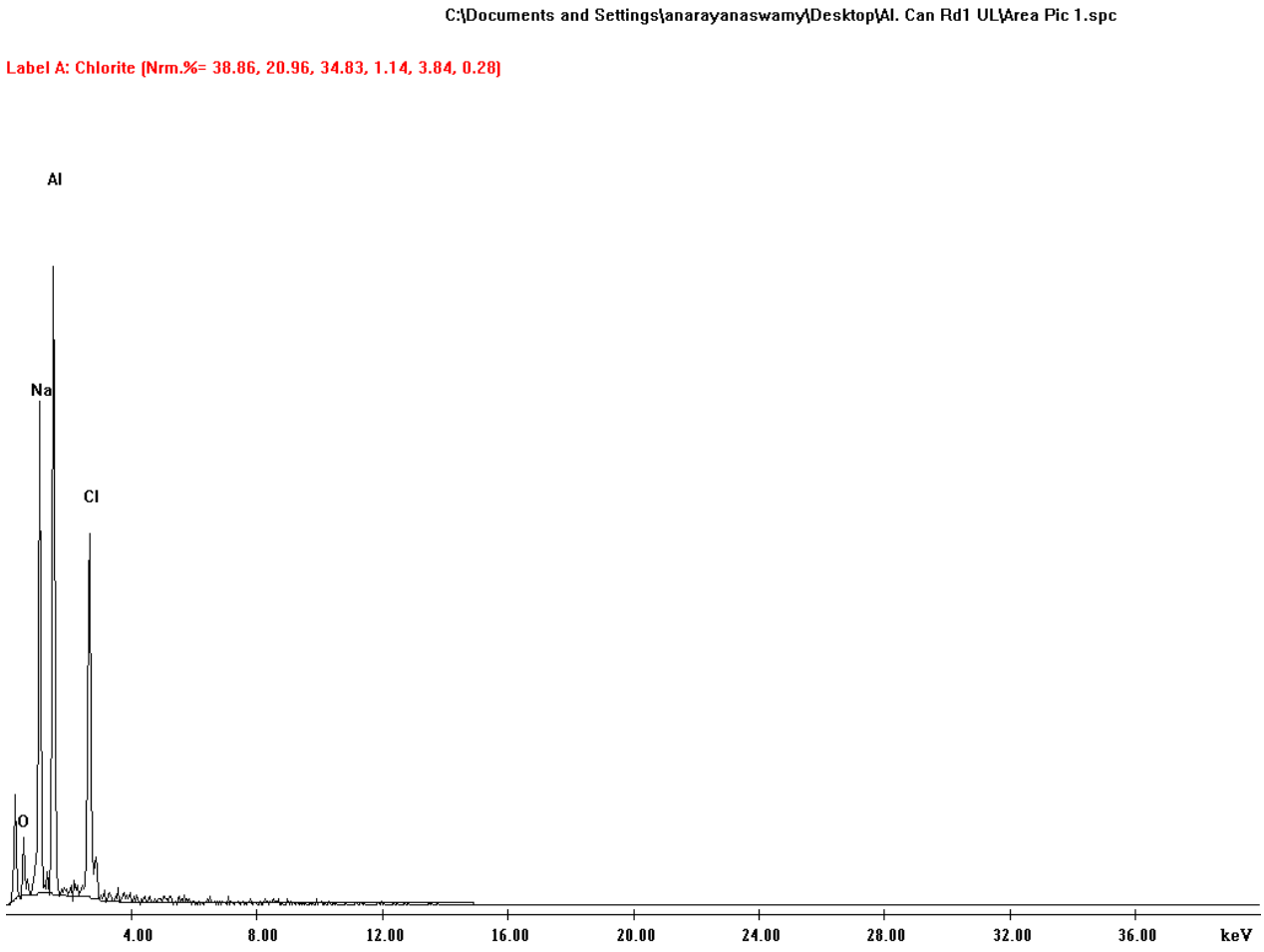

Figure 4.11: EDS spectrum for Al can unleached powder after 30 min milling with NaCl

4.3.2 Reactions of the Obtained Powders with Hot Water

Figure 4.12 shows the kinetic curves for the powders obtained from Al beverage cans (100-μm foil) by 30-min milling in air. It is seen that the final reaction was less than for the powders obtained from thinner foils. The increase in the milling time to 60 min significantly improved the results (Fig. 4.13). The fact that the maximum reaction extent still remains lower than for 15–36 μm foils may be attributed to the larger particle size and to the additives in aluminum used in the beverage cans (1 wt% Mg, 1 wt% Mn, 0.4 wt% Fe, 0.2 wt% Si, and 0.15 wt% Cu [76]).

As mentioned in the previous section, the observed S-shape kinetic curves have three stages: induction period, the middle stage and the saturation stage. At high temperatures (80 °C), the induction period is very short (<1 min) and also the final extent of reaction is high (up to 90%).

It should be noted that all the experiments reported above were conducted with deionized water. To study the effect of water composition, several experiments with powders obtained from Al foil (15–36 μm) were performed using tap water. The water temperature was 65 °C. For the leached powder, the induction time was 20 min and after 2 hours the reaction extent was only about 50 %. For unleached powders the reaction extent was faster but the reaction extent after 2 hours was about 65 %. The reaction rates were significantly lower than in the case of using deionized water, which accords well with the results for aluminum modified by metal oxides [77].

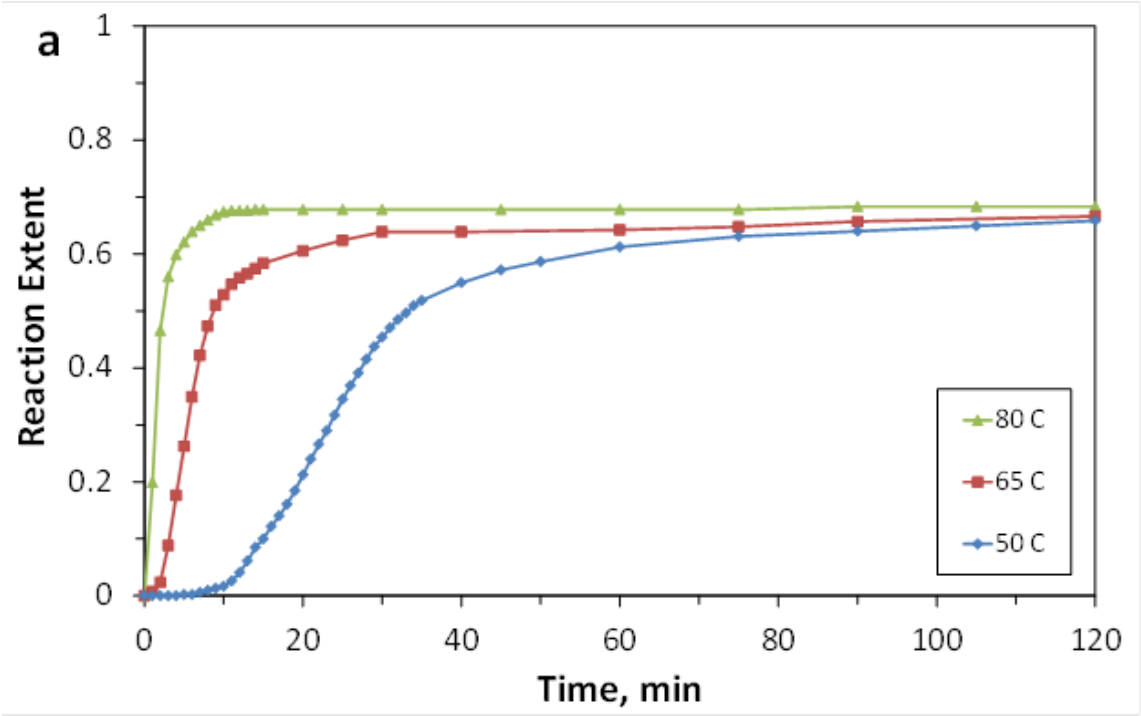

(a)

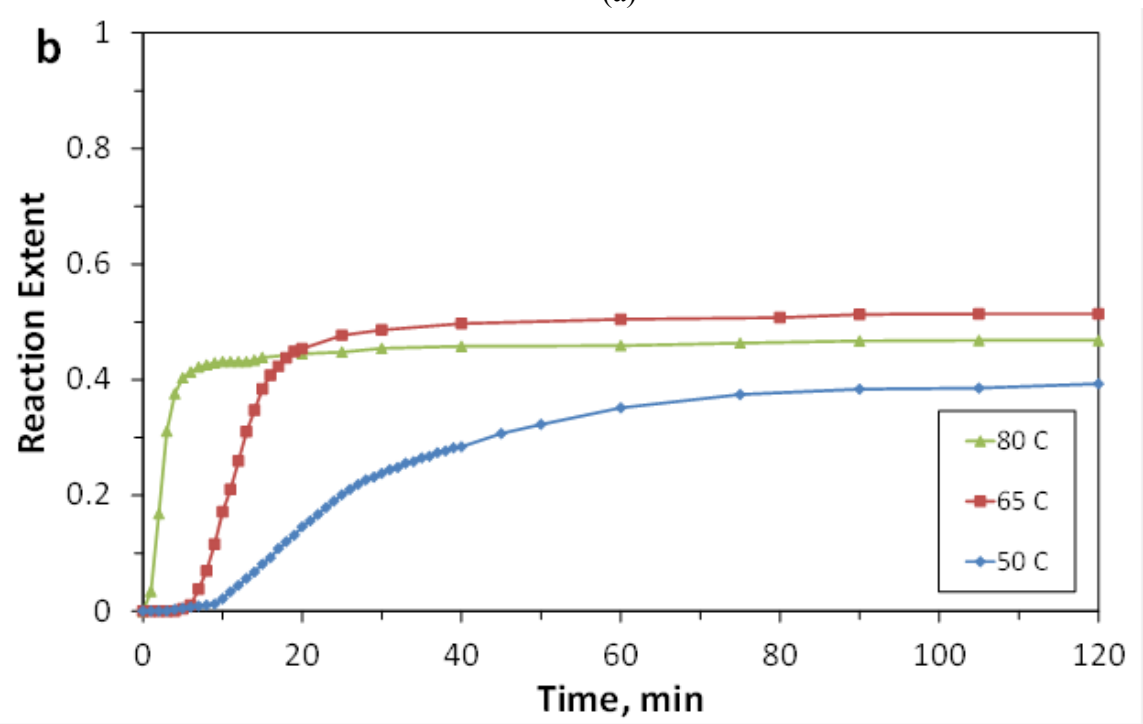

(b)

Figure 4.12: Kinetic curves for the powders obtained from Al cans by milling with NaCl in air (the milling time: 30 min): (a) Al/NaCl and (b) salt-free (leached by water) Al.

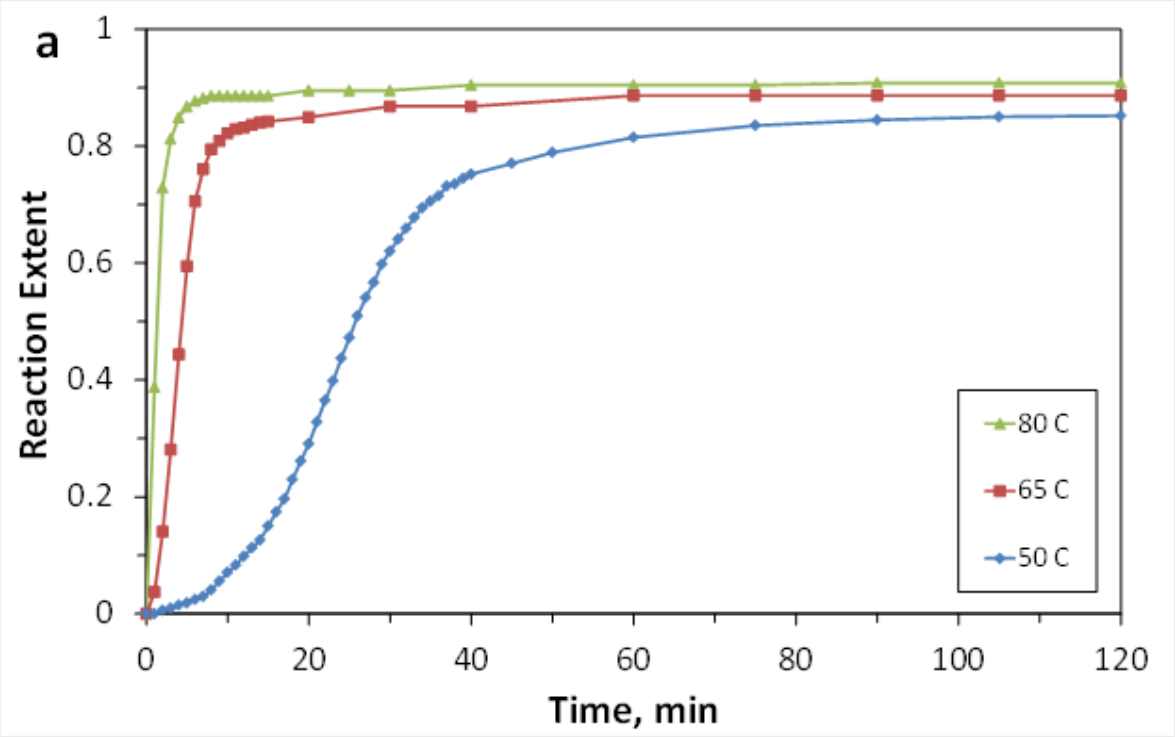

(a)

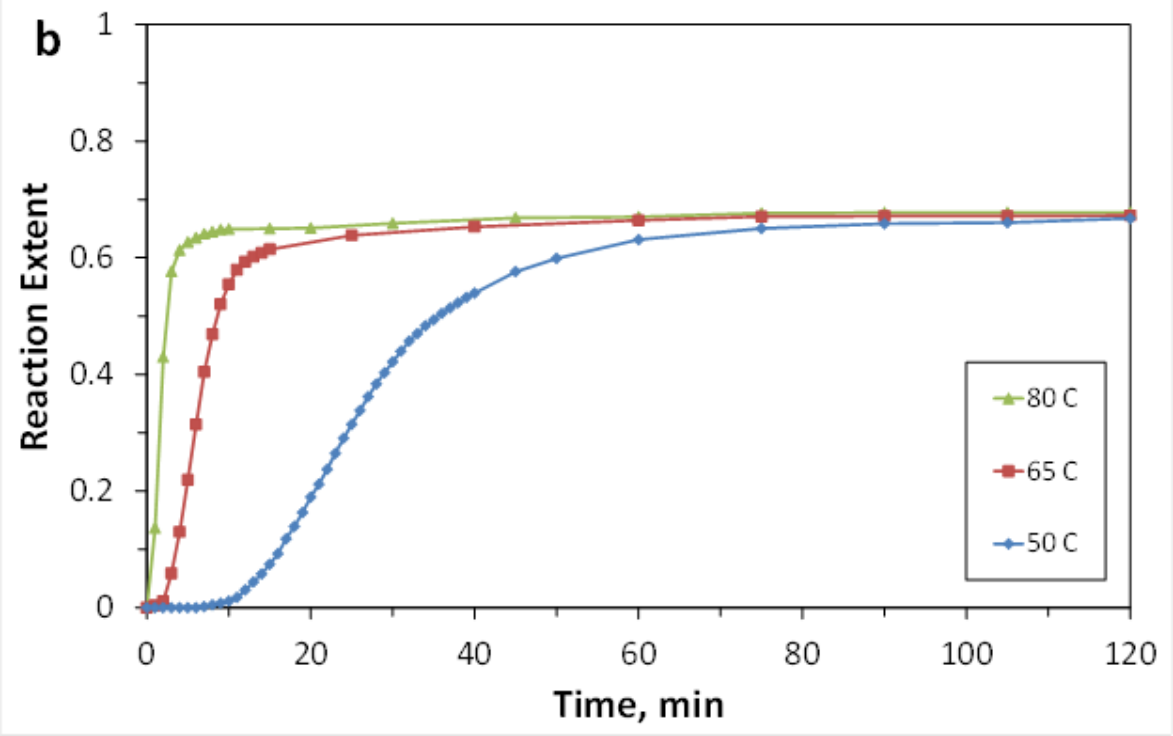

(b)

Figure. 4.13: Kinetic curves for the powders obtained from Al cans by milling with NaCl in air (the milling time: 60 min): (a) Al/NaCl and (b) salt-free (leached by water) Al.

4.4 Discussion of the Effect of Leaching on the Induction Period and the Final Reaction Extent

Figures 4.6, 4.8, and 4.12 show that for the salt-free (leached) Al powders, the induction period is longer than in the case of the unleached Al/NaCl mixtures. To verify that the shorter induction time for the unleached powders was not created by Cl^- ions transferred from the powder to water upon its immersion, an experiment was conducted where the same amount of NaCl as in the Al/NaCl samples was dissolved in the water and then a leached Al powder was immersed. The kinetic curve in this experiment was exactly the same as for the leached powder immersed in the water without NaCl. Thus, the longer induction period for leached powders is caused by the higher protective properties of the Al surface layer and not by Cl^- ions in water.

Initially, it was suggested that this protective layer forms due to oxidation during washing in cold water. As noted in table 4.2, washing in methanol led to full dissolution of NaCl and a lesser content of oxygen than for water-washed powders. However, the obtained kinetic curve at 50°C (Fig. 4.14) had essentially the same induction period as for the powder leached in water (Fig. 4.8b). As methanol does not oxidize Al, it is reasonable to suggest that formation of an aluminum hydroxide film during leaching in cold water cannot be responsible for the increased induction period as compared with unleached (Al/NaCl) powder. Apparently, the increased induction period was caused by the formation of the alumina film during drying, which followed washing in either water or methanol.

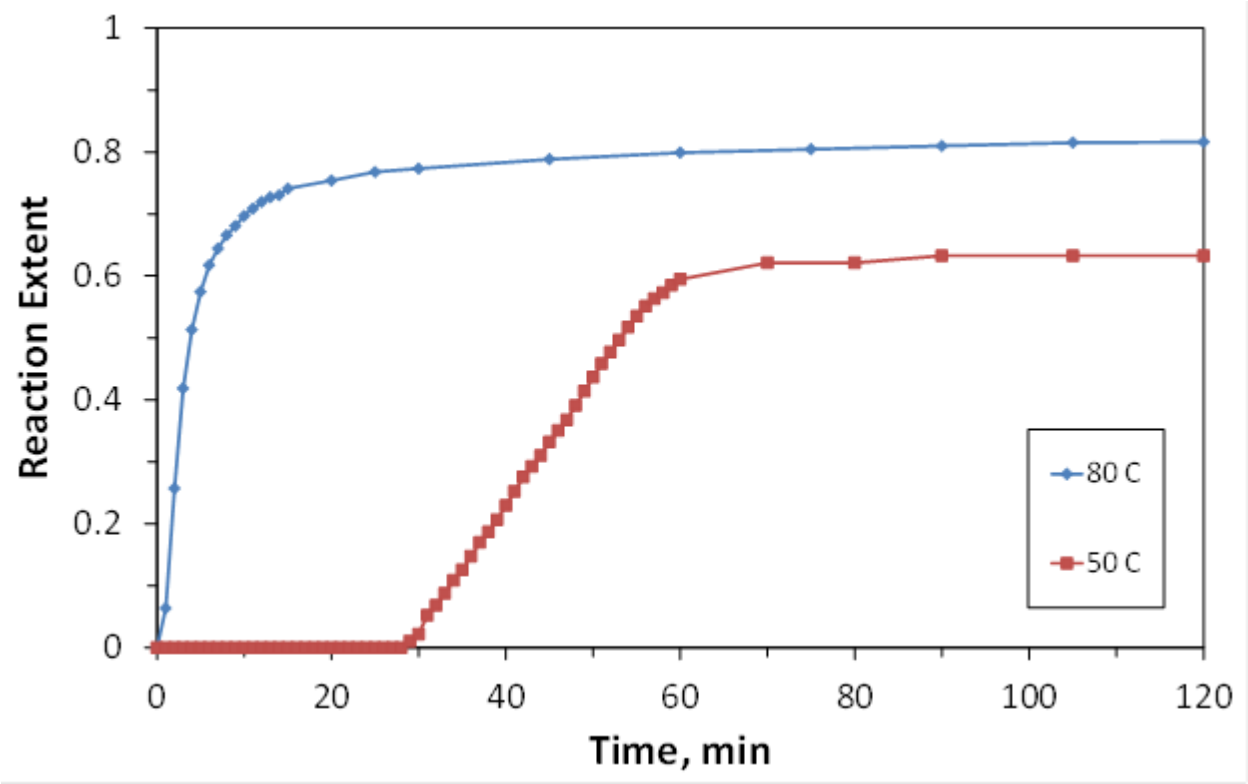

Figure 4.14: Kinetic curves for the powder obtained by ball milling of Al foil with NaCl in Ar and leached by methanol.

This conclusion has important implications for practice. The removal of salt would be desired in portable applications. It is clear that the removal can be conducted using cold water, but drying will decrease the activity of the obtained salt-free Al powder due to the growth of the protective alumina film.

Figures 4.6, 4.8, 4.12, and 4.14, show that leaching by water or methanol decreases the final reaction extent. Oxidation during drying after leaching may partly explain this decrease. The oxidation before the injection of the powder into the reactor, however, cannot explain the observed dependence of the final reaction extent on the temperature. Thus, there is another mechanism that decreases the reaction extent.

Apparently, this decrease may be caused by premature cessation of the reaction due to the resistance to diffusion of OH groups through the growing product layer. The obtained XRD spectra of the reaction products did not allow an unambiguous conclusion on the presence of metallic Al. To detect unreacted aluminum in the products, which mainly contain boehmite or bayerite, they were tested in the

thermogravimetric analyzer. Specifically, the tested materials were produced by the reaction of Al powder obtained from 23 μm foil by milling with NaCl in air and washing in cold water. The samples (13 mg) were placed in alumina crucibles and heated in argon flow (20 mL/min) to 760 °C at a heating rate of 20 °C/min. The calculated differential thermal analysis (c-DTA) for the reaction products of the leached powder with water at 35 °C, 50 °C, and 65 °C revealed an endothermic peak at 660 °C, which is the melting point of Al. The c-DTA test at 80 °C, however, did not indicate the peak at 660 °C. Thus, the thermal analysis detected unreacted Al in the products of the reaction at 35-65 °C and did not detect it in the products of the reaction at 80 °C.

4.5 THE ACTIVATION ENERGY OF AL-H_2O REACTION

Figures 4.6, 4.8, 4.12, and 4.13, show that the reaction rate (the slope of the kinetic curve) during the middle stage of the process is approximately the same for the unleached and leached powders. This indicates that by the end of the induction period the alumina layer, formed during the washing-drying procedure loses its protective properties; the metal core is shrinking and a layer of boehmite is growing.

For each of the 38 kinetic curves shown in Figs. 4.6, 4.8, 4.12, 4.13, and 4.14, time variation of the reaction rate was calculated. The reaction rate was defined as the derivative of the reaction extent with respect to time. In the calculations, the reaction rate at each point was determined as the change in the reaction extent between two consecutive measurements divided by the time between these measurements.

Figure 4.15 shows the Arrhenius plot obtained for the maximum reaction rates in the 38 experiments. The standard deviation of slope was determined using LINEST function in Microsoft Excel. The effective activation energy determined from the Arrhenius plot is equal to 63.1 ± 3.1 kJ/mol. The obtained values of the maximum reaction rates and the activation energy are in a good agreement with the data reported for Al particles activated by ball-milling with graphite [22] (the effective activation energy determined in that study was 61 ± 10 kJ/mol). The observed good agreement is not surprising as during the middle stage of the reaction, the Al core is shrinking and the layer of boehmite is growing, while the surface properties of the initial particle apparently do not play a significant role.

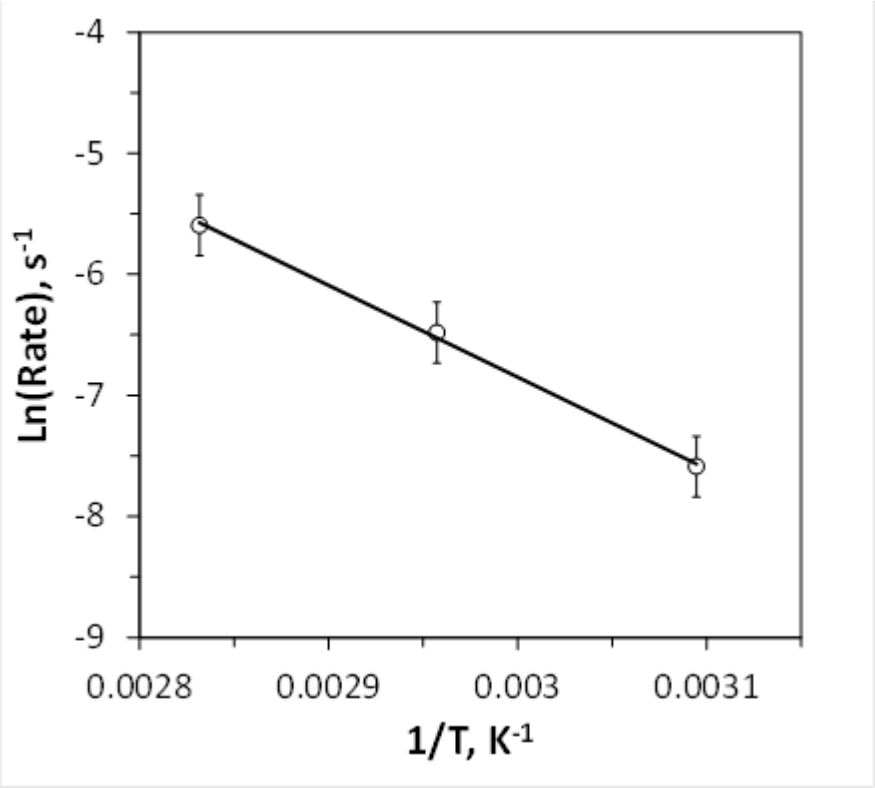

Figure 4.15: Arrhenius plot for the maximum rates of the reactions between the obtained powders and water.

4.6 Combustion of Activated Aluminum Powder with Water

At Al concentration of 30 wt%, the mixture did not ignite. In the range of Al concentrations from 40 wt% to 80 wt%, the mixture ignited easily and, upon ignition, a combustion front propagated downward. Figure 4.16 shows the images of the combustion front propagation for the mixture with 40 wt% Al. It is seen that the propagation was rather uniform. Despite the thermolysis of the plastic tube, the solid products retained the original sample shape.

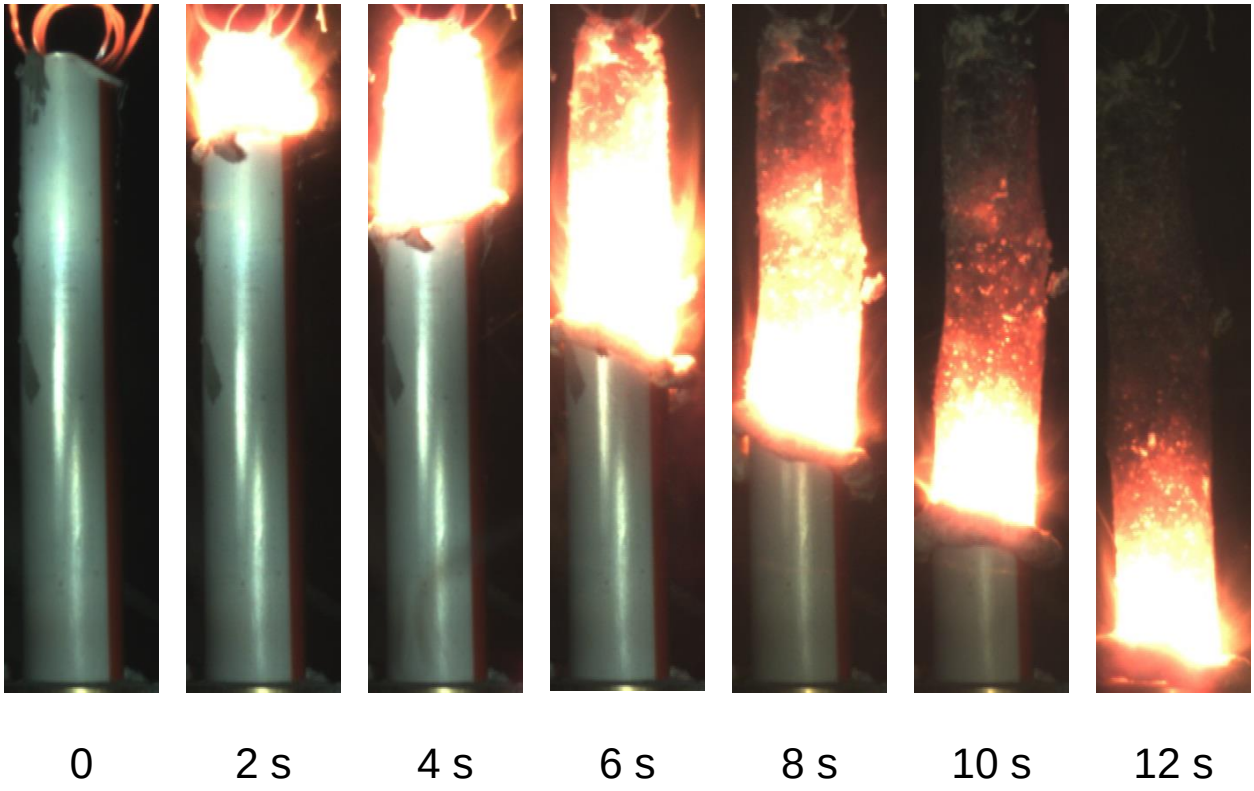

Figure 4.16: Propagation of the combustion front over Al/H_2O mixture at 40 wt% Al. Time zero was selected arbitrarily. The thermocouple is not visible as it was embedded in the rear side of the sample.

At Al concentrations 50–70 wt%, the combustion propagation was accompanied by numerous sparks and dispersion of solid products over the chamber (Fig. 4.17). At the concentration of 80 wt%, less sparks were observed (Fig. 4.18), which is apparently explained by the decrease in the amount of evolved hydrogen. At 90 wt% Al, a thermal front still propagated over the sample, which was clearly seen due to melting and thermolysis of the tube, but visible reaction did not occur in the mixture and the propagation velocity was low.

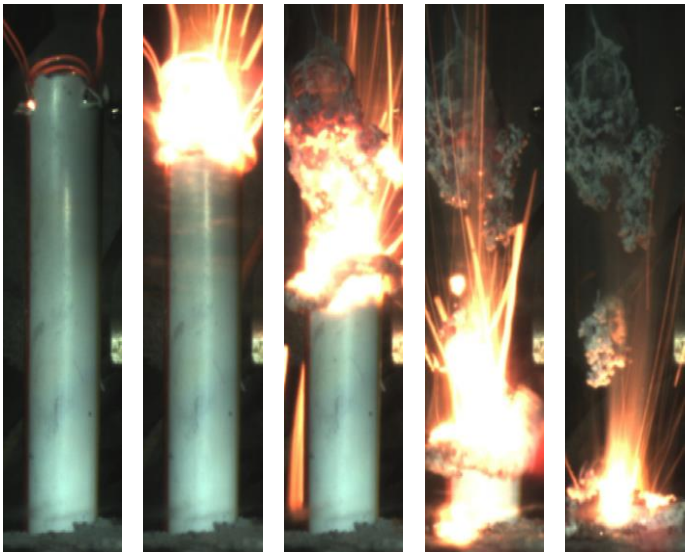

Figure 4.17: Propagation of the combustion front over Al/H_20 mixture at 60 wt% Al. Time zero was selected arbitrarily. The thermocouple is not visible as it was embedded in the rear side of the sample.

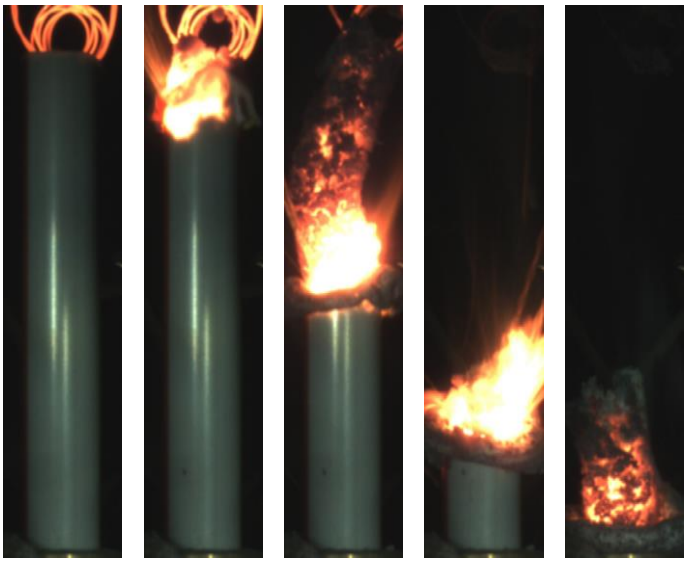

Figure 4.18: Propagation of the combustion front over Al/H_2O mixture at 80 wt% Al. Time zero was selected arbitrarily. The thermocouple is not visible as it was embedded in the rear side of the sample.

Figure 4.19 shows the maximum temperatures measured in the front for different concentrations of Al in the Al/H_2O mixture. Each point except one for 90 wt% Al was obtained by averaging the values measured in three experiments. For comparison, the adiabatic flame temperatures for Al-H_2O system at a pressure of 1 atm were calculated using software THERMO [78] and shown on the same plot. The plateaus on the calculated curve (one at 660 °C and two at 2054 °C) correspond to melting of Al and Al_2O_3, respectively. The complicated shape of the right side of the curve (an almost horizontal line between 60 and 80 wt% Al) is associated with the equilibrium between Al_2O_3 and gaseous suboxide of aluminum Al_2O. Formation of the latter instead of condensed Al_2O_3 significantly decreases the heat release and hence the adiabatic flame temperature. In the calculated product compositions, the maximum concentration of Al_2O was observed at 62 wt% Al. The measured temperatures were significantly lower than the predicted ones due to heat losses. It should be noted that the relatively large diameter of the thermocouples could lead to error in temperature measurements.

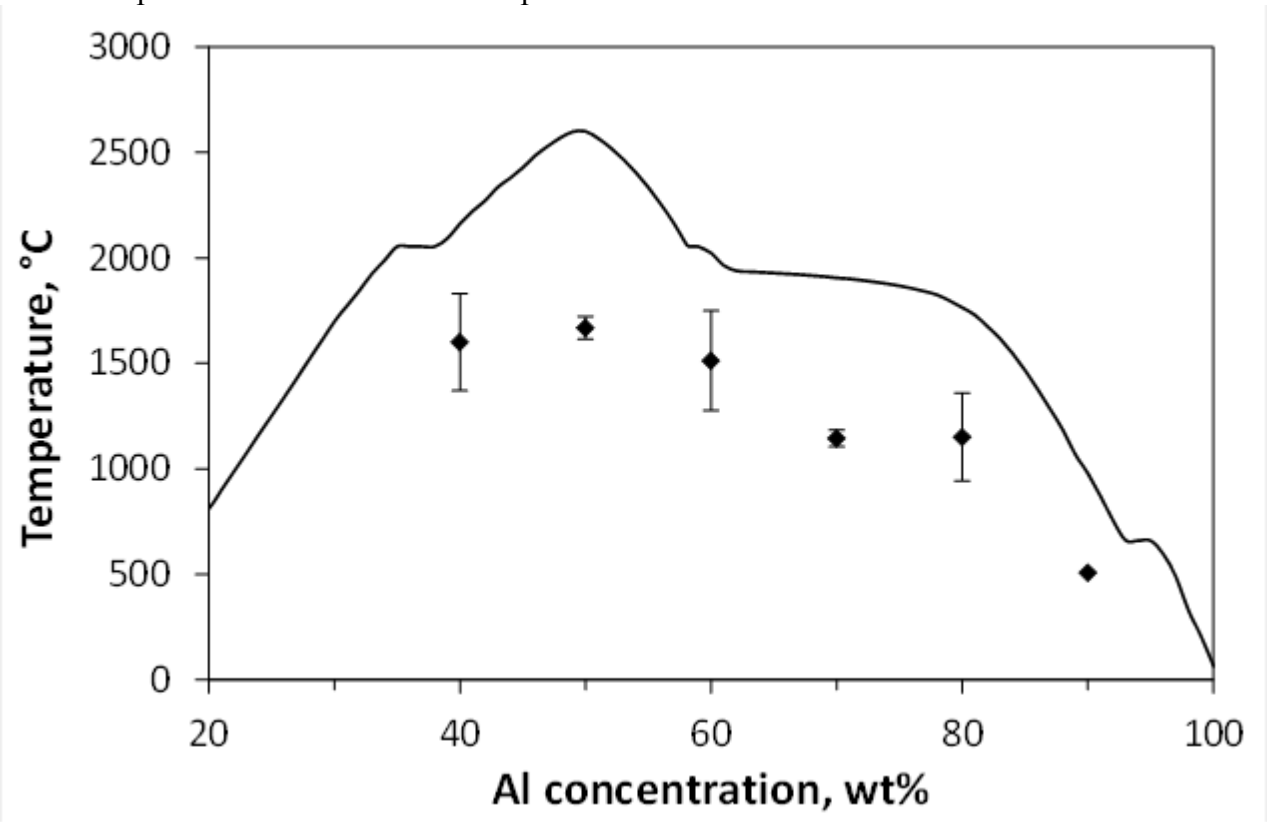

Figure 4.19: Maximum temperatures measured in the front (points) and calculated adiabatic flame temperatures (curve) for Al/H_2O mixtures.

Figure 4.20 shows the measured velocities of the front propagation. It is interesting that in the range of Al concentrations from 50 wt% to 80 wt%, the front velocity increases despite the decrease in the combustion temperature. This effect may be explained by the fact that the thermal diffusivity of solid Al (97.5 mm^2/s [79]) is higher by three orders of magnitude than that of liquid water (0.14 mm^2/s [79]). In the models of combustion wave propagation over Al-H_2O [55] and Mg-H_2O [48] mixtures, the difference in thermal diffusivities of the metal and water was taken into account but the increase in the front velocity moving away from the stoichiometry was not detected as only stoichiometric mixtures were analyzed.

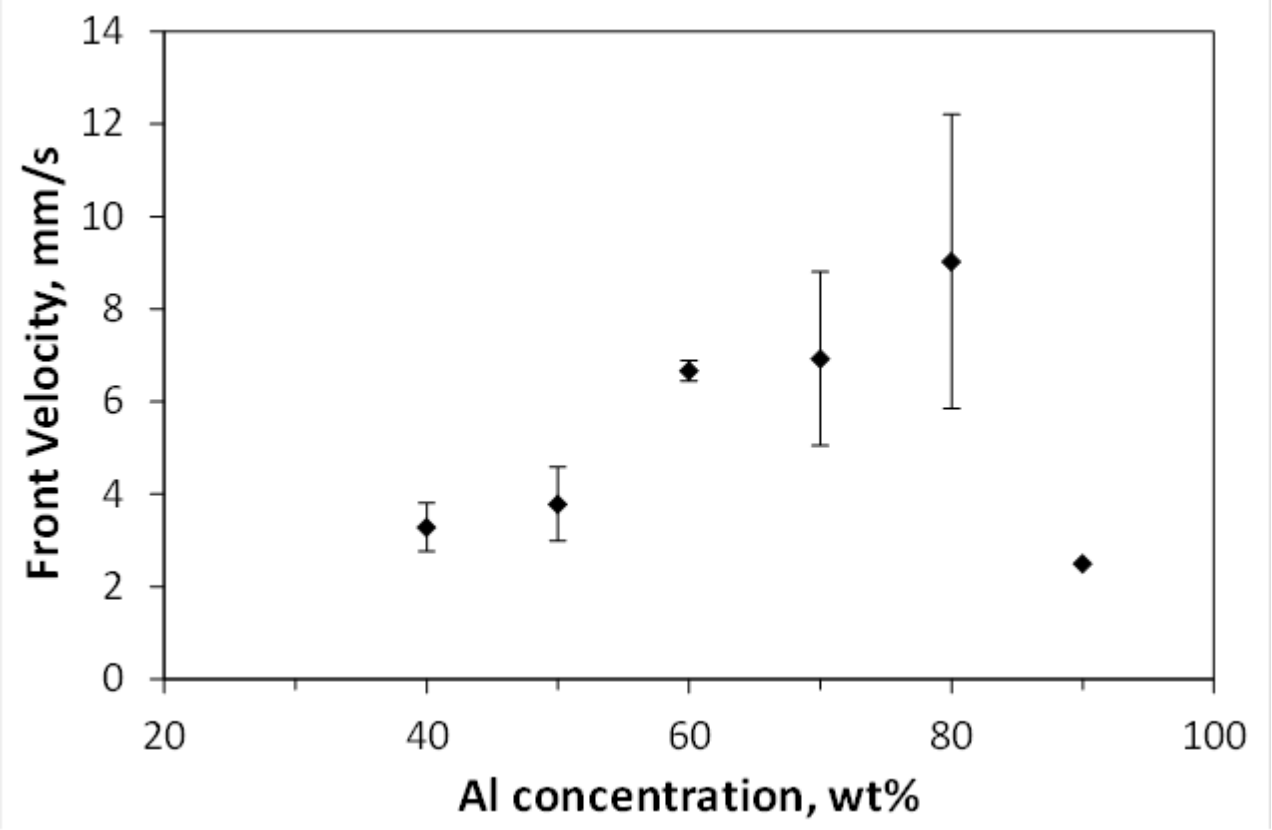

Figure 4.20: The front propagation velocities measured for Al/H_2O mixtures.

Figure 4.21 shows the EDS spectrum of the combustion products for Al/H_2O mixture (50 wt% Al). The obtained Al/O atomic ratio is close to Al/O ratio in Al_2O_3, which confirms the reaction as described in Eq. 3.

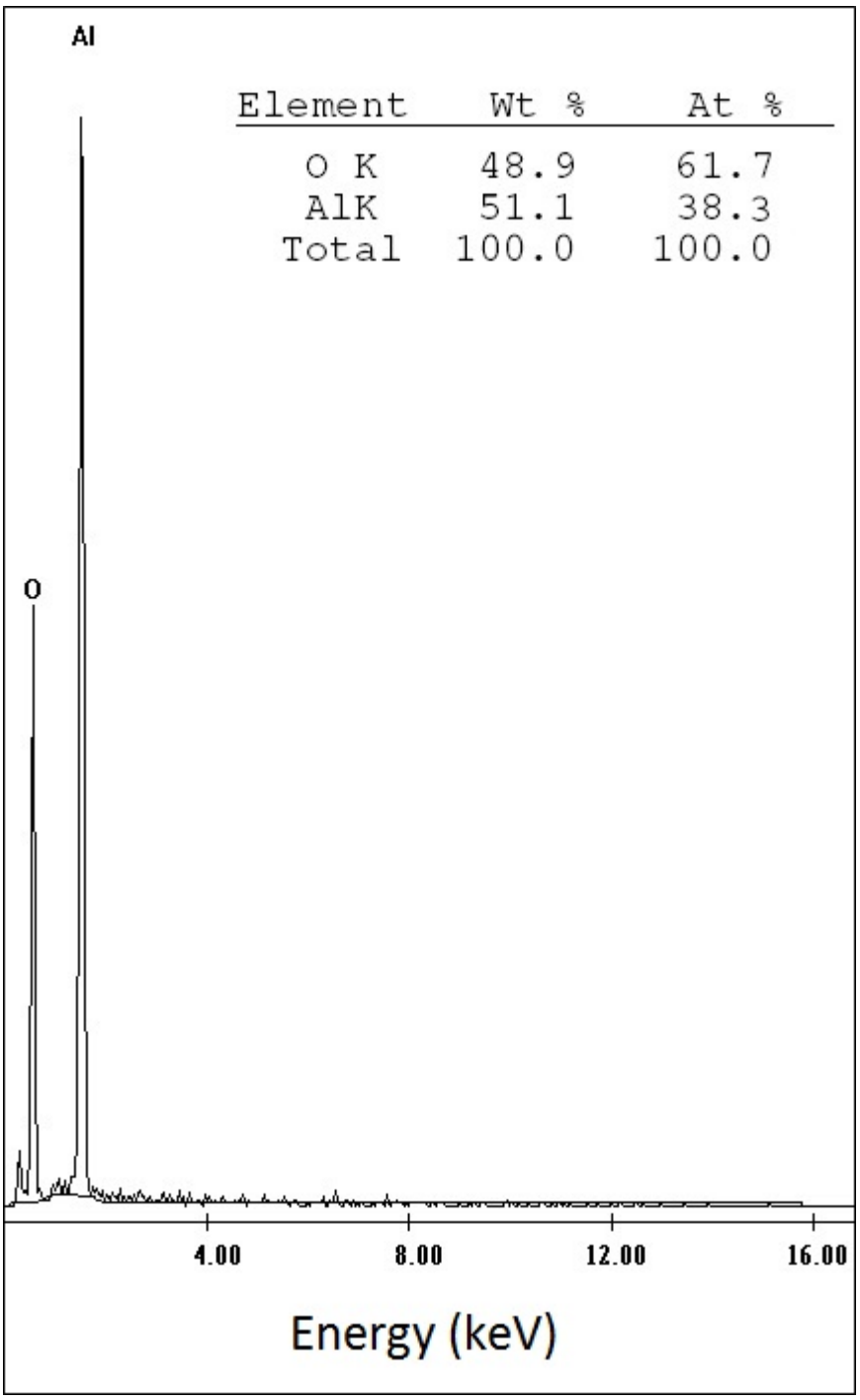

Figure 4.21: EDS spectrum of the combustion products for Al/H_2O mixture with 50 wt% Al.

Figure 4.22 shows XRD patterns of the combustion products for the mixtures with 40 wt% Al and 70 wt% Al. It is seen that some amount of unreacted Al is present in the products of the mixture with 40 wt% Al and that this amount increases with increasing Al concentration in the initial mixture, which is quite understandable. From the practical standpoint, the mixtures with Al concentrations 40–50

wt% are more attractive than those with a higher Al loading as they provide higher conversion efficiencies of Al. The traces of carbon detected on the XRD patterns originated from the plastic tubes, fragments of which were found in the combustion products.

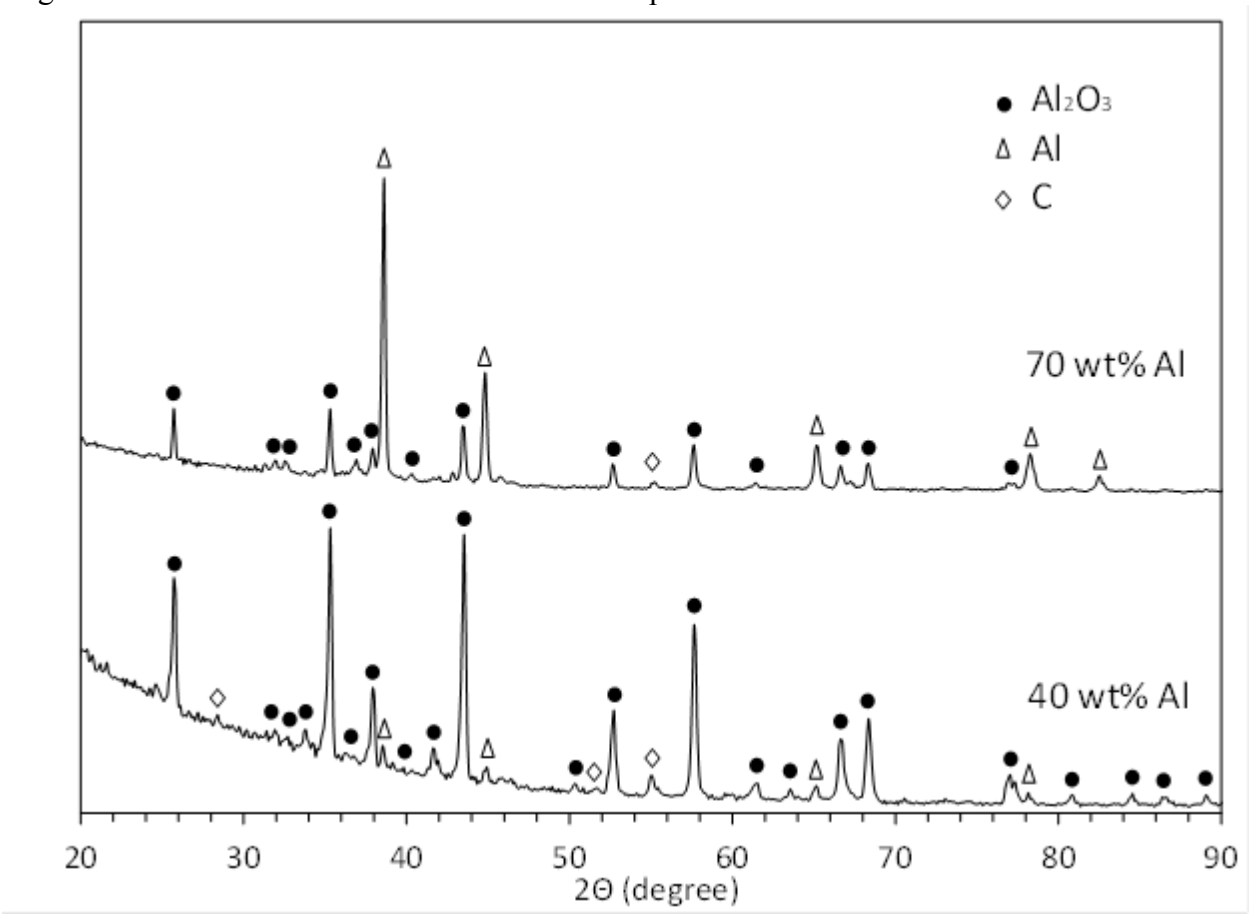

Figure 4.22: XRD patterns of the combustion products for Al/H_2O mixtures with 40 wt% Al and 70 wt% Al.

The measured combustion front velocities were compared with the data obtained for stoichiometric Al-H_2O compositions at a pressure of 1 atm (or 0.1 MPa) where water was gelified with 3 wt% polyacrylamide [45], [50]. The comparison shows that the front velocity for the micron-sized Al powder obtained from foil (4±1 mm/s) is between those for 120-nm Al powder (2 mm/s [45]) and for 38-nm Al powder (7 mm/s [50]). It is important that the 38-nm powder had active aluminum content as low as 54.3 wt% [50], while the micron-scale powder fabricated from foil has a much higher active Al content.

Note that conventional, commercially available micron-scale Al powders do not form combustible mixtures with water and their addition to nanoscale Al/water mixtures either prevents the ignition or dramatically decreases the burning rate [52], [53], [55].

4.7 Energy Considerations

The presented results confirm that through high-energy ball milling with NaCl, aluminum foil can be directly converted to a powder that readily reacts with water, releasing hydrogen. It is interesting to compare the energy required for milling of the Al foil with the energy that can be obtained from the generated hydrogen. In the presented experiments, the energy consumed by 30-min milling of a 4-g batch of Al foil was about 1800 kJ, i.e., about 450 kJ per gram of Al. The maximum theoretical yield of the reaction with water is 1.5 mol H_2 per mole of Al, i.e., 0.111 g H_2 per gram of Al, and the higher heating value of H_2 is 142 kJ per gram of H_2. Thus, the maximum energy that can be obtained from the produced hydrogen is 15.8 kJ per gram of Al, i.e., only 3.5% of the energy consumed for milling. The milled amount, however, could be increased by a factor of 5 in the same mill, which would increase the energy efficiency to 17.5%. Further optimization of the milling procedure could also increase the energy efficiency. Finally, it is expected that scale-up of the milling process for industrial applications will significantly reduce the required energy per unit mass of Al.

Note that in energy storage applications, the stored energy may remain significantly lower than the energy required for fabricating the energy carrier. For example, nuclear, hydroelectric, and other power plants generate unnecessary power during low-demand periods. This extra power can be used for fabricating energy carriers that could provide power during high-demand periods. This scheme is attractive even if the generated energy is less than the energy consumed for fabricating the carriers.

Also, for portable hydrogen storage systems and energetic materials, the most important characteristics are the energy per unit mass and the energy per unit volume. The use of activated Al powders could be especially attractive in applications using off-board or recycled water. Aluminum-water reactions provide 300 g H_2 per liter of Al. For comparison, the volumetric hydrogen capacities of compressed hydrogen gas at 700 bar, liquid hydrogen, and such a promising compound as ammonia borane are 30 g/L, 70 g/L, and 150 g/L, respectively [80].

4.8 SUMMARY

It has been demonstrated experimentally that high-energy ball milling of aluminum foil (thickness: 15–100 μm) with sodium chloride produces a powder that readily reacts with hot water, releasing hydrogen. After washing NaCl out of this powder, using cold water or methanol, the remaining Al powder retains the high reactivity with respect to hot water.

The reactions of the obtained powders with deionized water have been studied over a temperature range of 35–80 °C. Milling in inert (argon) environment increases the final reaction extent up to 98%. It has been shown that the induction period is longer for the leached (salt-free) powders, apparently due to aluminum oxidation during drying that follows the leaching process. The oxidation during drying may also explain the decreased reaction extent for the powders leached by either water or methanol.

The effective activation energy of the reaction between the obtained aluminum powders and water has been determined using the temperature dependence of the maximum reaction rate. The obtained value, 63.1 ± 3.1 kJ/mol, is in a good agreement with the data obtained previously for Al powders activated by ball milling with graphite.

The obtained activated Al powder was mixed with gelled (3 wt% polyacrylamide) water over a wide range of Al–H_2O mass ratios and combustion of these mixtures was studied in argon environment at 1 atm. Stable propagation of the combustion front was observed at Al concentrations from 40 wt% to 80 wt%. With increasing Al concentration, the combustion front velocity increased despite the decrease in the combustion temperature, apparently due to the high thermal diffusivity of Al. The obtained micron-scale Al powders provide the combustion front velocities that are comparable with those for nanoscale Al powders, while offering a higher content of active aluminum.

The conversion of aluminum foil to activated powders may help mitigate the problem of growing surplus of Al scrap and waste in the U.S. The obtained powder could be used for low-temperature and combustion reactions with water in various applications.

Chapter 5: Results-Gallium Oxide Synthesis

5.1 Characterization of Ball Milled GaN Powders

Figure 5.1 shows the SEM microphotographs of the GaN powders. Figure 5.1a shows the original GaN powder, while fig. 5.1b shows the planetary ball milled GaN powder at the same magnification. It can be clearly seen that ball milling does reduce particle size and makes the powder more uniform. The average particle size of the ball milled GaN powder is less than 1 μm. Figure 5.1c demonstrates that many particles in this powder are as small as 100 nm.

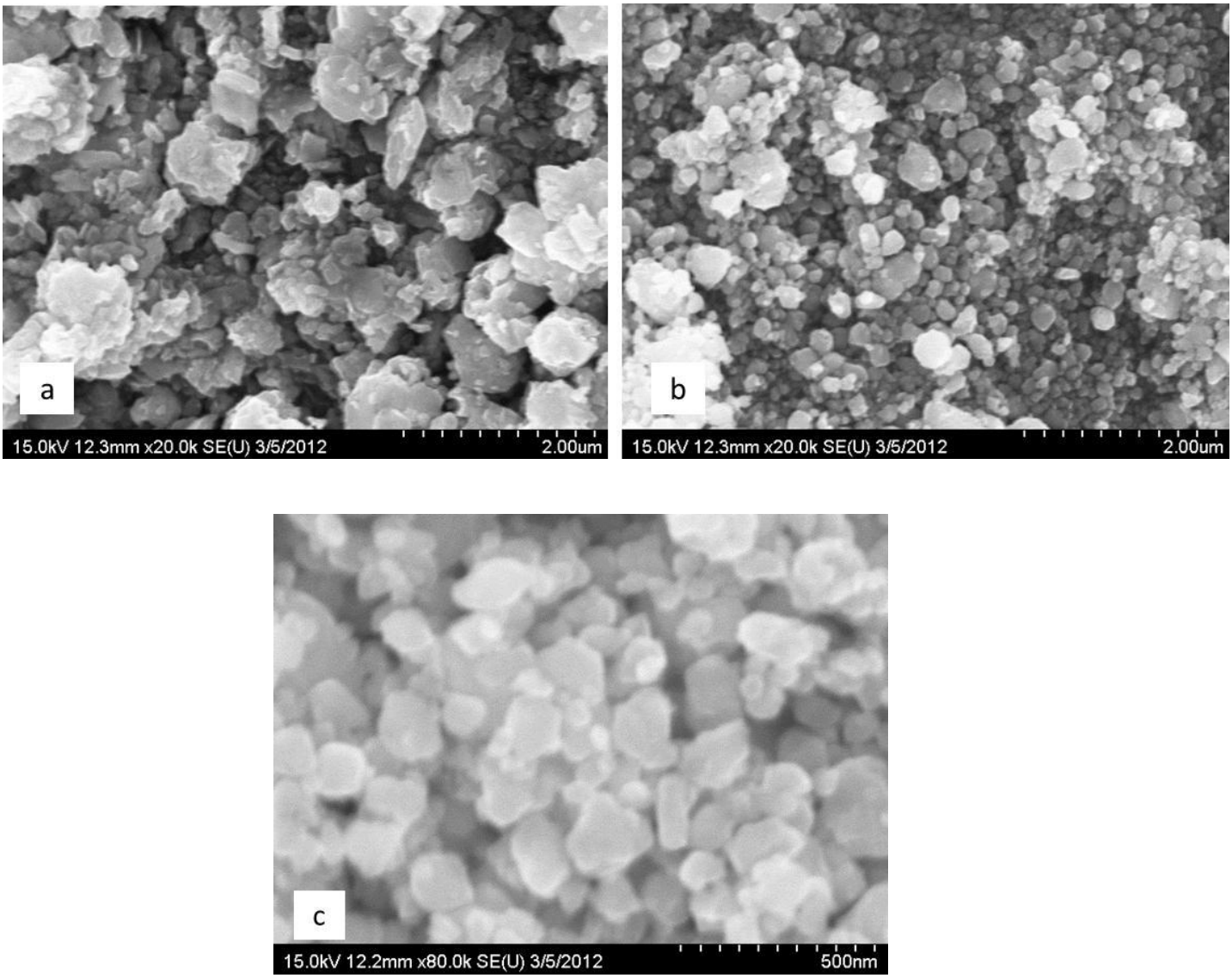

Figure 5.1: SEM microphotographs of GaN powders: (a) Original GaN powder, (b) Ball milled GaN powder, and (c) Ball milled GaN powder at higher magnification.

Figure 5.2 shows a comparison between the XRD patterns of the original GaN powder and the planetary ball milled GaN powders. It is seen that the 04/13/12 GaN powder peaks (black) are much smaller than the original GaN powder peaks (green). This indicates that ball milling does induce a reduction in particle size by repeated fracturing and cold welding of GaN particles. This result is coherent with the results shown in previous research [45]. It should be noted, however, that the milling time is significantly shorter (70 min) in the present research as compared to previous studies (10h, 20h, and 40h [45]). For the present research, all GaN powders used were milled using the parameters mentioned for 04/13/12 powder.

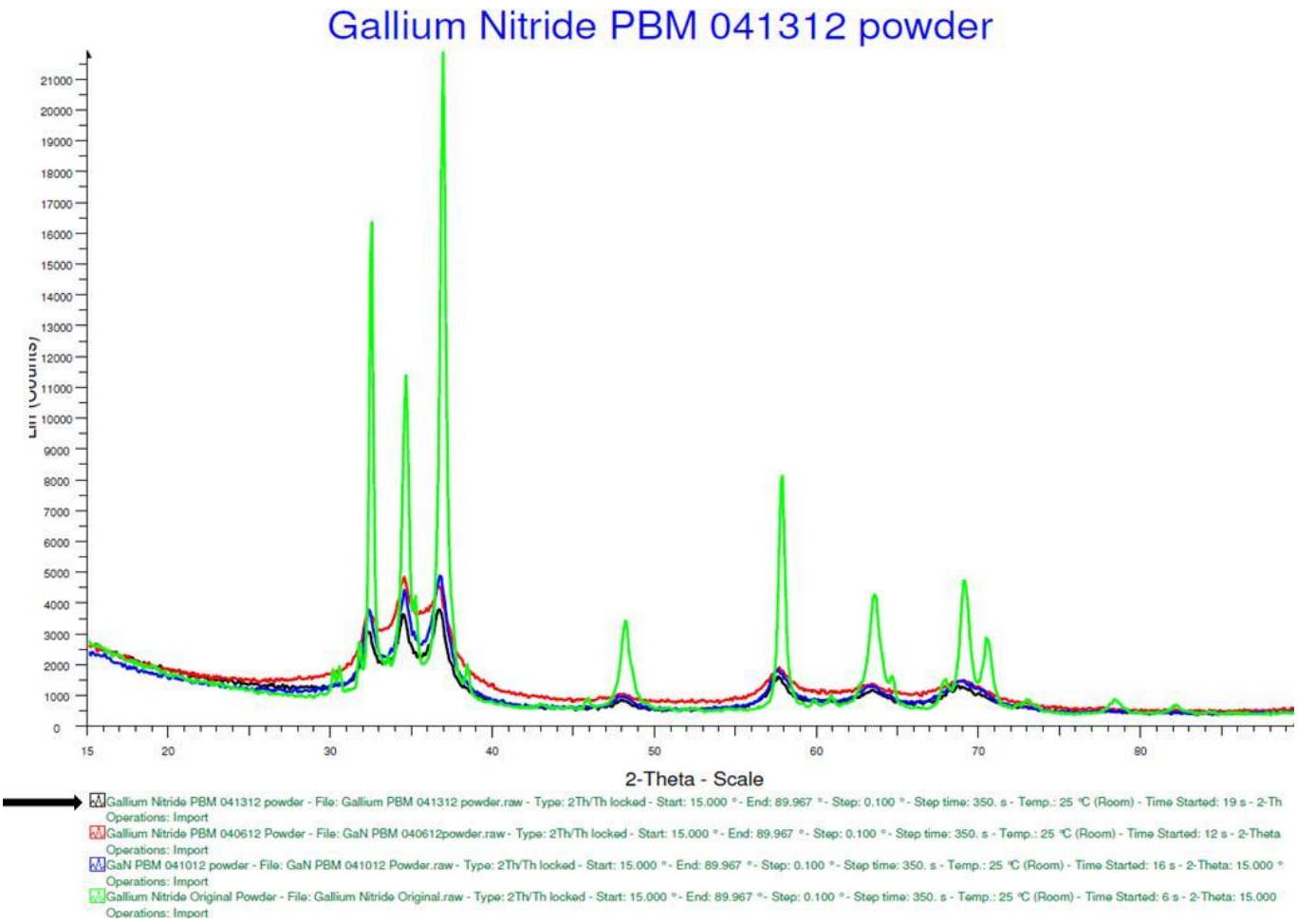

Figure 5.2: XRD pattern of the GaN powders showing comparison of the peaks obtained for different milling parameters: (a) Green peaks: Original powder and (b) Black peaks: 04/13/12 powder (see section 3.2.1)

The amount of ball milled GaN powder obtained was not sufficient to perform BET specific surface area analysis. The surface area analysis will be performed in the future as mentioned in the proposed plan of work.

5.2 Oxidation Reactions of Ball Milled GaN Powders

During the initial heating experiments, it was noted that the tube furnace was not properly sealed. As such, excess air leaked into the furnace during the heating and all GaN was converted to a white powder. XRD analysis confirmed the presence of β-Ga_2O_3 in the powder. SEM microphotographs showed the presence of nano particles. However, nano belts or nano ribbons were not found in the powder. Thus, to prevent excessive air leakage into the furnace, the end caps were sealed using vacuum grease. All experiments were run assuming that there was no air leakage into the system.

5.2.1 Case 1

Figure 5.3 shows the SEM microphotographs of the obtained products. Nanobelts are seen in fig. 5.3a, b, and c. Nano sheet-like structures are seen is fig. 5.3b. A unique saw-like structure is seen in fig. 5.4d. Preliminary observations using SEM software Quartz PCI revealed that the belts had a width in the range of 10-15 nm and were several microns long. Other nano particles seen in the images are spherical in shape and more uniform.

EDS analysis of an area of the image shows the presence of gallium, nitrogen, and oxygen (fig. 5.4b). Thus, not all GaN powder was converted to Ga_2O_3. Spot analysis of the nanobelts using EDS confirmed the presence of Ga and O (fig. 5.4a). Elemental analysis suggests that the nanobelts consist of Ga_2O_3.

XRD analysis of the reaction products showed peaks consistent with Ga0.97N0.9O0.09 (fig 5.5). However, very few nanobelts can be seen from the SEM images. A possible reason for this is the use of high-purity nitrogen and not ultra-high purity nitrogen as suggested by Lee *et al* [45]. High-purity nitrogen has heavy oxygen super saturation which hinders the growth of nano structures. The aim of the present research is to increase the yield of β-Ga_2O_3. Thus different cases have been taken into account.

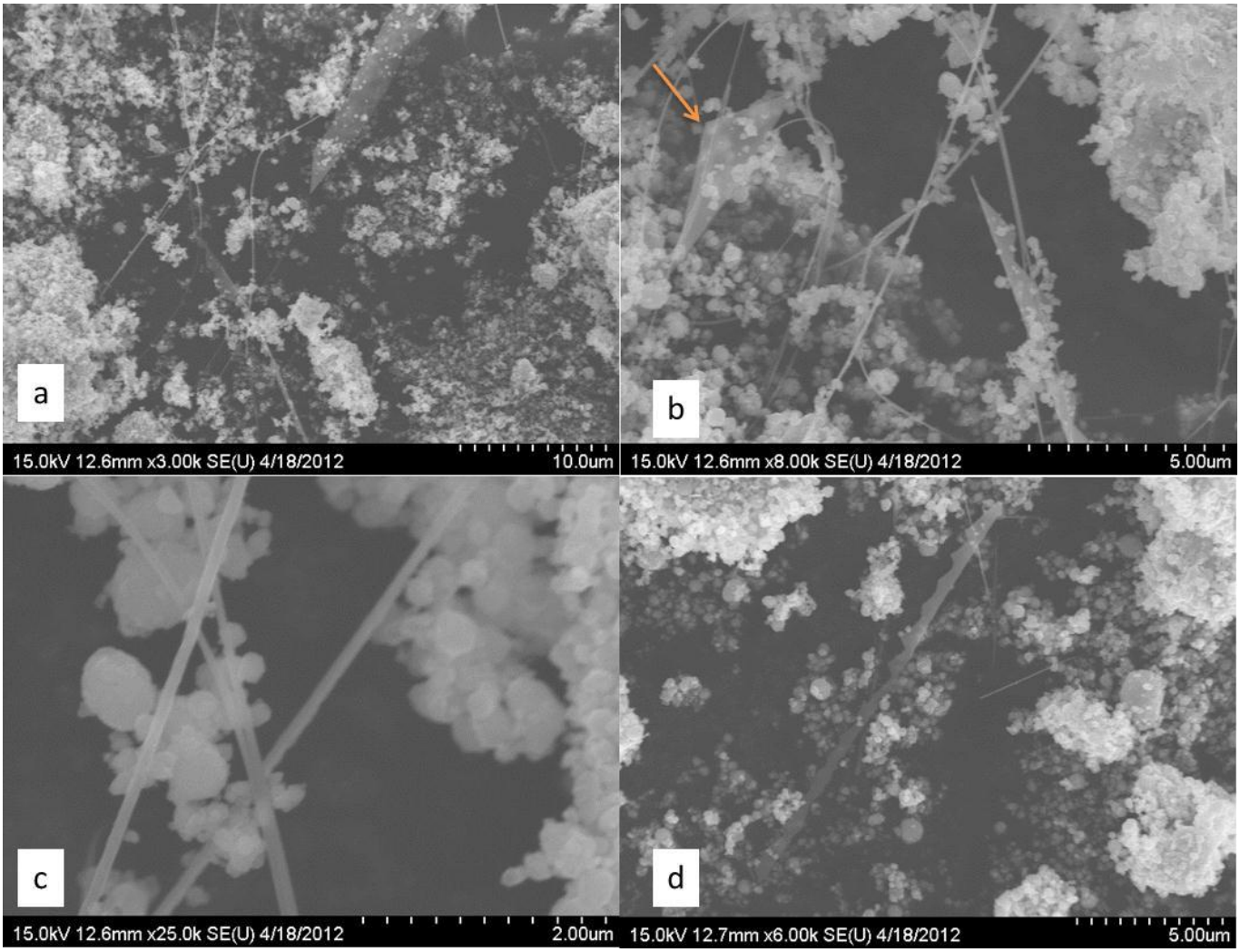

Figure 5.3: SEM microphotographs of the reaction products obtained by heating ball milled GaN powder in a tube furnace: (a) nanobelts seen, (b) sheet like structures (see arrow), (c) magnified view of the belts, and (d) saw-like nano structures

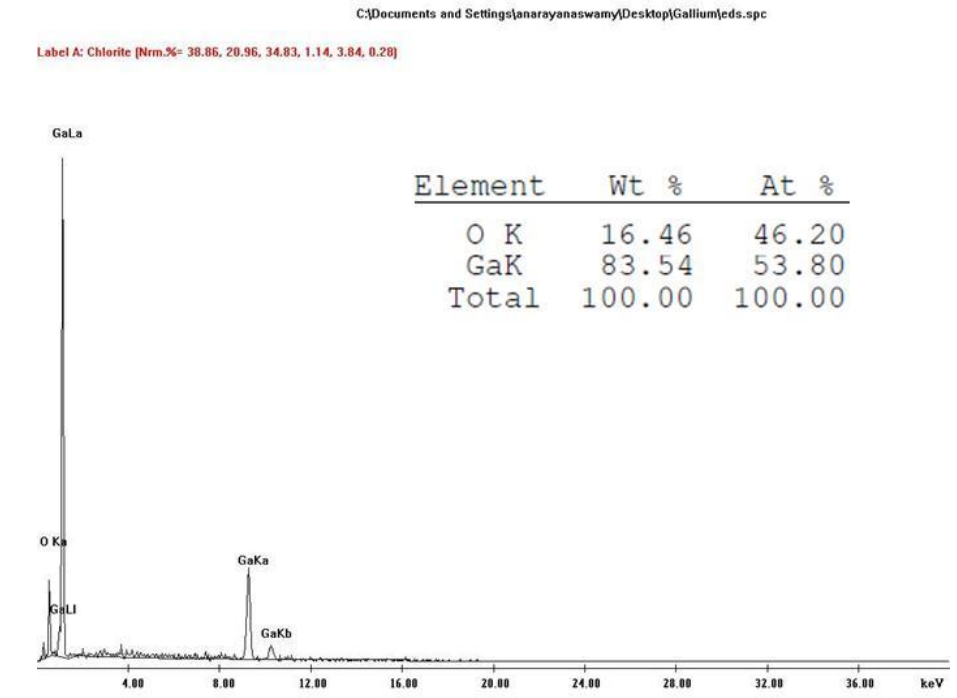

Element	Wt %	At %
O K	16.46	46.20
GaK	83.54	53.80
Total	100.00	100.00

(a)

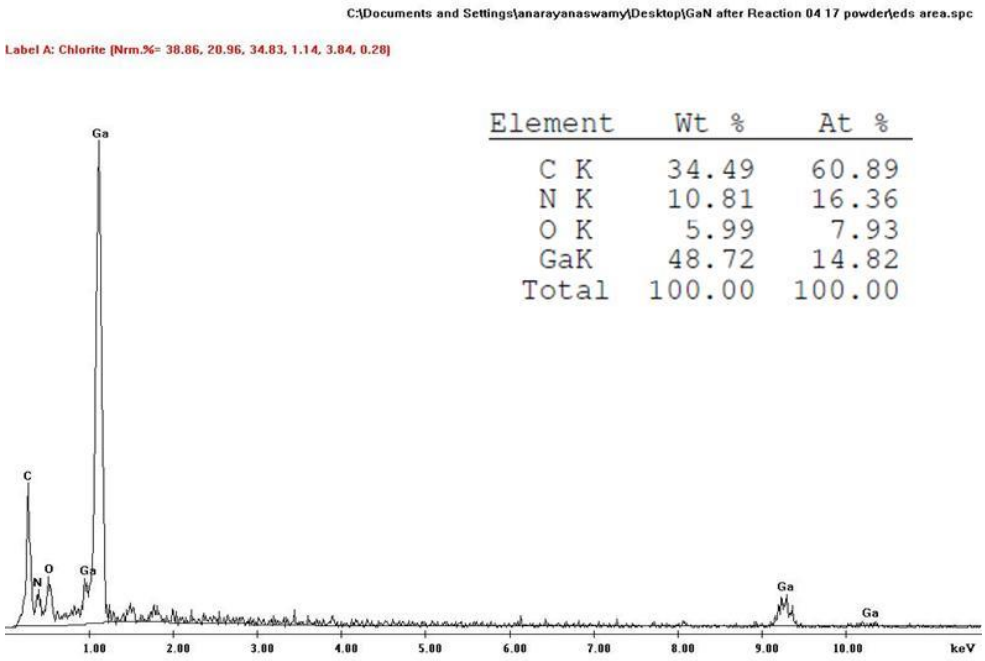

Element	Wt %	At %
C K	34.49	60.89
N K	10.81	16.36
O K	5.99	7.93
GaK	48.72	14.82
Total	100.00	100.00

(b)

Figure 5.4: EDS spectra of the reaction products (a) EDS spectrum of the nanobelts by spot analysis (b) EDS spectrum of the obtained powder by area analysis

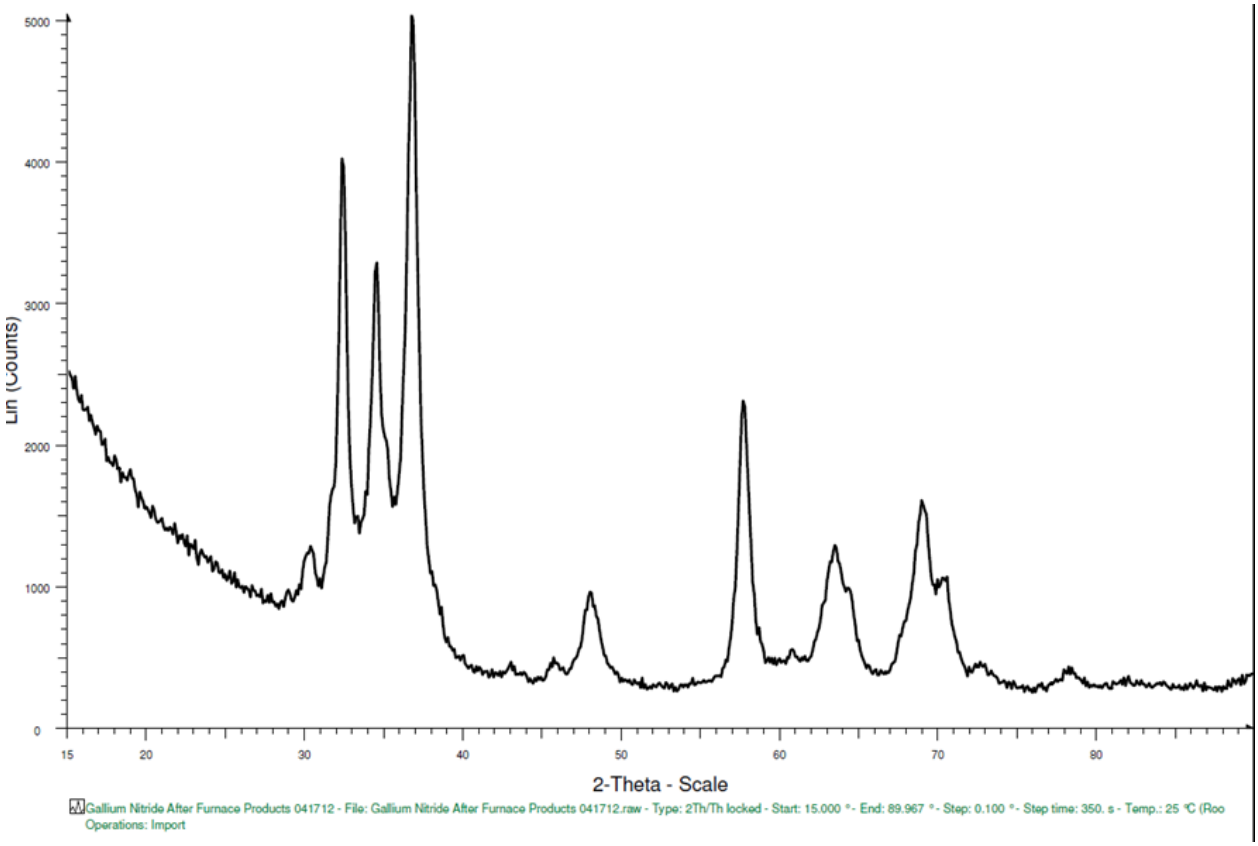

Figure 5.5 XRD pattern of the reaction products obtained by heating GaN powder: peaks consistent with $Ga_{0.97}N_{0.9}O_{0.09}$.

5.2.2 Case 2

To see the effect of small carrier gas molecules, high-purity helium gas was used for heating experiments instead of nitrogen. It was assumed that the helium molecules can penetrate better into the GaN matrix than nitrogen molecules owing to their diminutive size. Figure 5.6 shows the SEM microphotographs of the products. No nanobelts or other nanostructures can be seen. Again, this may be attributed to the insufficient purity of the helium gas used. For all cases presented henceforth, an ultra-high purity nitrogen gas is used for heating experiments.

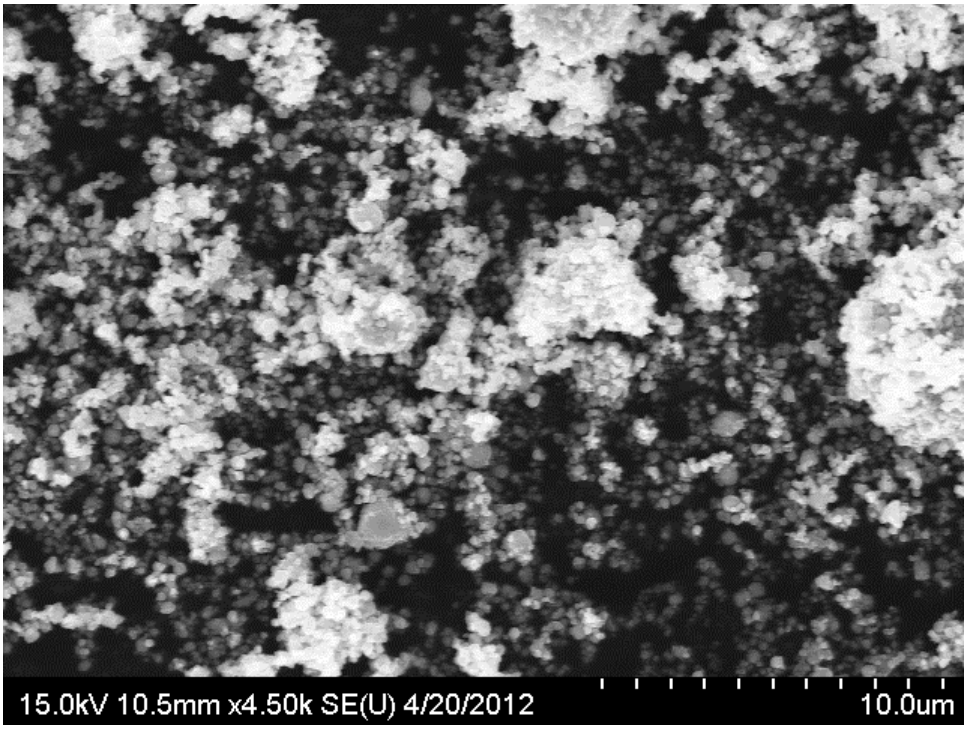

Figure 5.6: SEM microphotograph of the reaction products obtained by heating ball milled GaN powder in a helium atmosphere

5.2.3 Case 3

For this case, a pellet was compacted out of 1.5 g of PBM GaN powder by applying a load of 2 tons in a uniaxial hydraulic press. After the heating experiment, the pellet was retrieved and placed in the SEM sample holder. No nanostructures were found. Unreacted GaN powder was found in the product indicating that the experiment was unsuccessful. Moreover, the pellet broke during sample handling. For case 4, the applied load was increased to 3 tons to prevent any fracture of the pellet.

5.2.4 Case 4

Figure 5.7 shows the SEM microphotographs of the pellet retrieved after the combustion experiment. Figure 5.7a shows a closely packed structure of the obtained products. Nanorod-like structures can be seen (fig. 5.7b) embedded inside a powder matrix. EDS analysis of the rod-shaped structures showed the presence of Ga and O (see table 5.1). Figure 5.7c shows thin sheet-like structures on the surface of the pellet. These structures consist of Ga, O, and traces of N as confirmed by XRD. From the analysis of the results obtained in cases 3 and 4, it is evident that compaction of the ball milled

GaN powder did not have any significant changes towards the yield of nanostructures. In both cases, most of the powder remained unreacted even at high temperatures (> 1000 °C). This contradicts the results reported by Jung *et al* [48] where compaction increased the yield of nanostructures.

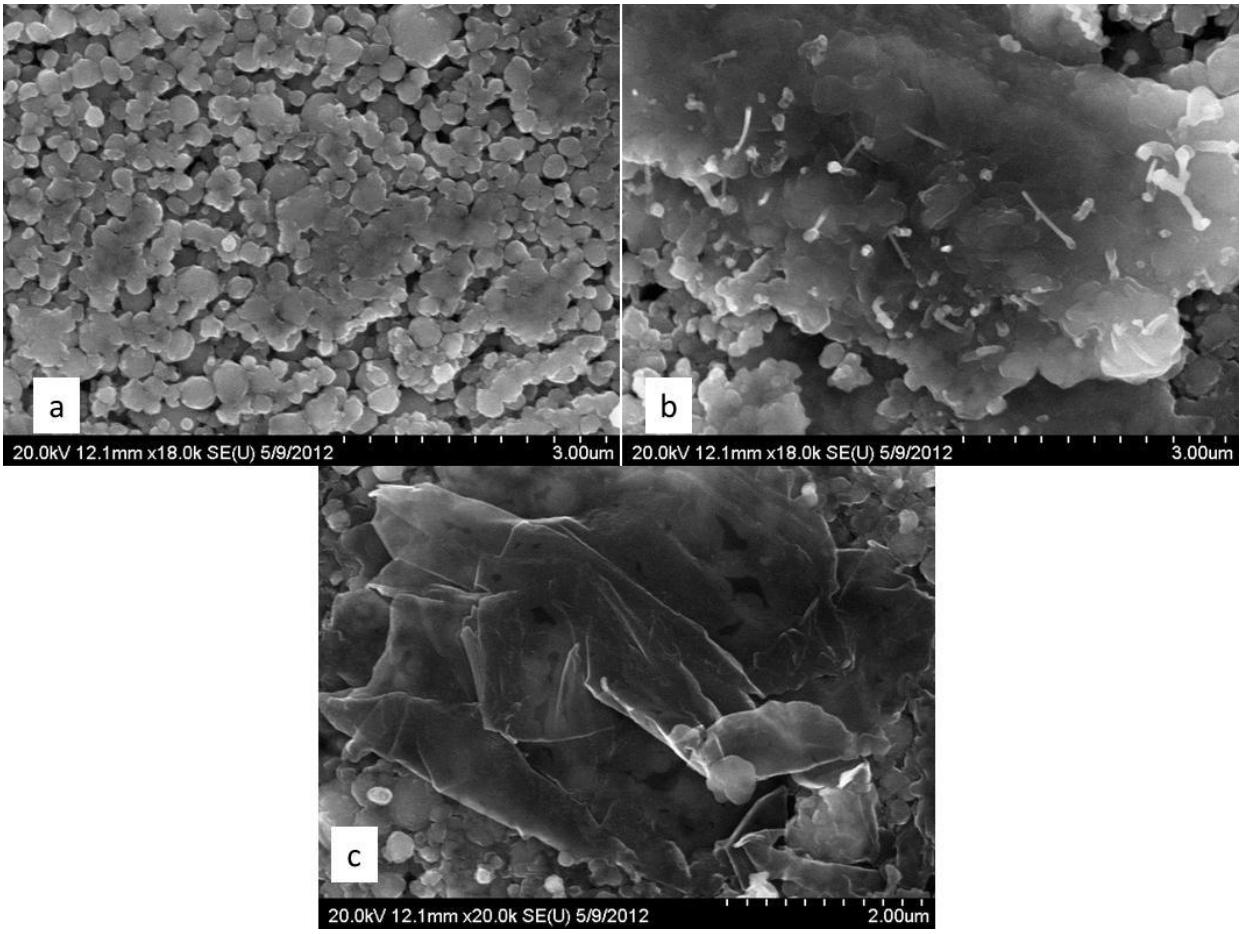

Figure 5.7: SEM microphotographs of the reaction products obtained by heating GaN pellet: (a) closely pack structure, (b) small, wire-like structures embedded in a dense powder matrix, and (c) thin sheet-like structures on the surface of the pellet

Table 5.1 Elemental composition of nano structures seen in fig. 5.7b obtained from spot analysis using EDS

Element	wt %	at %
O	33.16	68.38
Ga	66.84	31.62
Total	100.00	100.00

5.2.5 Case 5

Figure 5.8 shows images of the alumina crucible after retrieval from the furnace. White wool-like structures can be seen on the outer rim of the crucible (fig. 5.8a). Yellow unreacted GaN powder is seen inside the crucible (fig 5.8b).

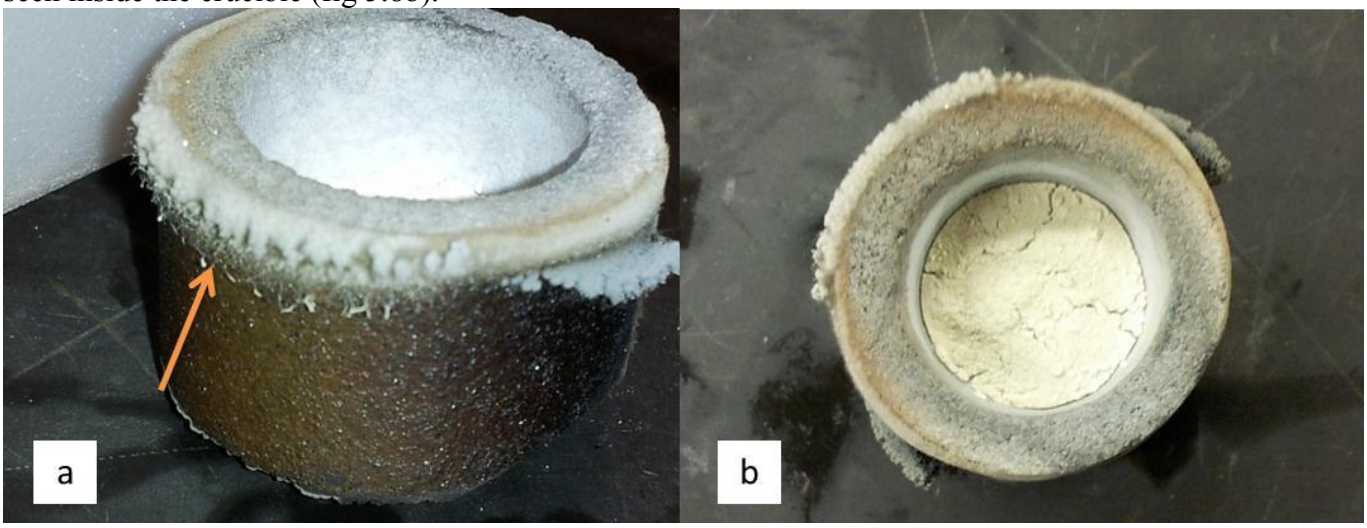

Figure 5.8: Digital photographs of the alumina crucible retrieved after heating ball milled GaN powder: (a) white wool like structures on the outer rim of the crucible, and (b) top view of the crucible with unreacted GaN powder inside

Figure 5.9 shows the SEM microphotographs of the white wool like products. Figure 5.9a shows extensive belts/wire like structures, while fig. 5.9b shows thick rod-shaped structures.

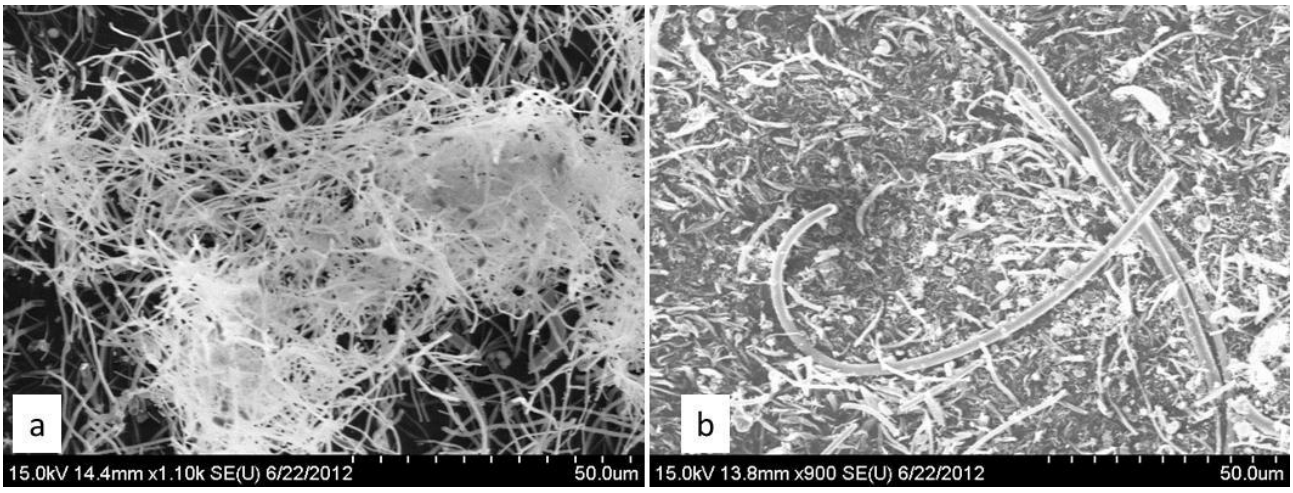

Figure 5.9: SEM microphotographs of the reaction products obtained by heating ball milled GaN powder: (a) Extensive belts/wire like structures, and (b) rod-like structures

EDS analysis of the wool-like products confirmed the presence of Ga, O and traces of silicon (Si). Upon further investigation it was found that the silicon was originated from the rings at the end of the tube furnace. The dimensions of the nano rods/wires were determined using the software Quartz PCI. The rods were 250-300 nm thick and several microns long. The large thickness can be attributed to the presence of Si on the outer layer of the Ga_2O_3 nano belts. The products were weighed using a micro balance (Mettler Toledo). The mass of the white wool-like products was 0.1 g whereas the mass of the unreacted GaN powder was 0.4 g.

Analysis of the products indicates that a shorter heating time and a higher furnace temperature lead to an increased yield of nanostructures.

5.2.6 Case 6

Figure 5.10 shows SEM microphotographs of the products obtained after heating GaN powders in N_2 atmosphere and subsequent cooling in air. Rod-like dentate-shaped structures can be seen in fig, 5.10a. Figure 5.10b shows nanorods, nanosheets, and nanoparticles. A single nanorod growing from a powder matrix can be seen in fig. 5.10c. Fig. 5.10d shows triangular and rectangular sheets amongst nano particles. These sheets have an average width of about 4 μm and a length of 10 μm.

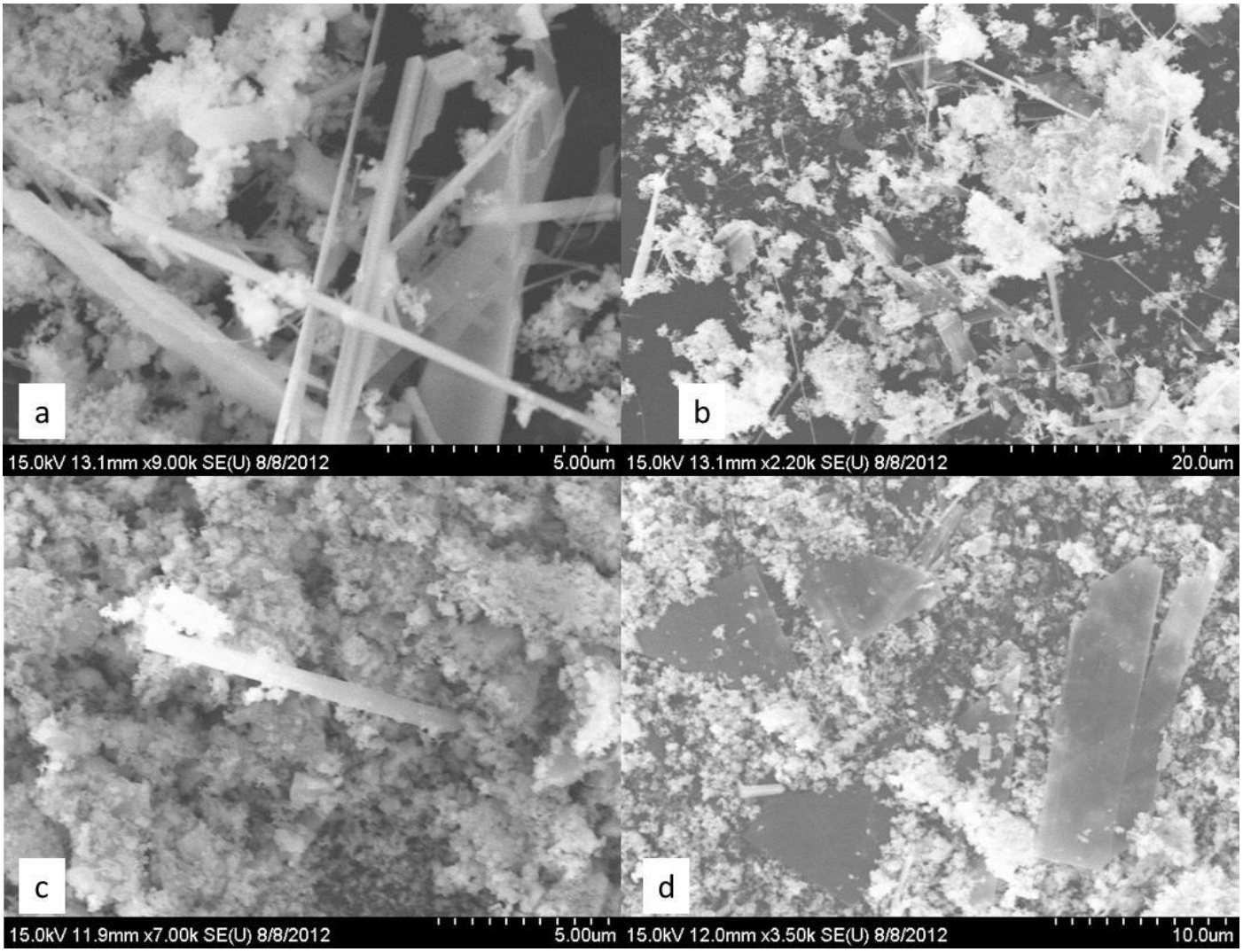

Figure 5.10: SEM microphotographs of the products obtained by haeting GaN powder: (a) three-dimensional nanorods of different sizes, (b) nanorods, nanosheets, nanowires seen in between agglomerated particles, (c) close up view of a nanorod grown from the GaN nanoparticles, and (d) clusters of sheets

EDS analysis of the sheets is presented in fig. 5.11. Elemental composition shows the presence of Ga and O. XRD pattern of the products is shown in figure 5.12. The peaks indicate the presence of β-Ga_2O_3 (red lines) and GaN (green lines). This explains the presence of gallium oxide structures dispersed in a GaN matrix. An important finding in the present research is the presence of nanostructures in the products after the tube furnace was exposed to air. This means that excessive air leakage into the chamber did not completely stop the formation of nano rod/wire like structures.

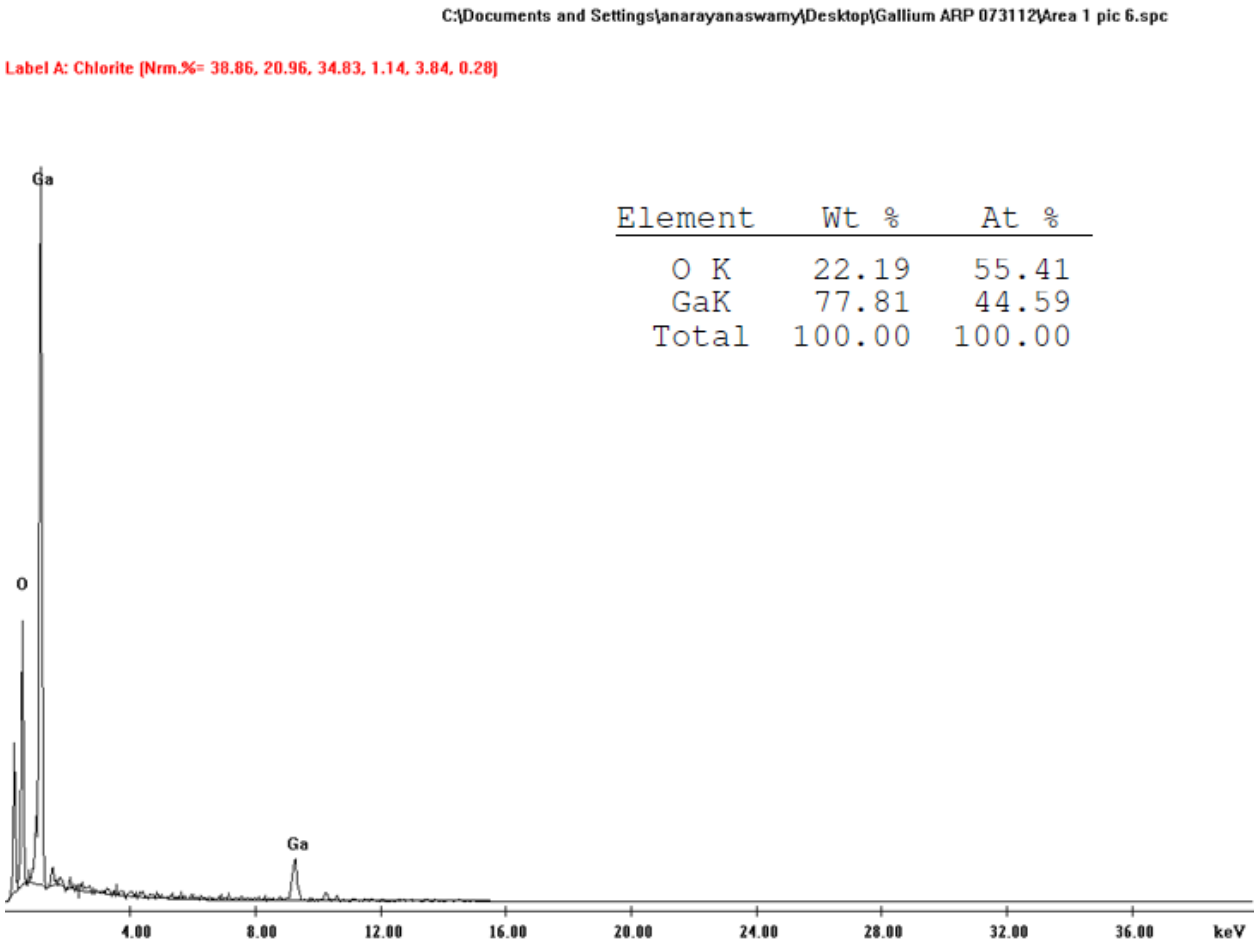

Figure 5.11: EDS spectra using area analysis of the nanosheets shown in fig. 5.10d: (inset: elemental composition)

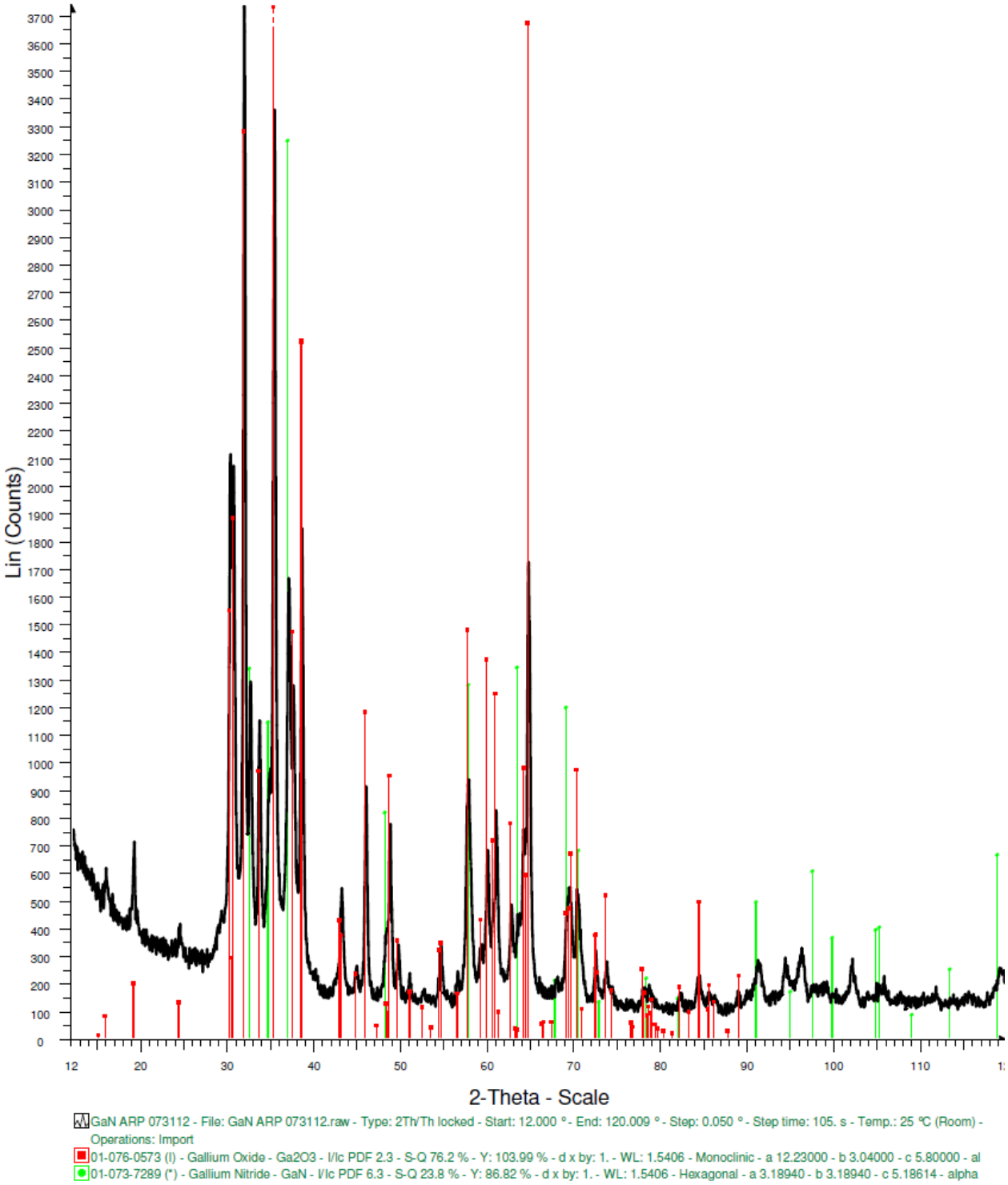

Figure 5.12: XRD pattern of the products obtained by heating GaN powder: red lines show presence of β-Ga_2O_3 mixed with unreacted GaN powder (green lines)

5.3 SUMMARY

β-Ga_2O_3 nano structures were successfully synthesized by GaN powders using a simple method. Ball milling of GaN powders reduced the particle size and made the powder more uniform. It was also found that the growth of nanostructures depends on the purity of the carrier gas used. Higher furnace temperatures and shorter annealing times resulted in higher yields of the nanostructures. A vapor-solid mechanism is apparently the growth route for the obtained nanomaterials.

.

Chapter 6: Conclusions

High-energy mechanical milling is an advanced powder processing technique for the production of homogeneous materials. Mechanical milling can reduce particle size to nano-range, can cause alloying of two elemental phases, or lower the reaction temperature of the powders. In this thesis, this technique has been successfully employed for the synthesis of activated aluminum (Al) powder from foil and β-Gallium Oxide (β-Ga_2O_3) nano-structures from gallium nitride (GaN).

A reactive Al powder was produced by milling Al foil with sodium chloride (NaCl) in an air environment for a short milling duration. The obtained powders were reacted with warm deionized water over a temperature range of 35-80°C. A maximum reaction extent of 93% (hydrogen yield per gram of Al) was achieved. The NaCl as removed from the Al powders by washing in cold water. The resulting powders retained high reactivity with respect to hot water. The reaction extent was lower for leached (salt-free) powders due to additional oxidation during the drying that follows the leaching process. Milling in an inert argon environment increased the final reaction extent to 98%. This was explained by the fact that argon reduced the oxidation of Al during the milling process. This was confirmed by using energy dispersive spectroscopy (EDS) analysis.

The obtained activated Al powder was mixed with gelled (3 wt% polyacrylamide) water over a wide range of Al–H_2O mass ratios and combustion of these mixtures was studied in argon environment at 1 atm. Stable propagation of the combustion front was observed at Al concentrations from 40 wt% to 80 wt%. With increasing Al concentration, the combustion front velocity increased despite the decrease in the combustion temperature, apparently due to the high thermal diffusivity of Al. The obtained micron-scale Al powders provide the combustion front velocities that are comparable with those for nanoscale Al powders, while offering a higher content of active aluminum.

The conversion of aluminum foil to activated powders may help mitigate the problem of growing surplus of Al scrap and waste in the U.S. The obtained powder could be used for low-temperature and combustion reactions with water in various applications.

Synthesis of Ga_2O_3 nanostructures from GaN powder through high-energy mechanical milling and annealing in nitrogen was investigated. The employed high-energy milling of GaN powder reduced

the particle size to sub-micron range and made the powder more uniform. The use of high-energy milling dramatically shortened the milling time as compared to conventional ball milling procedures. When annealing was conducted in ultra-high purity (O_2 < 1 ppb) nitrogen flow, a variety of Ga_2O_3 one-dimensional nanostructures such as rods, belts, sheets, and leaf-like shapes were obtained. The formation and growth of gallium oxide nanostructures during annealing of GaN in nitrogen gas is explained by thermal decomposition of GaN followed by reaction of gallium atoms with oxygen present in the gas flow. When the oxygen content in the gas exceeds some value, the competing process of heterogeneous oxidation of GaN prevails over the growth of Ga_2O_3 one-dimensional nanostructures via a vapor-solid mechanism.

These results are important for practical applications as Ga_2O_3 based materials are widely used in the field of nano-electronics.

Bibliography

[1] "World Nuclear Association," June 2010. [Online]. Available: http://www.world-nuclear.org/info/inf70.html. [Accessed 10 August 2012].

[2] E. T. T. Center, "Hydrogen Fuel Cell Engines and Related Technologies," December 2001. [Online]. Available: http://www1.eere.energy.gov/hydrogenandfuelcells/tech_validation/pdfs/fcm00r0.pdf. [Accessed 10 August 2012].

[3] C. A. Powell and B. D. Morreale, "Materials Challenges in Advanced Coal Conversion Technologies," *Materials Research Society Bulletin,* vol. 33, p. 309, 2008.

[4] N. Docquier and S. Candel, "Combustion Control and Sensors: A Review," *Progress in Energy and Combustion Science,* vol. 28, p. 107, 2002.

[5] P. Walker and W. H. Tarn, CRC Handbook of Metal Etchants, Florida: CRC Press LLC, 1990.

[6] G. Favero and P. Jobstraibizer, "The Distribution of Aluminum in the Earth: from Cosomogenesis to Sial Evolution," *Coordinated Chemical Review,* vol. 149, pp. 367-400, 1996.

[7] P. F. Pokhil, A. F. Belyaev, Y. V. Frolov, V. S. Logachev and A. I. Korotkov, Combustion of Powdered Metals in Active Media, Foreign Technology Division, 1973.

[8] F. K. Shan, G. X. Liv, W. J. Lee, G. H. Lee, I. S. Kim and B. C. Shiw, "Structural, Electrical and Optical Properties of Transparent Gallium Oxide Thin Films Grown by Plasma Enhanced Atomic Layer Deposition," *Journal of Applied Physics,* vol. 98, pp. 023504-6, 2005.

[9] M. Ogita, K. Kobayashi, Y. Yamada, Y. Nakanishi and Y. Hatanaka, "Properties of Gallium Oxide Thin Film Sputtered from Powder Target for High Temperature Oxygen Sensor," in *The 27th Annual Conference of the IEEE Industrial Electronics Society*, Colorado, 2001.

[10] C. Suryanarayana, "Mechanical Alloying and Milling," *Progress in Materials Science,* vol. 46, no. 1-2, pp. 1-184, 2001.

[11] C. C. Koch, O. B. Cavin, C. G. McKamey and J. O. Scarbrough, "Preparation of Amorphous Ni60Nb40 by Mechanical Alloying," *Applied Physics Letters,* vol. 43, pp. 1017-9, 1983.

[12] G. B. Schaffer and P. G. McCormick, "Reduction of Metal Oxides by Mechanial Alloying," *Applied Physics Letters,* vol. 55, pp. 45-6, 1989.

[13] W. Wang, "Ph.D. Thesis," University of Waikato, Waikato, NZ, 2000.

[14] K. Blok, R. H. Williams, R. E. Katofsky and C. A. Hendriks, "Hydrogen Production From Natural Gas, Sequestration of Recovered CO2 in Depleted Gas Wells and Enhanced Natural Gas Recovery," *Energy,* vol. 22, no. 2/3, pp. 161-168, 1997.

[15] L. Leibowitz and L. W. Mishler, "A Study of Aluminum-Water Reactions by Laser Heating," *Journal of Nuclear Materials,* vol. 23, pp. 173-182, 1967.

[16] O. V. Kravchenko, K. N. Semenenko, B. M. Bulychev and K. B. Kalmykov, "Activation of Aluminum metal and its Reaction with Water," *Journal of Alloys and Compounds,* vol. 397, pp. 58-62, 2005.

[17] J. H. Brewer and D. L. Allgeier, "Disposable Hydorgen Generator," *Science,* vol. 147, no. 3661, pp. 1033-1034, 1965.

[18] L. F. Kozin and V. A. Sakharenko, "Kinetics and Mechanisms of Interaction Between Aluminum-Base, Gallium-Base and Thallium-Base Base Alloys and Water," *Ukrainskii Khimicheskii Zhurnal,* vol. 50, no. 1, pp. 9-15, 1984.

[19] V. A. Zasukha, L. F. Kozin and B. I. Danil'tsev, "Kinetics of the Reduction of Water by Activated Aluminum Powder," *Theoretical and Experimental Chemistry,* vol. 31, no. 4, pp. 196-199, 1995.

[20] K. Hanada, K. A. Khor, M. J. Tan, Y. Murakoshi, H. Negishi and T. Sano, "Aluminum-Lithium/SiCp Composites Produced by Mechanically Milled Powders," *Journal of Materials Processing Technology,* vol. 67, pp. 8-12, 1997.

[21] K. Uehara, H. Takeshita and H. Kotaka, "Hydrogen Gas Generation in the Wet Cutting of Aluminum and its Alloys," *Journal of Materials Processing Technology,* vol. 127, pp. 174-177, 2002.

[22] A. N. Streletskii, I. V. Kolbanev, A. B. Borunova and P. Y. Butyagin, "Mechanochemical Activation of Aluminum: 3. Kinetics of Interaction Between Aluminum and Water," *Colloid Journal,* vol. 67, no. 5, pp. 631-637, 2005.

[23] A. V. Parmuzina and O. V. Kravchenko, "Activation of Aluminum Metal to Evolve Hydrogen from Water," *International Journal of Hydrogen Energy,* vol. 33, pp. 3073-3076, 2008.

[24] B. Alinejad and K. Mahmoodi, "A Novel Method for Generating Hydrogen by Hydrolysis of Highly Activated Aluminum Nanoparticles in Pure Water," *International Journal of Hydrogen Energy,* vol. 34, pp. 7934-7938, 2009.

[25] E. Czech and T. Troczynski, "Hydrogen Generation Through Massive Corrosion of Deformed Aluminum in Water," *International Journal of Hydrogen Energy,* vol. 35, pp. 1029-1037, 2010.

[26] L. Soler, A. M. Candela, J. Macanas, M. Munoz and J. Casado, "Hydrogen Generation by Aluminum Corrosion in Seawater Promoted by Suspensions of Aluminum Hydroxide," *International Journal of Hydrogen Energy,* vol. 34, pp. 8511-8518, 2009.

[27] M. Watanabe, "Chemical Reactions in Cracks of Aluminum Crystals: Generation of Hydrogen from Water," *Journal of Physics and Chemistry of Solids,* vol. 71, pp. 1251-1258, 2010.

[28] L. Soler, A. M. Candela, J. Macana, M. Munoz and J. Casado, "Hydrogen Generation from Water and Aluminum Promoted by Sodium Stannate," *International Journal of Hydrogen Energy,* vol. 35, pp. 1038-1048, 2010.

[29] J. Macanas, L. Soler, A. M. Candela, M. Munoz and J. Casado, "Hydrogen Generation by Aluminum Corrosion in Aqeous Alkaline Solutions of Inorganic Promoters: The AlHidrox Process," *Energy,* vol. 36, pp. 2493-2501, 2011.

[30] V. Rosenband and A. Gany, "Application of Activated Aluminum Powder for Generation of Hydrogen from Water," *International Journal of Hydrogen Energy,* vol. 35, pp. 10898-10904, 2010.

[31] A. V. Ilyukhina, O. V. Kravchenko, B. M. Bulychev and E. I. Shkolnikov, "Mechanochemical Activation of Aluminum with Gallams for Hydrogen Evolution from Water," *International Journal of Hydrogen Energy,* vol. 35, pp. 1905-1910, 2010.

[32] Z. Zhao, X. Chen and M. Hao, "Hydrogen Generation by Splitting Water with Al-Ca Alloy," *Energy,* vol. 36, pp. 2782-2787, 2011.

[33] P. Dupiano, D. Stamatis and E. L. Dreizin, "Hydrogen Production by Reacting Water with Mechanically Milled Composite Aluminum-Metal Oxide Powders," *International Journal Of Hydrogen Energy,* vol. 36, pp. 4781-4791, 2011.

[34] S.-H. Hong, D. W. Lee and B. K. Kim, "Manufacturing of Aluminum Flake Powder from Foil Scrap by Dry Ball Milling Process," *Journal of Materials Processing Technology,* vol. 100, pp. 105-109, 2000.

[35] S. H. Hong and B. K. Kim, "Fabrication of Aluminum Flake Powder from Foil Scrap by a Wet Ball

Milling Process," *Materials Letters,* vol. 51, pp. 139-143, 2001.

[36] Y. A. Aleksandrov, E. I. Tsyganova and A. L. Pisarev, "Reaction of Aluminum with Dilute Aqueous NaOH Solutions," *Russian Journal of General Chemistry,* vol. 73, no. 5, pp. 689-694, 2003.

[37] S. S. Martinez, W. L. Benites, A. A. Alvarez Gallegos and P. J. Sebastian, "Recycling of Aluminum to Produce Green Energy," *Solar Energy Materials and Solar Cells,* vol. 88, pp. 237-243, 2005.

[38] R. Cownden and M. Nahon, "Performance Modeling and Improvements of a Solid Polymer Fuel Cell System," *Proceedings of the 2nd International Fuel Cell Conference, Kobe, Japan,* pp. 355-358, 1996.

[39] I. Dincer, "Technical, Environmental and Exergetic Aspects of Hydrogen Energy Systems," *International Journal of Hydrogen Energy,* vol. 27, pp. 265-285, 2002.

[40] H. J. Neef, "International Overview of Hydrogen and Fuel Cell Research," *Energy,* vol. 34, no. 3, pp. 327-333, 2009.

[41] J. P. Foote, B. R. Thompson and J. T. Lineberry, "Combustion of Aluminum with Steam for Underwater Propulsion," *Gabirel D.Roy (Ed.),Advances in Chemical Propulsion:Science to Technology, Office of Naval Research, Arlington, Virginia, USA,* pp. 154-167, 2001.

[42] T. F. Miller and J. D. Herr, "Green Rocket Propulsion by Reaction of Al and Mg Powders and Water," *AIAA Paper 2004-4037,* 2004.

[43] A. Ingenito and C. Bruno, "Using Aluminum for Space Propulsion," *Journal of Propulsion and Power,* vol. 20, no. 6, pp. 1056-1063, 2004.

[44] V. G. Ivanov, S. N. Leonov, G. L. Savinov, O. V. Gavrilyuk and O. V. Glazkov, "Combustion of Mixtures of Ultradisperse Aluminum and Gel-Like Water," *Combustion, Explosion and Shockwaves,* vol. 30, pp. 569-570, 1994.

[45] V. G. Ivanov, O. V. Gavrilyuk, O. V. Glazkov and M. N. Safronov, "Specific Features of the Reaction between Ultrafine Aluminum and Water in a Combustion Regime," *Combustion, Explosion and Shockwaves,* vol. 36, pp. 213-219, 2000.

[46] E. Shafirovich, V. Diakov and A. Varma, "Combustion of Novel Mixtures for Hydrogen Generation," *Combustion and Flame,* vol. 144, pp. 415-418, 2006.

[47] E. Shaifrovich, V. Diakov and A. Varma, "Combustion Assisted Hydrolysis of Sodium Borohydride for Hydrogen Generation," *International Journal of Hydrogen Energy,* vol. 32, pp. 207-211, 2007.

[48] M. Diwan, V. Diakov, E. Shafirovich and A. Varma, "Noncatalytic Hydrothermolysis of Ammonia Borane," *International Journal of Hydrogen Energy,* vol. 33, pp. 1135-1141, 2008.

[49] G. A. Risha, S. F. Son, R. A. Yetter, V. Yang and b. C. Tappan, "Combustion of Nano-Aluminum and Liquid Water," *Proceedings of Combustion Institute,* vol. 31, pp. 2029-2036, 2007.

[50] G. A. Risha, J. L. Sabourin, V. Yang, R. A. Yetter, S. F. Son and B. C. Tappan, "Combustion and Conversion Efficiency of Nanoaluminum-Water Mixtures," *Combustion Science and Technology,* vol. 180, pp. 2127-2142, 2008.

[51] J. L. Sabourin, G. A. Risha, R. A. Yetter, S. F. Son and B. C. Tappan, "Combustion Characteristics of Nano Aluminum, Liquid Water, and Hydrogen Peroxide Mixtures," *Combustion and Flame,* vol. 154, pp. 587-600, 2008.

[52] T. L. Connell Jr, G. A. Risha, R. A. Yetter, G. A. Young, D. S. Sundaram and V. Yang, "Combustion of Alane and Aluminum with Water for Hydrogen and Thermal Energy Generation," *Proceedings of Combustion Institute,* vol. 33, pp. 1957-1965, 2011.

[53] Y. L. Sun and B. Z. Zhu, "Combustion Characteristics of an Al/H2O Mixture with Polyoxyethylene," *Industrial and Engineering Chemistry Research,* vol. 50, pp. 14136-14141, 2011.

[54] J. Wan, S. Z. Cai, Y. Liu, C. S. Xie, X. P. Xia and D. W. Zeng, "Reaction Characteristics of Nano-Aluminum and Water by In-Situ Investigation," *Mateirals Chemistry and Physics,* vol. 136, pp. 466-471, 2012.

[55] D. S. Sundaram, V. Yang, T. L. Connel Jr, G. A. Risha and R. A. Yetter, "Flame Propagation of Nano/Micron-Sized Aluminum Particles and Ice (ALICE) Mixtures," *Proceedings of Combustion Institute,* vol. 34, pp. 2221-2228, 2013.

[56] T. R. Sippel, T. L. Pourpoint and S. F. Son, "Combustion of Nanoaluminum and Water Propellants: Effect of Equivalence Ratio and Safety/Aging Characterization," *Propellants, Explosions and Pyrotechnics,* vol. 38, pp. 56-66, 2013.

[57] T. X. Phuoc and R. H. CHen, "Spontaneous Ignition of Low-Concentration Nano-Sized Al-Water Slurry," *Applied Energy,* vol. 101, pp. 567-571, 2013.

[58] S. Iijima, "Helical Microtubles of Graphitic Carbon," *Nature,* vol. 354, p. 56, 1991.

[59] C. Y. Lee, T. Y. Tseng, S. Y. Li and P. Lin, "Growth of Zinc Oxide Nanowires on Silicon (100)," *Tamkang Journal of Science and Engineering,* vol. 6, no. 2, pp. 127-132, 2003.

[60] E. I. Givargizov, "Growth of Si Whiskers by V-L-S Mechanism," *Journal of Crystal Growth,* vol. 31, p. 20, 1975.

[61] Z. R. Dai, J. L. Gole, J. D. Stout and Z. L. Wang, "Tin Oxide Nanowires, Nanoribbons, and Nanotubes (0)," *Journal of Physical Chemistry,* vol. 106, pp. 1274-1279, 2002.

[62] V. M. Mikushkin, S. E. Sysoev and Y. S. Gordeev, "Nano-Structure Creation by Ion Bombardment of Semiconductor and High Temperature Super Conductors," *Russian Academy Science News Seria Physical,* vol. 66, no. 4, pp. 588-592, 2002.

[63] R. S. Wagner and W. C. Ellis, "V-L-S Mechanism of Single Crystal Growth," *Applied Physics Letters,* vol. 4, no. 5, 1964.

[64] J. Zhang and F. Jiang, "Catalytic Growth of Ga2O3 Nanowires by Physical Evaporation and their Photoluminescence Properties," *Chemical Physics,* vol. 289, pp. 243-249, 2003.

[65] H. Z. Zhang, Y. C. Kong, Y. Z. Wang, X. Du, Z. G. Bai, J. J. Wang, D. P. Yu, Y. Ding, Q. L. Hang and S. Q. Feng, "Ga2O3 Nanowires Prepared by Physical Evaporation," *Solid State Communications,* vol. 109, pp. 677-682, 1999.

[66] M. Ogita, N. Saika, Y. Nakanishi and Y. Hatanaka, "Ga2O3 Thin Films for High-Temperature Gas Sensors," *Applied Surface Science,* vol. 142, pp. 188-191, 1999.

[67] J. S. Lee, K. Park, S. Nahm, S. W. Kim and S. Kim, "Ga2O3 Nanomaterials Synthesized from Ball-Milled GaN Powders," *Journal of Crystal Growth,* vol. 244, pp. 287-295, 2002.

[68] A. Glushenkov and Y. Chen, "Synthesis of ZnO Nanowires Using Ball-Milling and Annealing Method," *Materials Forum,* vol. 30, pp. 1-6, 2006.

[69] H. D. Xiao, H. L. Ma, W. Liang, C. S. Xue, H. Z. Zhuang, J. H. Ma and W. R. Hu, "Ga2OH, a-Ga2O3 and b-Ga2O3 Powders Synthesized from Ball-Milled GaN Powders," *Materials Chemistry and Physics,* vol. 94, pp. 261-265, 2005.

[70] W. S. Jung, H. U. Joo and B. K. Min, "Growth of beta-Gallium Oxide Nanostructures by the Thermal Annealing of Compacted Gallium Nitride Powder," *Physica E,* vol. 36, pp. 226-230, 2007.

[71] Y. Wang, L. Hou, X. Qin, S. Ma, B. Zhang, H. Gou and F. Gao, "Fabrication of Single-Crystalline beta-Gallium Oxide Nanowires and Zigzag-Shaped Nanostructures," *Journal of Physical*

Chemistry, vol. 111, pp. 17506-17511, 2007.

[72] L. Cao, M. K. Li, Z. Yang, Q. Wei and W. Zhang, "Synthesis and Characterization of Dentate-Shaped beta-Ga2O3 Nano/Microbelts via a Simple Method," *Applied Physics A,* vol. 91, pp. 415-419, 2008.

[73] W. Z. Gai, W. H. Liu, Z. Y. Deng and J. G. Zhou, "Reaction of Al Powder with Water for Hydrogen Generation Under Ambient Condition," *International Journal of Hydrogen Energy,* vol. 37, pp. 13132-13140, 2012.

[74] K. Mahmoodi and B. Alinejad, "Enhancement of Hydrogen Generation Rate in Reaction of Aluminum with Water," *International Journal of Hydrogen Energy,* vol. 35, pp. 5227-5232, 2010.

[75] Z. Y. Deng, Y. B. Tang, L. L. Zhu, Y. Sakka and J. Ye, "Effect of Different Modfication Agents on Hydrogen Generation by the Reaction of Al with Water," *International Journal of Hydrogen Energy,* vol. 35, pp. 9561-9568, 2010.

[76] W. F. Hosford and J. L. Duncan, "The Aluminum Beverage Can," *Scientific American,* pp. 48-53, 1994.

[77] H. W. Wang, H. W. Chung, H. T. Teng and G. Cao, "Generation of Hydrogen from Aluminum and Water- Effect of Metal Oxide Nanocrystals and Water Quality," *International Journal of Hydrogen Energy,* vol. 36, pp. 15136-15144, 2011.

[78] A. A. Shiryaev, "Thermodynamics of SHS: Moden Approach," *International Journal of Self-Propagating High Temperature Synthesis,* vol. 4, pp. 351-362, 1995.

[79] Y. A. Cengel, J. M. Cimbala and R. H. Turner, Fundamentals of Thermal-Fluiid Sciences, New York: McGraw Hill, 2012.

[80] J. Yang, A. Sudik, C. Wolverton and S. DJ, "High Capacity Hydrogen Storage Materials: Atributes for Automotive Applications and Techniques for Materials Discovery," *Chemical Society Reviews,* vol. 39, no. 2, pp. 656-675, 2010.

Appendix A

Peer Reviewed Journal Articles

Narayana Swamy, A.K. and Shafirovich, E., "Conversion of Aluminum Foil to Powders that React and Burn with Water," *Combustion and Flame*, 2013, in review.

Narayana Swamy, A.K., Shafirovich, E., and Ramana, C.V., "Synthesis of One-dimensional Ga_2O_3 Nanostructures via High-Energy Ball Milling and Annealing of GaN," *Ceramics International*, Vol. 39, 2013, pp. 7223-7227.

Álvarez, F., Delgado, A., Frias, J., Rubio, M., White, C., **Narayana Swamy, A.K.**, and Shafirovich, E., "Combustion of Thermites in Reduced Gravity for Space Applications," *Journal of Thermophysics and Heat Transfer*, June 3, 2013, doi: 10.2514/1.T3876

Álvarez, F., White, C., **Narayana Swamy, A.K.**, and Shafirovich, E., "Combustion Wave Propagation in Mixtures of JSC-1A Lunar Regolith Simulant with Magnesium," *Proceedings of the Combustion Institute*, Vol. 34, 2013, pp. 2245–2252.

Shafirovich, E., Garcia, A., **Narayana Swamy, A.K.**, Mast, D.J., and Hornung, S.D., "On Feasibility of Decreasing Metal Fuel Content in Chemical Oxygen Generators," *Combustion and Flame*, Vol. 159, 2012, pp. 420-426.

Conference Proceedings Papers/Presentations

Narayana Swamy, A.K., and Shafirovich, E., "Combustion of Activated Aluminum with Water," The 8th U.S. National Combustion Meeting, May 19-22, 2013, Park City, UT, Paper 1G12.

Narayana Swamy, A.K., and Shafirovich, E., "Activated Aluminum Powder Obtained from Foil: Reactions with Hot Water and Combustion of Al/H_2O Mixtures," 51st AIAA Aerospace Sciences Meeting, January 7-10, 2013, Grapevine, TX, AIAA Paper 2013-0595.

Narayana Swamy, A.K., and Shafirovich, E., "Water Splitting by Aluminum Powder Obtained from Foil," Proceedings of ASME 2012 International Mechanical Engineering Congress and Exposition (IMECE2012), November 9-15, 2012, Houston, TX, IMECE2012-88150 (***Best Poster Award***).

Narayana Swamy, A.K., and Shafirovich, E., "Fabrication of Activated Aluminum Powder from Foil," 2012 Materials Research Society Fall Meeting, Boston, MA, November 25-30, 2012.

Álvarez F., White, C., Delgado, A., Frias, F., **Narayana Swamy, A.K.**, and Shafirovich, E., "Combustion of JSC-1A Lunar Regolith Simulant Mixed with Magnesium," 48th AIAA/ASME/SAE/ASEE Joint Propulsion Conference, July 30 – August 1, 2012, Atlanta, GA, AIAA Paper 2012-4092.

Narayana Swamy, A.K., and Shafirovich, E., "Hydrogen generation from water using activated aluminum," 2nd Southwest Energy Science and Engineering Symposium, El Paso, Texas, March 2012.

Álvarez F., Delgado, A., Frias, F., Rubio, M., White, C., **Narayana Swamy, A.K.**, and Shafirovich, E., "Microgravity Combustion of Thermite Mixtures for Welding in Space and for Production of Structural Materials from Lunar Regolith," 50th AIAA Aerospace Sciences Meeting, January 9-12, 2012, Nashville, TN, AIAA Paper 2012-1119.

Garcia, A., **Narayana Swamy, A.K.**, and Shafirovich, E., "Study of CO_2 reduction in SnO_2/SnO thermochemical cycle," 1st Southwest Energy Science and Engineering Symposium, El Paso, Texas, April 2011.

Vita

Ashvin Kumar Narayana Swamy is a doctoral student in the Environmental Science and Engineering program, specifically in its Energy Science and Engineering track, managed by the Department of Mechanical Engineering at The University of Texas at El Paso (UTEP). Originally from Bangalore, India, Ashvin received his bachelor's degree in mechanical engineering at the National Institute of Technology Durgapur, India. He moved to the United States in 2007 to pursue master's degree in mechanical and aerospace engineering at Oklahoma State University. Under the mentorship of Dr. David G. Lilley, he studied combustion and smoke propagation of flammable materials in compartmentalized structures. He was also involved in the development of a computer code for fire dynamics. To gain further insight into the field of combustion and energy, he decided to enroll into the doctoral program at UTEP. Ashvin is currently working in Dr. Evgeny Shafirovich's group in the Department of Mechanical Engineering. His research focuses on the fabrication of advanced materials for energy applications. His main topic is the production of hydrogen from water using secondary aluminum like foil scrap and waste. For this purpose he uses high-energy ball milling to produce activated micro- and nano-scale powders as well as studies reactions of the produced powders with hot water and combustion of their mixtures with liquid and solid water. He is also involved in a DOE-sponsored project titled "*Gallium Oxide Nanostructures for High Temperature Sensors,"* also under the guidance of Dr. Shafirovich. In this project, gallium oxide nano-belts and nano-sheets were successfully synthesized by employing high-energy milling and high-temperature reactions. Ashvin has also worked on developing chemical oxygen generators with improved fire safety and process stability and helped the UTEP microgravity team in preparation of lunar regolith samples for combustion experiments onboard reduced gravity research aircraft in Houston, Texas in June 2011 and June 2012. Ashvin is highly skilled in particle characterization techniques such as BET specific surface area analysis, particle size analysis, scanning electron microscopy (SEM), energy dispersive X-ray spectroscopy (EDS), X-ray diffraction analysis (XRD), and thermogravimetric analysis (TGA). Ashvin's research interests include combustion synthesis, high-energy mechanical milling, energetic materials, and development of nano-

composite materials. After graduation, Ashvin plans to work in the field of nano-composites for energy applications.

Permanent address: No. 4, 1st Cross Nayak Layout, B.K. Circle, Kothannur Dinne
J.P. Nagar 8th Phase, Bangalore, India, 560076

This dissertation was typed by Ashvin Kumar Narayana Swamy.